

A Novel Constitutive Law for Describing Materials Behaviour at High Strain Rate and Large Deformation

by

A.M.S. Hamouda, *BSc, MEng, MIMechE, MASME, MAAM*

This thesis is submitted to Dublin City University as the fulfilment of
the requirement for the award of Degree of

Doctor of Philosophy

Supervisor: Professor M.S.J. Hashmi

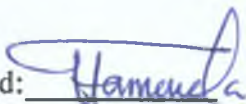
*School of Mechanical & Manufacturing Engineering
Dublin City University*

March 1995

Dedicated to My Late Father

DECLARATION

I hereby certify that this material, which I now submit for assessment on the programme of study leading to the award of Doctor of Philosophy is my own work and has not been taken from the work of others save and to the extent that such work has been cited and acknowledged within the text of my work.

Signed: 

I.D No.: 91700931

Date: 20 March 1995

LIST OF CONTENTS

	Page
DECLARATION	I
TABLE OF CONTENTS	II
ACKNOWLEDGMENTS	VI
ABSTRACT	VII
NOMENCLATURE	VIII

CHAPTER ONE. INTRODUCTION AND JUSTIFICATION

1.1 INTRODUCTION	1
1.2 IMPORTANT OF STRESS-STRAIN DATA OF ENGINEERING MATERIALS TO DESIGN	1
1.3 AIM OF THE STUDY	2
1.4 METHOD OF APPROACH	3
1.5 LAYOUT OF THESIS	4

CHAPTER TWO: LITERATURE REVIEW

2.1 INTRODUCTION	5
2.2 DYNAMIC LOADING OF ENGINEERING MATERIALS	5
2.2.1 Impact Loading of Structures	5
2.2.2 High Speed Forming and Metal Cutting	6
2.2.3 Dynamic Crack Propagation	8
2.3 CLASSIFICATION OF STRAIN RATE REGIMES	9
2.3.1 Creep Rate Regime	10
2.3.2 Quasi-static Strain Rate Regime	10
2.3.3 Intermediate Strain Rate Regime	10
2.3.4 High Strain Rate Regime	10
2.4 TECHNIQUES FOR HIGH STRAIN RATE TESTING	11
2.4.1 Techniques Used for Intermediate Strain Rate Testing	11
2.4.2 Techniques Used for High Strain Rate Testing	13
2.4.3 Techniques Used for Very High Strain Rate Testing	18
2.4.4 Measurement Techniques	18
2.5 FACTORS AFFECTING THE DYNAMIC COMPRESSION TEST	21
2.5.1 Interfacial Friction	21
2.5.2 Inertia Effects	24

2.5.3 Adiabatic Shear Phenomena	25
2.5.4 Specimen Geometry	27
2.5.5 Microstructural Changes	28
2.6 EFFECT OF STRAIN RATE ON FLOW STRESS	29
2.6.1 Metallic Materials	29
2.6.2 Composite Materials	32
2.6.3 Polymeric Materials	33

CHAPTER THREE: FORMULATION AND IMPLEMENTATION OF A NOVEL RATE-DEPENDENT CONSTITUTIVE LAW

3.1 INTRODUCTION	35
3.2 REVIEW OF EXISTING CONSTITUTIVE LAWS	35
3.3 FORMULATION OF A NEW CONSTITUTIVE LAW	38
3.3.1 Effect of Thermal Softening on Strain Hardening	39
3.3.2 Effect of Strain Rate on Strain Hardening	40
3.4 THEORETICAL FORMULATION: FINITE-DIFFERENCE MODEL	41
3.4.1 Equation of Motion	42
3.4.2 The Displacement-Strain Relations	44
3.4.3 Idealised Cross-Section Model	44
3.4.4 Stress Calculations	45
3.4.5 Inertia Effects	49
3.4.6 Effect of Friction	50
3.4.7 Effect of Stress Waves	50
3.4.8 Initial and Boundary Conditions	51
3.4.9 Stability of Solution and Selection of Time Increments	52
3.5 ENERGY DISTRIBUTION IN THE SYSTEM	53
3.6 IMPLEMENTATION OF FINITE-DIFFERENCE MODEL	54
3.6.1 Code Description	54
3.6.2 Code Input and Output	55
3.6.3 Condition to Terminate the Simulation of the Deformation	55
3.7 A COMPUTATIONAL EXAMPLE AND VALIDATION	57
3.7.1 High Velocity Impact of a Steel Bar Against a Rigid Boundary	57
3.7.2 Finite-Element Model	57
3.7.3 Finite-Difference Model	57
3.7.4 Results & Comparison	59
3.8 ON THE ENERGY DISSIPATION DURING IMPACT TEST	60

CHAPTER FOUR: EXPERIMENTAL INVESTIGATIONS

4.1 INTRODUCTION	65
4.2 SELECTION OF MATERIALS AND SPECIMEN DESIGN	65
4.3 HIGH STRAIN RATE TESTING	68
4.3.1 Ballistic Test Apparatus	68
4.3.2 Ballistic Test Procedure	75
4.3.3 Preparation of Projectile	76
4.4 TYPICAL TEST RESULTS AND LIMITATIONS	78
4.5 INTERMEDIATE STRAIN RATE TESTING	81
4.6 STUDY ON THE EFFECT OF WATER SATURATION ONTO THE MECHANICAL PROPERTIES OF NYLON	85

CHAPTER FIVE: ANALYSIS AND DISCUSSION OF RESULTS

5.1 INTRODUCTION	87
5.2 DETERMINATION OF MATERIALS CONSTANTS	87
5.3 DYNAMIC BEHAVIOUR OF METALLIC MATERIALS	88
5.3.1 Dynamic Stress-Strain Curves	89
5.3.2 Adiabatic and Isothermal Stress-Strain Curves	90
5.3.3 Strain Rate Sensitivity	93
5.3.4 Comparison with Earlier Studies	95
5.4 DYNAMIC BEHAVIOUR OF METAL MATRIX COMPOSITES	97
5.4.1 Primary Remarks	97
5.4.2 Quasi-Static Properties	97
5.4.3 Dynamic Stress-Strain Curves of MMC	99
5.4.4 Adiabatic and Isothermal Stress-Strain Curves	101
5.4.5 Strain Rate Sensitivity	102
5.5 DYNAMIC BEHAVIOUR OF NYLON	103
5.5.1 Introduction	103
5.5.2 Primary Remarks	103
5.5.3 Low Strain Rate	103
5.5.4 Dynamic Stress-Strain Curves of Nylon	104
5.5.5 Strain Rate Sensitivity	105
5.5.6 Thermal Softening Effect	107
5.6 FACTORS AFFECTING STRAIN RATE SENSITIVITY	108
5.6.1 Interfacial Friction Effect	108
5.6.2 Inertia Effects	108

5.6.3 Thermal Softening Effect	109
5.6.4 Energy Losses Effect	109
5.7 VERIFICATION OF THE DEVELOPED LAW	112
5.7.1 Introduction	112
5.7.2 High Strain Rates Tests	112
5.7.3 Intermediate Strain Rates Tests	113
CHAPTER SIX: GENERAL CONCLUSIONS	
6.1 INTRODUCTION	116
6 2 STATEMENT OF PROBLEM	116
6.3 SUMMARY OF THEORETICAL AND EXPERIMENTAL INVESTIGATIONS	117
6 4 GENERAL CONCLUSIONS	117
5.4.1 A Novel Constitutive Law	117
5.4.2 Dynamic Behaviour of Metallic Alloys	118
5.4.3 Dynamic Behaviour of Metal Matrix Composites	118
5.4.4 Dynamic Behaviour of Nylon	118
6 5 THESIS CONTRIBUTION	119
6 6 RECOMMENDATION FOR FUTURE WORK	120
REFERENCES	121
APPENDIX (A)	A1
APPENDIX (B)	B1
APPENDIX (C)	C1

ACKNOWLEDGEMENTS

The author wishes to express his deep indebtedness to Professor M S J. Hashmi, Dean of Faculty of Engineering and Design for his supervision, encouragement and guidance during the course of this project.

The author would also like to express his appreciation to Professor S.A. Meguid, Director of Engineering Mechanics and Design, Toronto University, Canada, and Dr Lisa Looney for their constructive suggestions, helpful advice and comments on the initial draft of the thesis.

The author wishes to express his thanks to the following people for their assistance and encouragement at various stages of the work: Dr M. El-Baradie; Mr Liam Domican; Mr F. Connor, from the School of Electronic Engineering; all the workshop staff; and Ms Lesley Lawlor.

The author is grateful to the following people who helped directly and indirectly to complete this work: Dr T.Y. Reddy, Professor S.T.S Al-Hassani, Department of Mechanical Engineering, University of Manchester Institute of Science & Technology (UMIST), for their help with the drop hammer tests.

The author is appreciative to his external examiner Professor S.R. Reid, Applied Mechanics Division, UMIST, for his constructive suggestions and comments.

Thanks to all the Research Student in the School of Mechanical & Manufacturing Engineering, for their encouragement.

Last, but not least, very special thanks are due to my loving mother, family and friends at home for their constant love and support. The patience, understanding, and encouragement of my brother Mohammed and his wife and their children are greatly appreciated.

A Novel Constitutive Law for Describing Material Behaviour at High Strain Rate and Large Deformation

A.M.S. Hamouda

ABSTRACT

Determination of stress-strain properties of materials and formulation of suitable constitutive laws is very important in order that: (i) the elastic-plastic response and collapse mode of structures can be analysed for improving subsequent design, and (ii) analysis of high speed metal cutting and metal forming processes may provide improved estimations of process parameters and better understanding of material flow behaviour.

Numerous techniques of high strain rate testing have been reported in the literature and most require transient measurements using sophisticated and often expensive instrumentation. The main criticism of these techniques is that there is always some inherent inaccuracy present especially when measurement of transient load is involved. In recent years, a new technique was reported in which high speed photographic means were employed. The technique avoids the measurement of transit load but is very tedious and expensive.

This thesis is devoted to the development and verification of a novel rate-dependent constitutive law which is capable of describing the elasto-plastic behaviour of three classes of engineering materials under dynamic loading conditions and large deformation. The materials examined were: metallic alloys (aluminium, brass, copper and steel); metal matrix composites (Al-Cu MMC and AL-Li MMC); and a polymeric material (Nylon).

Both theoretical and experimental investigations were conducted to achieve the above set objectives. In the theoretical investigations, finite difference algorithms were developed to describe the elasto-plastic behaviour of the examined materials using a novel constitutive law. The algorithms take into account the effect of inertia, interfacial friction, strain hardening and thermal softening.

The experimental investigations were divided into two main sections. In the first, ballistic test experiments were conducted in conjunction with the theoretical work to evaluate the material constants needed in the newly developed constitutive law. In the second, the ballistic tests were used to verify the proposed law. In this case, both the deformation and loading history were measured and compared with the theoretical predictions. The results reveal good agreement between the two.

NOMENCLATURE

A	Cross-section area.
f	Plastic work converted into heat energy.
G	Temperature softening parameter affecting strain hardening index.
G_1	Temperature softening parameter affecting strength coefficient.
K	Strength coefficient.
m	Strain rate sensitivity constant.
M	Mass per unit length.
N	Axial force.
p	Strain rate sensitivity constant.
r	Current radius of an element.
R	Strain rate parameter affecting strain hardening index.
s	Specific heat.
U	Acceleration.
U	Displacement.
ρ	Density.
ΔS	Link length in numerical model.
Δt	Time interval.
ε	Total true strain.
$\dot{\varepsilon}$	Total true strain rate.
σ	True stress.
α	Parameter combining strain rate and temperature effects on strain hardening

Subscripts

1	The mass number and the number of the preceding link.
j	Instant of time.

Superscripts

p	Plastic
n	Strain hardening index
(-)	Overbar indicate equivalent.

CHAPTER ONE: INTRODUCTION AND JUSTIFICATION

1.1 INTRODUCTION

In this introductory chapter, we justify the undertaking of the work, identify the aims of the study and outline the method of approach adopted in achieving the set objective. Finally, a summary of the content of the different chapters is provided under the heading " Layout of Thesis".

1.2 IMPORTANCE OF DYNAMIC STRESS-STRAIN DATA OF ENGINEERING MATERIALS TO DESIGN

The understanding of material response at high strain rate has taken on a much greater significance over the last few decades as many of the problems confronting engineers involve dynamic loadings at high rates of strain. Many of these problems result from military interests; such as the development of advanced armour systems, vulnerability assessment of military targets, design of lightweight armour systems including fabric body armour for the protection of personnel, analysis of blast loading effects, and penetration [1.1-1.10]. Furthermore, meteorite impacts on satellites [1.11], crashworthiness of vehicles and the protection of their components [1.12-1.16] are other examples of dynamic loadings at high rates of strain. Potential industrial development of impact forming techniques and explosive welding [1.17] also require that characterization of the behaviour of materials at high strain rate be developed.

A recent study conducted by the National Materials Advisory Board (NMAB), U.S.A on " Material Response to Ultra-High Loading Rates", summarizes the state-of-the-art of dynamic behaviour of materials as well as provides recommendations for future research in the area of dynamic plasticity [1 18]. The NMBA report concerned itself with high velocity ordnance problems; such as, shape-charge jets, self-forging

projectiles, and fragmentation devices as well as their interaction with armour targets. In each case, the behaviour of the material involves high rates of strain, large deformation, high pressure, and high temperatures due to adiabatic heating in both projectile and the target. The NMAB recommended that "*the most fruitful course for advance development appeared to be an iterative combination of ballistic test firings, numerical simulations with computer codes, and dynamic material determinations*". This was one of the motivating factors behind the present work.

In the view of the fact that direct measurements of the governing constitutive laws are difficult to obtain over much of the ranges of interest in impact situations, it is desirable to develop theoretical models which do not require extensive experimental data for their calibration. This indeed was a second motivating factor behind the proposed studies.

1.3 AIM OF THE STUDY

The objectives of the present study can be summarised as follows:

- (i) to develop a nonlinear finite difference scheme which is capable of describing the elasto-plastic behaviour of engineering materials under impact loading using a novel constitutive law,
- (ii) to account for the effects of inertia, interfacial friction, strain hardening and thermal softening in the developed algorithms,
- (iii) to verify the theoretical result with experimental measurements using a ballistic test rig. Both the deformation and loading history must be examined, and
- (iv) to obtain dynamic stress strain data for different types of engineering materials; such as, metallic alloys, metal matrix composites and polymeric materials.

To achieve the above-stated objectives, the following method of approach was adopted

1.4 METHOD OF APPROACH

The method of approach, which is shown schematically in Figure 1.1, is divided into two main sections.

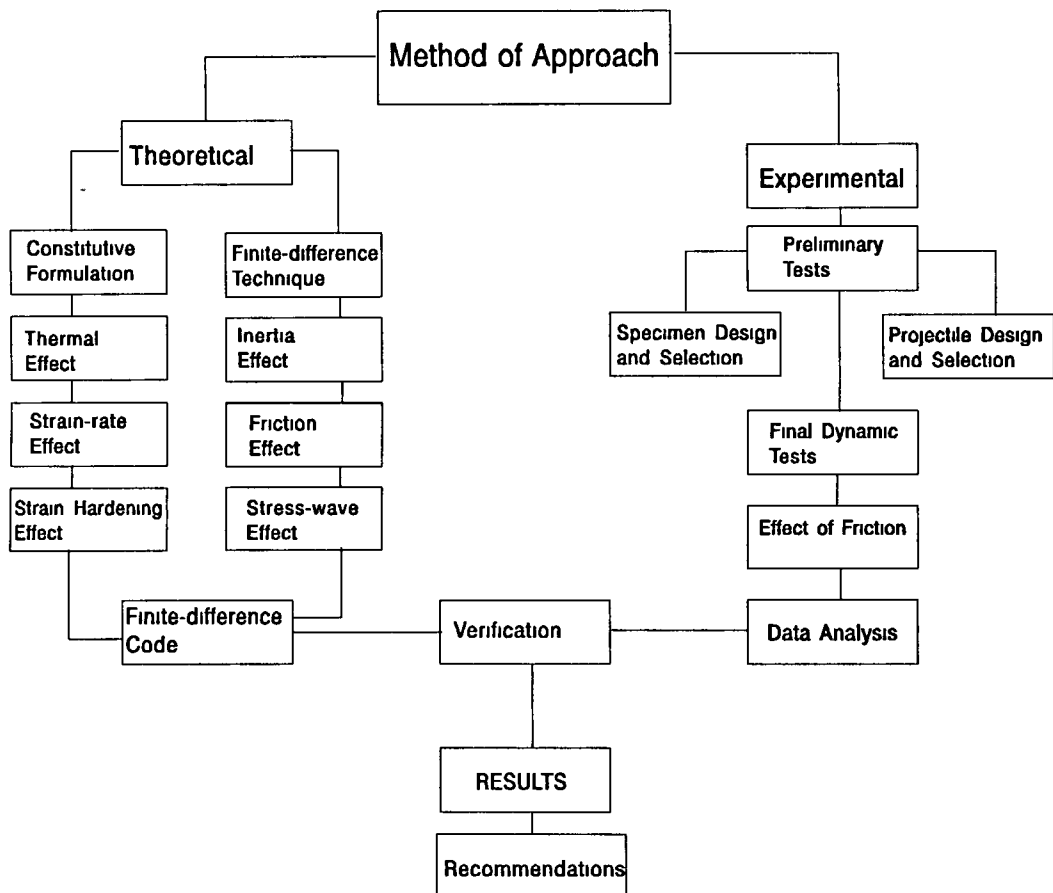


Figure 1.1 *The Method of Approach Adopted in the Present Study.*

The first is devoted to the development of a theoretical model, which consists of developing a nonlinear finite-difference algorithm and formulating a novel constitutive

law for materials subjected to high rates of strain and large deformation. In this context, convergence and accuracy tests were conducted to verify the model. The second section is concerned with the experimental investigations. This is devoted to (i) design and selection of projectiles and specimens materials, (ii) conducting dynamic compression tests, (iii) examining friction effects, and finally, (iv) data analysis and interpretation of the results.

1.5 LAYOUT OF THESIS

This thesis is divided into six chapters. Following this introductory chapter, chapter two gives the importance of high strain rate to impact loading of structures, high speed forming and machining, and dynamic crack propagation. The factors affecting strain rate sensitivity and a critical review of the relevant literature are also presented and discussed. Chapter three is devoted to the development of a theoretical model for the dynamic system using a new form of a constitutive law which takes into account high strain rate and large strain effects. The convergency and accuracy of the developed code are examined and assessed. Also, a study on the energy dissipation during the impact is presented. Chapter four examines, the details of the selection of the materials, the test specimen and projectile design, the ballistic test apparatus used and the test procedure. Typical results are also given in this chapter. Chapter five is devoted to the analysis and discussion of results. Finally, in chapter six conclusions are drawn based on the present work.

CHAPTER TWO: LITERATURE REVIEW

2.1 INTRODUCTION

The aim of this chapter is to provide the fundamental and background information necessary to pursue the subject of high strain-rate mechanical behaviour of materials. Accordingly, the fundamental applications of high strain-rate are first reviewed. These are then followed by describing the techniques available for determining the high strain-rate properties of materials. These range from split Hopkinson bar to flat plate impact. The effects of friction, inertia, and temperature rise during the dynamic compression tests are also reviewed and discussed. No attempt is made to deal in depth with any specific applications involving high strain-rate such as penetration and crashworthiness. However, numerous references are given for the readers to explore these topics in greater detail.

2.2 DYNAMIC LOADING OF ENGINEERING MATERIALS

Recent advances in materials and manufacturing technology have resulted in situations involving dynamic loading at high rates of strain. In the past, impact problems were of primary concern to the military only. But at present, as civilian technology becomes more competitive, intense demands are being made for developing equations of state to describe the behaviour of materials at high strain-rates. The main areas of interest to this study which involve high strain-rates are: (i) impact loading of structures, (ii) high speed forming and metal cutting, and (iii) dynamic crack propagation.

2.2.1 Impact Loading of Structures

In view of its importance to design, the impact behaviour of structures has received considerable attention over the years. For example, energy absorbing devices are required to provide crashworthiness protection for cars, airplanes and other vehicles [2.1]. Many civil, nuclear and ocean engineering structures are subjected to dynamic loads. The impact resistance of structures is a major concern in the building and

maintenance of an aircraft and spacecraft, since they may be subjected to impact with runway or space debris, bird impact, or even the dropping of tools on critical structural components. Moreover, engineers often have to decide whether or not a structure is safe to operate after it has been subjected to low energy impacts.

Most of the practical problems mentioned above are very complex. They not only involve dynamic effects, but structures often possess intricate structural geometries which undergo finite displacements, finite rotations with large inelastic strains together with tearing and fracture of the material.

It has been observed by many authors [2.2-2.5] that the influence of the strain rate sensitivity of the material plays an important role on the response of structures.

Cowper-Symonds [2.6] proposed a deformation model for strain rate sensitive materials which is used extensively in numerical studies. Perrone's simplification [2.7] has allowed the influence of material strain-rate sensitivity to be incorporated into rigid perfectly plastic analysis. Reid and Reddy [2.8,2.9] described how the effect of strain-rate can be incorporated into the analysis of the crushing of layered tube systems at moderate speed using the Cowper-Symonds model. They raised the question of how one can represent strain-rate sensitivity in the context of large structural deformations. Jones [2.10] modified Cowper-Symonds to cater for those particular situations involving large plastic strains.

2.2 2 High Speed Forming and Metal Cutting

Metal forming: In recent years there has been a remarkable interest in high speed metal forming technology. The design of metal forming processes often requires knowledge of the load and energy requirement for a given forming operation. It is important that metal processing engineers know the influence of the strain-rate, friction, material properties and tool geometry on the final product.

A considerable effort has been devoted during the past thirty years to determining the effect of strain-rate in metal forming [2.11-2.16]. The work by Ghosh [2.17] illustrates the application of dynamic plasticity in sheet metal forming. The influence of strain-rate on cold forming has been reviewed by Martensson [2.18]. Application of dynamic plasticity to metal forming and their relation to stress wave propagation phenomena is covered in detail in the book by Johnson [2.19].

One should also mention *High-Energy-Rate-Forming* (HERF) in which the material is formed explosively. The important distinguishing characteristics of HERF processes is that the rate of energy transfer to the workpiece is high during a short period. The subject of HERF was reviewed in references [2.20-2.22]. Table 2.1 gives some of the typical deformation velocities for various energy sources.

Table 2.1 *Some Typical Deformation Velocities for Various Energy Sources.*

System	Velocity ms ⁻¹
<i>Hydraulic press</i>	0.04
<i>Brake press</i>	0.05
<i>Mechanical press</i>	0.9
<i>Drop hammer</i>	0.3-6
<i>Gas-mechanical</i>	3-76
<i>Explosive gas</i>	9-101
<i>Low explosive</i>	9-101
<i>High explosive</i>	31-213
<i>Electro-hydraulic</i>	30-213
<i>Electro-magnetic</i>	30-213

Metal cutting: During the process of metal chip removal, even at conventional machining speeds, the strain-rates are very high; often increasing substantially with the flow stresses opposing the progress of the tool within the work-piece. A number of researchers have investigated the effects of high strain-rate on machining. Among the published papers on strain-rates effects in machining one can cite Boothroyd and Bailey [2.23], Spaans [2.24], Hashmi [2.25], and Oxley and Hastings [2.26]. Reviews of investigations into metal cutting have been presented by von Turkovitch [2.27] and Boothroyd [2.28].

An important aspect of the analysis of machining processes is the estimation of the strain rate in the region ahead of the tool and determination of the distribution of the strain rate throughout the workpiece as a function of time. As pointed out by Oxley [2.29] the problem is further complicated by the fact that machining is generally a discontinuous process. This was brought out very clearly in the work of LeMaitre *et al.* [2.30]. Furthermore, at very high machining speeds the chip formation may even be accompanied by adiabatic shearing. In spite of these difficulties, Oxley and Stevenson [2.31] have developed a model to predict the strain-rates in the plastic zone in which the chip is formed in front of the cutting tool. By the measurement of grids inscribed on the work-piece they were able to deduce the velocity gradients and strain-rates in the deformation zone. It was found that the mean shear strain-rate in that zone is equal to the shear velocity divided by the depth of cut.

2.2.3 Dynamic Crack Propagation

Along with the deformation and flow behaviour of materials, failure is one of the most important aspects of dynamic materials characterization for engineering applications. The dynamic failure process is, in general, strongly influenced by the strain-rate, stress, and loading history. During the past three decades, a number of investigators have addressed the problem of crack propagation in metals under impact loading [2.32,2.33]. The original work of Griffith [2.34] and its engineering formulation by Irwin [2.35] remains the basis for many of the theoretical approaches to the problem. Central to the fracture problem is the concept of fracture toughness K_{Ic} . In this case, the critical applied stress at which a crack of length a may propagate under mode I loading is given by:

$$\sigma = \beta \frac{K_{Ic}}{\sqrt{a}} \quad (2.1)$$

where β is a configuration coefficient which depends upon the crack geometry and applied load. The quantity K_{Ic} is dependent on various factors including specimen thickness, temperature and crack velocity. Problems involving the fracture-toughness and rate-sensitivity concepts have been discussed in a review by Kenny and Campbell

[2.36], where it was pointed out that progress depended on the development of an adequate description of stress and strain distribution within the plastic zone at the crack tip; such a description should incorporate strain-rate sensitivity effects.

Many techniques have been developed for the measurement of dynamic fracture toughness. Most methods employ the split Hopkinson pressure bar in one form or another. The obvious approach is to sandwich a pre-cracked specimen between the input and output bars, as has been investigated by Klepaczko [2.37] and Bassim *et al.* [2.38] with compact tension specimens. Kanninen *et al.* [2.39] have made measurements of the speed of crack propagation in steel-foil specimens, and showed that strain-rates of exceeding 10^4 s^{-1} existed in the plastic zone. Recently, the major issues in dynamic failure models of brittle and ductile materials have been reviewed and discussed by Nemat-Nasser [2.40].

2.3 CLASSIFICATION OF STRAIN RATE REGIMES

The plastic behaviour of materials is generally found to be sensitive to the rate of deformation. Since the deformation behaviour of materials within different strain regimes is governed by different mechanisms, it is convenient to identify certain dynamic loading regimes when considering strain rate as a parameter in mechanical testing. The entire range of strain rate in dynamic testing can be classified as shown in Table 2.2. This classification is similar to that proposed by Lindholm [2.41].

Table 2.2 *Classifications of Strain Rate.*

Strain rate	Creep (10^{-8} - 10^{-5} s^{-1})	Quasi-static (10^{-4} - 10^{-1} s^{-1})	Intermediate (1 - 10^2 s^{-1})	Bar Impact ($> 10^2$ - 10^5 s^{-1})	Plate Impact ($> 10^5 \text{ s}^{-1}$)
Method of Loading	Constant load	Hydraulic or Screw machine	Pneumatic or explosive impact	Mechanical or Gas-gun	Gas-gun or explosive
Dynamic Considerations	Plane Stress				Plane strain
	Inertia forces neglected ----- Isothermal		Inertia forces important ----- Adiabatic		

2.3.1 Creep Rates Regime (10^{-8} to 10^{-4} s^{-1}).

Creep can be viewed phenomenologically as a process in which work hardening and recovery processes occur on the same time scale as the deformation process. Generally creep pertains to strain-rates less than 10^{-4} s^{-1} . Although creep can occur at any temperature, only at temperatures exceeding about 0.4 of the melting point of the material the effect significant [2.42].

2.3.2 Quasi-Static Strain Rate Regime (10^{-4} to 10^{-1} s^{-1})

Strain-rates less than 10^{-1} s^{-1} are generally treated as low strain-rates. Within this range, the conventional screw-driven machines with pen recorders are usually used for testing. The quasi-static stress-strain curve at constant strain-rates is used to describe the material behaviour. As higher strain-rates are encountered, the stress-strain curve may change, and therefore alternative testing techniques have to be employed.

2.3.3 Intermediate Strain Rate Regime (10^{-1} to 10^3 s^{-1})

The intermediate or medium strain-rates regime is the range of strain-rates from 10^{-1} to 10^2 s^{-1} . At these rates, it is necessary to use an energy storage system to supply energy to the specimen during the test. The most versatile test equipment for low and intermediate strain-rates is a system which employs kinetic energy from moving mass (a pendulum, a drop hammer or a rotating flywheel). For adequate measurements of load and deformation at this range of strain-rate, oscilloscope recording is always used.

2.3.4 High Strain Rate (10^3 to 10^5 s^{-1})

Strain rate of 10^3 s^{-1} or higher are treated as the range of high strain-rates. Most investigators assume that during plastic deformation of the specimen, a uniform stress condition exists. The existence of a uniform stress condition depends upon the method of load application and the geometry of the specimen. The deformation of the specimen is achieved by means of impact or impulsive sources. The dimensions of the specimen normal to the plane of the loading are as small as possible. In this regime, inertia, friction, temperatures and wave propagation effects become important in interpretation of experimental data.

2.4 TECHNIQUES FOR HIGH STRAIN RATE TESTING

High strain rate testing began slowly in the early 19th century, as discussed by Rinehart [2.43] in a review of high strain-rate deformation and fabrication. A surge in the study of high strain-rate deformation began during World War II. This activity has been reviewed in references [2.44-2.50]. This section gives a brief review of the state-of-the-art of high strain-rate testing techniques used to characterize dynamic material properties. These techniques are listed in Table 2.3 with the appropriate range of strain-rate. Each technique has its limitations and these restrict the useful range of strain rate testing.

Table 2.3 *Experimental Techniques for High Strain-Rate Testing.*

MODE	APPLICABLE STRAIN RATE, s^{-1}	TESTING TECHNIQUES
Compression	<0.1	Conventional testing machine
	0.1 to 100	Servo-hydraulic machine
	0.1 to 500	Cam plastometer and drop test
	200 to 10^4	Hopkinson pressure bar
	10^4 to 10^5	Direct impact using air gun apparatus
Tension	<0.1	Conventional testing machine
	0.1 to 100	Servo-hydraulic machine
	100 to 10^4	Hopkinson pressure bar in tension
	10^4	Expanding ring
	$>10^5$	Flyer plate
Shear	<0.1	Conventional testing machine
	0.1 to 100	Servo-hydraulic machine
	10 to 10^3	Torsional impact
	100 to 10^4	Hopkinson pressure bar in torsion
	10^3 to 10^4	Double-notch shear and punch
	10^4 to 10^7	Pressure-shear plate impact

2.4.1 Techniques Used for Intermediate Strain Rate Testing (up to $10^2 s^{-1}$)

Cam Plastometer Test: The cam plastometer is a device designed to achieve constant strain-rates in compression. This machine consists of two platens between which a specimen is compressed when one of the plates is driven by a logarithmic shaped cam, and the other remains fixed to the machine frame.

The first published results of experiments using a plastometer with a rotating cam are those of Loizou and Sims [2.51] which were carried out on lead. A modified version of the rotating flywheel cam plastometer was first used by Hockett [2.52]. He made a more detailed study on aluminum, and has obtained true stress-strain curves at elevated temperatures in strain-rates ranging from 0.1 to 240 s⁻¹. Hockett and Zukas [2.53] used the cam plastometer to determine the compressive true stress-strain curves for annealed iron at constant true strain-rates from 10⁻² to 200 s⁻¹, over a range of temperature from 253 to 873 K. A common trend observed in all the data collected from the cam plastometer experiments was that the flow stress and the temperature at a particular value of strain, increases with an increase in strain-rate.

Expanded Ring Test: The expanded ring test provides another method for obtaining high strain-rate properties of materials. Clark and Duwez [2.54] have dynamically expanded thin tubes filled with mercury through axial impulse loading of the mercury. They have achieved strain-rates below 200 s⁻¹. Dynamic deformation of the ring has been achieved using electromagnetic forces by Niordson [2.55] or by detonating explosive charges by Hoggatt and Recht [2.56]. Rajeendran and Fyfe [2.57] used another technique of vaporizing a copper wire at the centre of the ring.

The expanding ring test has received limited use because of the difficulties in performing the test and its requirement for a very precise displacement measurement. The major difficulty in data reduction is the process of double differentiating the displacement measurement in order to calculate the stress. Warnes *et al.* [2.58] conducted a series of tests on copper specimens and compared the results with Hopkinson bar tests at equivalent strain-rates. The data from the ring tests produced higher stresses which were attributed to shock-induced hardening. The amount of this hardening was equivalent to approximately 5% of the pre-strain in uniaxial tension.

Drop Hammer Test: A typical drop hammer compression system usually consists of a drop tower with a massive foundation, a loading tup, and stop blocks. In the test, the loading tup is raised by a motor to a predetermined height and then dropped. The tup transfers the impact load from the cross-head to the specimen through a shaft.

The drop hammer compression test has been used to determine the compressive stress-strain behaviour of material at medium strain-rates of the order of 10^2 s^{-1} and higher. Lengyel and Mohitpour [2.59] used a high-energy-forging press to subject specimens to small increments of deformation at high loading rates through a series of repetitive tests. In this manner, they tended to avoid any rapid temperature build up or any possibility of non-constant strain-rate at large strains and high strain-rates. They achieved strain-rates of up to 10^3 s^{-1} in these incremental tests. Using a single test, however, the stress-strain results fell well below those of the incremental test. They attributed this to the substantial temperature rise at large strains as well as decrease in strain-rate during the test. It is interesting, however, that strain-rate history effects were not considered as a contributing factor.

An advanced application of the drop forging test is described by Holzer and Brown [2.60] in which load cell is used for transient force measurement and a fibre-optics displacement transducer is used for transient strains. Force measurements are obtained with the aid of computer analyzed force-time data

2.4.2 Techniques Used for High Strain Rate Testing (10^3 to 10^5 s^{-1})

Split-Hopkinson Bar: The split Hopkinson bar dynamic testing technique was invented by Kolsky in 1949 [2.61], following the pioneering work of John and Bertram Hopkinson [2.62-2.66] and Davies [2.67]. The apparatus is described by Lindholm [2.68], among others, and a discussion of various modifications and uses of the apparatus can be found in the article by Nicholas [2.69].

In this approach, the dynamic stress-strain relation in uniaxial compression of a material is obtained by sandwiching a small sample between two elastic bars of equal cross-sectional area and elasticity, called the *incident* bar and the *transmission* bar, respectively.

An elastic stress pulse is imparted into the incident bar by a striking bar of a given cross-sectional area and material properties. By ensuring that all the three bars remain elastic, plastic deformation is induced in the (usually) ductile sample. The stress in the sample is obtained by measuring the transmitted pulse, and the strain of the sample is calculated from the pulse reflecting off the sample back into the incident bar, where it is measured by means of a strain gauge attached to each bar. It is assumed that the elastic waves propagate at constant velocity in an un-dispersed manner in the Hopkinson bars, an assumption which is valid for wave-lengths exceeding the bar diameter. The condition which must be met to obtain valid data from a SHPB test is that the stresses at both ends of the specimen are essentially identical at any instant time. This means that a large number of stress waves must be propagating back and forth in the specimen in order to have a valid test. As higher strain-rates are attempted, the amplitude of propagating waves increase and the number of wave reflections decreases eventually violating the basic assumptions. When different values of stress occur at the two ends of the specimen because of wave propagation phenomena, the assumptions of uniform or average stresses and strains are invalid and the test provides invalid data. Furthermore, at higher and higher strain-rates, the assumption of a state of uniaxial stress in the specimen and neglect of radial inertia, and end friction all tend to become invalid. Thus, there are fundamental limitations to the strain-rates which can be achieved with this technique. Strain-rates in compression up to 10^4 s^{-1} can be achieved in carefully performed tests, and strain-rates up to 10^5 s^{-1} have been documented using extremely small specimens (less than 1 mm height) for some materials. At these very high strain-rates, however, conflicting results have been reported leading to questions as to whether all the conditions for the accurate conduct of the test have been met satisfactorily.

A modification of the standard Hopkinson bar test involves the removal of the input bar and impacting the specimen directly with a projectile bar. In this situation, direct measurement of strain must be made on the specimen. Although higher strain-rates can be achieved with this technique, the same fundamental question about the validity of the experiment must be asked as for the SHPB experiment.

The SHPB has also been modified for use in tension, torsion, and shear as discussed in references [2.70-2.77]. A schematic showing the direct and indirect configuration for SHPB is presented in Figure 2.1.

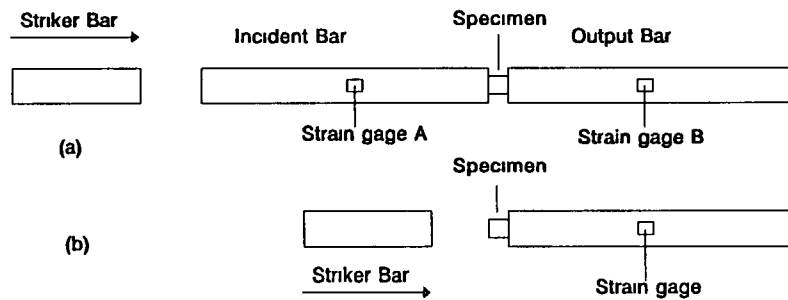


Figure 2.1 Shows the Direct and Indirect Configuration of the SHPB.

Taylor's Momentum Balance Model: Based upon experimental evidence and knowledge of the elasto-plastic wave propagation in a solid rod, Taylor [2.78] developed an analytical model to assess the dynamic yield strength of various materials at high strain rate. Taylor's technique involves impacting a cylindrical rod against a rigid target and taking post-impact measurement of the deformed shape. The change in the rod length can, by one-dimensional rigid-plastic analysis, be related to the dynamic strength as

$$Y = \frac{\rho U^2}{2} \ln\left(\frac{L}{L_0}\right) \quad \text{for } L < L_0 \quad (2.2)$$

where Y is the flow stress, ρ is the density, U is the striking velocity, L is the deformed length, and L_0 is the initial length. This relation was shown to be independent of both the rod aspect ratio and the impact velocity for a wide variety of materials.

Wiffens [2.79] carried out experimental tests on a wide range of metals, including several types of steel, aluminum, copper, and lead, and obtained the values for the dynamic yield stress at strain-rates of about 10^4 s^{-1} .

Hawkyard *et al.* recognized in Ref. [2.80] that Taylor's momentum balance across the rigid-plastic was not an accurate application of the conservation of momentum. They noted that 99% of the initial kinetic energy of the projectile is converted into plastic work. Since practically all the kinetic energy is converted to plastic work, the effective yield stress can be very simply related to the mean strain by equating the kinetic energy to the plastic work of the deformation. Hawkyard [2.81] used energy balance in his analysis to predict the final shape of mushrooming of flat ended projectiles fired onto a rigid anvil. He reported that with the use of energy balance across the plastic wave, a better overall approximation to the actual conditions can be obtained. In addition, Hawkyard extended the analysis to include strain hardening materials.

Hutching and O'Brien [2.82] noted that Taylor and Hawkyard theories were developed for use with metals at high velocities, where the elastic strain in the projectile was small compared with the final plastic strain. But this is not the case for polymers, nor for metallic projectiles at low impact speed. They examined the case of normal impact at low velocities of copper projectiles against a rigid target. They reported that the impact deformation of cylindrical copper projectiles is found to differ significantly from the theoretical predication of Taylor [2.78] and Hawkyard [2.81]. The differences arise because both theories assumed rigid-plastic behaviour, whereas at low velocity, account must be taken for elastic strain in the projectile which will be of comparable magnitude to the plastic strain.

Balendra and Travis [2.83] investigated the double-frustum phenomenon in the mushrooming of cylindrical projectiles when impacted at high speeds (304 m/s) onto a rigid anvil. They reported that the effects of radial inertia and yield behaviour at high strain-rate were responsible for the double-frustum phenomena. Erlich and Chartagnac

[2.84] have reported measurements of the radial deformation in 4340 steel cylinders when impacted in symmetric end-to-end tests. A hypothetical composite stress-strain curve consisting of a linear work hardening portion followed by a perfect-plastic portion was derived to fit the experiments. However, no independent check was made to determine whether the derived stress-strain curve could predict the results of an experiment under different conditions. Gillis and Jones [2.85] have further modified the one-dimensional analysis of the undeformed portion of the Taylor's analysis to include consideration of mass loss at high impact velocities.

Kuscher [2.86] has experimentally proved Taylor's theory using a laser velocity interferometer. The rod was stationary aligned and impacted by anvil projectile of high-strength steel. If Taylor's theory is true, the anvil will produce elasto-plastic waves that will accelerate the rod. The elastic part of the waves which will travel to the rear end of the rod will be reflected again, and so on. The movement of the rear end of the rod is observed with the VISAR interferometer, and the results show that the rear end of the rod has a stepwise acceleration, as postulated by Taylor.

Twenty-five years after Taylor's original work [2.78], the use of two-dimensional wave propagation codes provided better understanding and renewed interest in this technique. In 1972, Wilkins and Guinan [2.87], using a two-dimensional finite difference code and an elastic-plastic model with work hardening, were able to successfully simulate the final shapes and final lengths of Taylor test specimens of several metallic alloys at ambient temperatures. Their results showed good correlation between the dynamic yield strength and the final fractional change in rod length, for a wide range of impact velocities and rod aspect ratios, thus confirming many of the Taylor/Whiffin conclusions.

Johnson and Cook [2.88] used their empirical model to simulate numerically cylinder impact experiments. Johnson and Holmquist [2.89] showed how several of the constants for the Johnson-Cook model [2.88] can be determined from post-test measurements of

Taylor impact tests. Other numerical simulation of Taylor's impact test using different constitutive models can be found in several papers in DYMAT 85 [2 90]. The results showed in general that simulations are more realistic when an accurate constitutive model is used to represent the dynamic behaviour.

2.4.3 Techniques Used for Very High Strain Rate Testing ($> 10^5 \text{ s}^{-1}$)

The Plate Impact Experiment: Plate impact experiments provide the highest strain-rates attainable today in essentially one-dimensional deformation. They show great promise, particularly in efforts to relate macroscopic behaviour to microstructural changes. A full description of the experiment is given in references [2.91,2.92]. The apparatus can be modified to suit different purposes. For instance, by subjecting the specimen to normal impact, and by supplementing the impact test with microscopic observations one can perform investigations into dislocation dynamics. On the other hand, the specimen may be struck obliquely, thus leading to pressure-shear loading. The purpose of the latter test is to determine the stress-strain behaviour at strain-rates beyond the range that can be attained with the SHPB.

The apparatus for oblique impact used by Kim and Clifton [2.93] consists in principle of a thin specimen which is mounted between two hard loading plates. Since the plates are tilted relative to the direction of propagation of the flyer, the impact imposes both a normal and shear traction on the specimen surface. As in the SHPB experiment, the instrumentation can provide measurements of stress and strain in the specimen. Both are determined from the measurements made on the back face of the target plate upon arrival of the stress pulses which were originated at the interface with the specimen.

2.4 4 Measurement Techniques

Many of the standard techniques for measuring stress and strain at low strain-rate become unsuitable for testing at higher strain-rates. The frequency response of a measurement device, such as load cell, strain gage, etc , must be considered Testing in the high strain-rate regime involves unique experimental techniques that were

developed to circumvent difficulties encountered in directly measuring stress-strain in a specimen deforming at high strain-rates. Measurement of stress-strain data becomes more difficult as the strain-rate increases, general comments concerning the topic are discussed as follow:

Stress-strain measurements· In most of the cases of the SHPB, the incident, reflected and transmitted pulses are measured by means of resistance strain gauges mounted on the pressure bars. After amplification, the readings are displayed on an oscilloscope as strain versus time records.

Watson and Ripperger [2 94] extended the measuring technique used by Karnes and Ripperger [2 95], and Chalupnik and Ripperger [2.96]. They measured the load and strain simultaneously in the specimen while the specimen was inside a high temperature environment. During the deformation of the specimen, the average stress over its cross-section was measured by a quartz load cell. The strain in the specimen was measured by a strain gauge attached to the specimen. It was stated by the authors that this technique does not require any assumption of any uniformity of stress, strain and strain-rate over the entire length of the specimen. Strain measurements were also performed by Wulf [2.97] using a co-axial capacitor from which the position of the back face of the projectile could be measured, following deformation of the specimen, and hence the specimen strain could be calculated.

In the compressive tests performed by Lindholm [2.68], the measured reflected pulse was integrated so that the oscilloscope displayed stress verses strain directly rather than strain verses time Some researchers [2.98, 2.99] developed a microcomputer-based SHPB to record the pulses instead of the conventional way. In the conventional way, the pulses were recorded using a triggered oscilloscope from which manual analysis can take several hours for every experiment. The microcomputer-based system reduces the analysis time to a few minutes and has much greater flexibility in signal capture.

Velocity Measurement Techniques: Time interval measurement is an important basic requirements in impact and ballistic tests. The velocity measurement is a specific application of time measurement. The velocity usually is determined by dividing a distance by the measured time interval. A basic instrument comprise of two detectors and a counter-measurement to record the time interval. Velocity measurement systems are necessary to control the impact velocity, measure residual velocities of projectiles, shock wave velocities, particles, and free surface velocities, etc.

A convenient way to make instantaneous velocity measurement is the use of the Doppler Radar Technique. The Doppler principle is based on the fact that the frequency of a harmonic signal will change when it is reflected from a moving object. More details about the Doppler principle are given in reference [2.100].

High Speed Photography: The high speed photography of ballistic and impact events is another important technique in ballistic research. Most ballistic events are very fast, and therefore the exposure time used is short. Since there has been some extensive development in high speed photographic methods, it is not possible to discuss all methods in this chapter; only a limited survey is given.

Proceedings of High Speed Photography and Cinematographic Symposium [2.101-2.104] are an excellent and productive source of information. Speyer [2.105] developed a new high speed video camera system specifically to address the problem of recording projectiles in flight and other associated ballistic events. The system known as SV-553 BR camera, and is capable of capturing fast moving events with exposure times selectable from 1 millisecond to 200 nanoseconds. Haque and Hashmi [2.106] used a high speed camera which has a framing rate of up to 10^6 frames per second, to record the deformation-time history of an impact event. A high speed camera has also been used by Parry *et al.* [2.107] to investigate the high strain-rate properties of polymeric materials. Gorham [2.108] incorporated a high speed camera into a modified version of SHPB system to record the strain distribution along the specimen.

Laser Interferometry: In the past decade laser interferometry has developed into a very precise method for obtaining velocity-time or displacement-time profiles of the motion of impact-loaded specimens, projectile motion in barrels, etc. The most common interferometer is the Velocity Interferometer System for Any Reflection (VISAR). This instrument can measure velocity-time history with excellent accuracy, and time resolution for wide variety of materials and arrangements. The main characteristics of the VISAR are (i) high time resolution, of order of 1 nsec, and (ii) high accuracy, but costs of the VISAR are very high. The data acquisition requires high quality and high frequency transient recorders or oscilloscopes.

The first application of the VISAR was on the measurement of the deceleration process of a penetrating rod projectile into a steel plate [2.109]. The VISAR was used to measure continuously the velocity-time history of the rear side of the penetrating rod. Birch and Jones [2.110] have used the laser Doppler velocimeter system to record the deceleration of the tup mass during impact tests on a drop hammer apparatus.

2.5 FACTORS AFFECTING THE DYNAMIC COMPRESSION TEST

2.5.1 Interfacial Friction

The experimental condition which is likely to cause the most significant deviation from the assumption of uniaxial and uniform stress within the specimen, as well as large quantitative errors in stress measurement, is that of friction at the specimen interfaces. The analysis of Siebel [2.111] assuming a friction coefficient, μ , at the interface gives the pressure to be:

$$\bar{P} = \sigma_y \left[1 + \frac{2\mu a}{3h} \right] \quad (2.3)$$

where \bar{P} is the mean applied pressure, σ_y is the material yield stress, a is the specimen radius, and h is the specimen height. Knowing the value of μ , leads to an estimate of error introduced by frictional restraint for a given specimen aspect ratio.

One of the most thorough analysis of the SHPB technique was presented by Bertholf and Karnes [2.112] using a two-dimensional elastic-plastic finite-difference computer code. They investigated the effects of interfacial friction as well as aspect ratio. They conducted comparisons between the calculated stress-strain response with the experimental data obtained under dry and lubricated conditions. Their results have shown the importance of lubrication in eliminating friction at the specimen interfaces, as the specimen tends to expand radially under axial compression. Klepaczko and Malinowski [2.113] presented the results of a simplified theoretical analysis to estimate the effects of both friction and inertia in the SHBP using an energy approach. They derived the following relationship.

$$\sigma_o = -P_{av} \left[1 - \frac{2\mu a}{h} \right] - \rho \left[\frac{a^2}{8} + \frac{h^2}{12} \right] \varepsilon + \rho \left[\frac{a^2}{16} - \frac{h^2}{12} \right] \varepsilon \quad (2.4)$$

where σ_o is the true axial stress, P_{av} is the average of the forces on either side of the specimen, μ is the coefficient of friction between the specimen and the bar, and a and h are the radius and the length of the specimen, respectively. In the case of no friction, this approximation reduces to that of Davies and Hunter [2.114]. The approximation is in overall qualitative agreement with numerical analysis of Bertholf and Karnes [2.112].

Based on Avitzur's analysis [2.115], Gorham *et al.* [2.116] gave the following expression for the magnitude of the friction correction

$$\bar{p} = \sigma_y \left[1 + \frac{2ma}{3\sqrt{3} h} \right] \quad (2.5)$$

where \bar{P} is the measured mean pressure, and m is the friction parameter. It can be seen that the measured stress depends not only on the friction parameter m but also on the aspect ratio a/h

Male and Cockcraft [2.117] developed a technique for studying the coefficient of friction between rigid tools and plastically deformed metals at elevated temperature. They indicated that at low strain-rate the coefficient of friction increases as the amount of deformation increases. Sheikh *et al* [2 118] studied the effect of impact speed on lubricant in hot forging and reported that the coefficient of friction decreases with increases of impact velocity. Narayanasamy *et al* [2.119] developed a method of predicting the barrelling of solid cylindrical specimen under uniaxial compression load. Hashmi [2.120] presented a numerical technique for the study of upsetting of cylindrical billets between a free falling tup and a stationary anvil with unequal end friction. He reported that no significant variation of the load on either the tup or anvil occurs as long as friction at one interface remains negligible. However, he noted that a significant increase in tup and anvil load occurs when friction at both ends is considerably high. Venugopal *et al.* [2.121] studied the effect of strain-rate and temperature on the friction factor of pure titanium. They reported that as the strain-rate increases, the friction coefficient increase under both dry and lubricant conditions. The reason for this behaviour could be that as the strain-rate increase, the adiabatic heating causes a temperature rise which results in lubricant break-down. Some other investigators [2 122, 2.123] supported the idea of lubricant break-down, although there is growing evidence that maintenance of lubricant is less of a problem at higher strain-rates than it is at low strain-rates. Loss of lubricant can result from its extrusion during compression. The viscous nature of the lubricants introduces time as a variable for this process, and as the strain-rate increases, there is less time available for loss of lubrication [2.124].

The ASTM [2.125] has recommended that, the most favourable L/D ratio for minimizing the errors due friction is:

$$1.5 \geq \frac{L}{D} \leq 2.0 \quad (2.6)$$

where L and D are the specimen height and diameter, respectively.

2.5.2. Inertia Effects

As the rate of deformation increases so the force required to accelerate material also increases. If the magnitude of this force is significant compared with the deformation loads, then the measured total load history is no longer considered an accurate record of the plastic yield stress. Several authors have made estimations of the inertia stress, to various levels of precision and with application to various experimental configurations, including Davies and Hunter [2.114], Haddow [2.126], Sturgess and Jones [2.127], Tirosh and Kobayashi [2.128], and Samanta [2.129]. The first comprehensive treatment of the inertia effect was published by Davies and Hunter [2.114] and further paper by Samanta [2.129], added an extra term to the equation which Davies and Hunter had omitted, apparently by oversight. The principal difference in their derivations is that Davies and Hunter used engineering strain whereas Samanta adopts natural strain in his paper. The latter convention is more appropriate where large strains are encountered. Subsequently Bertholf and Karnes [2.112] claimed that Samanta's analysis included an error and they published an equation which differed from Samanta's in some numerical factors. There is no evidence in their paper or elsewhere to support their conclusion. Dharan and Hauser [2.130] used a SHPB to determine the stress-strain relationship of aluminum at strain-rates up to $1.2 \times 10^2 \text{ s}^{-1}$. They reported that during high impact velocity compression, in addition to the axial particle velocity, the radial and tangential particle velocities may be subjected to high values of compression stresses in three directions.

The above conclusions were in direct conflict with the results obtained by some other investigators who proved that inertia effect could be ignored. Holzer and Brown [2.60] investigated the behaviour of steel in compression at strain-rate up to 10^4 s^{-1} . They reported that there is no significant radial inertia effect, because there is no large separation between the stress-strain curves at high and low strain-rates. Haque and Hashmi [2.106] ignored the effect of radial inertia and reported that the radial inertia and temperature effects will cancel each other. Malatynski and Klepaczko [2.131] conducted a series of experiments on lead under compression up to strain-rates of $2 \times$

10^3 s^{-1} using different aspect ratio specimens, and found that inertia effects are negligible within the range of test conditions used.

In view of this confusion, Gorham [2.132] proposed the use of miniature specimens (< 1 mm dimensions) to eliminate inertia effects. His calculations reveal that an error of less than 0.1% is expected at a strain rate of 10^5 per second.

2.5.3 Adiabatic Shear Phenomena

Mechanism. Adiabatic shear is a deformation mechanism which is unique to high strain-rates of deformation. In metals and alloys, it is well known that at room temperature, about 95% of the work done in plastic flow is converted to heat. Adiabatic shearing is a particular situation in which the heat generated in a localized band cannot be dissipated because of the high strain-rate and the thermal properties of the material [2.133]. In fact, a truly adiabatic deformation does not exist, some part of the heat is being lost to the surrounding, but the term adiabatic is taken here to show that large part of the heat is retained in the band.

When the metals and alloys are deformed at large strains and very high strain-rates such as in ballistic impact and penetration, machining, and high speed forging, localized shearing can occur, leading to localization of heat generation. Generally, the flow stress increases with increasing strain and strain-rate. However, in localized shearing, the increased temperature reduces the flow stress.

There have been a number of attempts to measure the temperature rise associated with shear bands. Costin *et al.* [2.134] measured temperature rises of the order of 100 °C associated with shearing in mild steel. There was some uncertainty because the width of the optical sensor was greater than the shear bandwidth. Hartley *et al.* [2.135] used an infrared radiation detection method to measure temperature rises across shear bands in mild steel. Temperatures of the order of 400 °C were recorded, and there was a variation in temperature across the bands. Woodward *et al.* [2.136] measured the

temperature rise in nickel-based alloys during torsion tests. The temperature rise was in agreement with simple thermo-mechanical calculation. However, adiabatic shear was not observed because of the low strength of the material.

Temperature Rise During Deformation: The mechanical deformation of a material can lead to change in temperature. When the specimen is compressed nearly all the work of plastic deformation is converted into heat. If the deformation takes place slowly ($\dot{\epsilon} < 10^{-2} \text{ s}^{-1}$), then heat generated within the specimen can be lost at the same rate to the surroundings by means of natural cooling, and hence there will be no change in the temperature of the specimen itself. A compression test under these conditions may be considered isothermal. However, if, the deformation takes place at a high strain-rate ($\dot{\epsilon} > 1 \text{ s}^{-1}$), then there will be no time for the heat to escape, and the specimen temperature will rise according to the level of strain. A compression test may be considered adiabatic if the strain-rate is sufficiently high.

The critical strain-rate above which a compression test may be considered adiabatic depends not only on the specimen geometry but also the type of test apparatus and its thermal contact with the specimen. Frost and Ashby [2.137] have derived an expression for critical strain-rate based on a conventional compression test arrangement, in which a cylindrical specimen of radius R is sandwiched between two parallel steel faces. The strain rate ($\dot{\epsilon}_c$) is given by.

$$\dot{\epsilon}_c = \frac{4 \epsilon_c K}{C_p R^2} \quad (2.7)$$

where K is the thermal conductivity of the specimen, C_p is the volume specific heat of the specimen, and ϵ_c is the critical strain above which adiabatic shear may occur.

Dixon and Parry [2.138] studied the effect of temperature rise during deformation in carbon steel type 224. They reported that for strain-rate of less than 10^{-2} s^{-1} , the compression test on this type of steel can be regarded as isothermal. However, when the strain-rate exceeds about 4 s^{-1} the tests have definitely shown to be adiabatic. They

calculated the $\dot{\epsilon}_c$ using equation (2.7), and a close agreement with their experimental observation was found.

As mentioned above, the temperature of the metal rises during plastic deformation because of the heat generated by plastic work, the deformation energy per unit volume, w , is equal to the area under the stress-strain curve:

$$w = \int_0^{\epsilon} \sigma (\epsilon, \dot{\epsilon}, T) d\epsilon \quad (2.8)$$

Only a small fraction of this energy is stored, and the rest is released as heat, as shown by Farren and Taylor [2.139], who observed a discrepancy between the work done and heat generated in plastically deformed steel and aluminium specimens. Later, Taylor and Quinney [2.140] carried out tests on steel, copper and aluminium with the specific aim of establishing this latent energy. They found that the stored or latent heat energy was a constant percentage of the original work done, but varied for different materials. The mechanism by which latent energy is stored in a material is unclear, although it is likely that residual stresses within the deformed material are responsible. The existence of this phenomenon is acknowledged by other researchers, who account for its effect by using a material factor f (where $f < 1$) in their energy balance equation [2.141-2.143].

2.5.4 Specimen Geometry

Many researchers have investigated the effect of specimen size on the stress-strain behaviour of material at different strain-rates. Gunasekera *et al.* [2.144] conducted compression tests under lubricated conditions on steel specimens at low strain-rates of $2.2 \times 10^{-3} \text{ s}^{-1}$. They reported that larger aspect ratio (height/diameter) test specimens are desirable and kept their aspect ratio at 1.5 to avoid buckling and barrelling. Hauser [2.145] conducted compression and tensile tests using SHPB at strain-rates of up to 10^4 s^{-1} . He reported that if the test specimen is small enough, the transit time for the elastic wave will also be short, so equilibrium throughout the specimen is rapidly established

and plastic deformation takes place uniformly within the specimen. Holzer and Brown [2.60] reported that the measured flow stress value is influenced by specimen geometry, with stress increasing as the aspect ratio decreases. Although radial inertia effects might be suspected, these observations were made at both high and low strain-rates. The effect of friction, as discussed previously, would appear to be the contributing factor in the interpretation of these experimental results.

With the exception of the work by Stelly and Dormeval [2.146], all specimens were cylindrical. Various aspect ratios have been selected and used. These ratios can be grouped approximately as detailed in Table 2.4.

Table 2.4 Shows Various Aspect Ratios Favoured by Some Authors.

ASPECT RATIO	REFERENCES	COMMENTS
> 0.5	Lindholm [2.68], Samanta [2.147], Glenn and Bradly [2.148], Edington [2.149], and Bhushan and Jahsmann [2.150]	To minimise inertia effect and to maintain a constant stress level
0.5-2.0	Hawkyard <i>et al</i> [2.80], Kumar and Kumble [2.151], Wulf [2.97], Lindholm [2.152], Shiori <i>et al</i> [2.153], Haque and Hashmi [2.106], and Follansbee <i>et al</i> [2.154]	In this group a compromise between the previous group and an attempt to minimise the effect of friction
> 2.0	Watson and Ripperger [2.94] and Kishida and Senda [2.155]	

2.5.5 Microstructural Changes

The change in the microstructure of materials has been investigated by many researchers. Their investigations have considered the effects of grain size and orientation on deformation at low and high strain-rates. Review articles on the effect of high strain-rate on the microstructure of the material were published by Campbell [2.49] and Leslie [2.156], and also cited in the book edited by Argon [2.157]. Haque *et al*. [2.158] investigated the microstructure of high purity copper specimens deformed at strain-rate ranging from 10^{-4} to 10^4 s⁻¹. They reported that deformation twins were observed and this twinning increased with increasing strain-rate. Meguid [2.159]

conducted macro and microstructural analyses of aluminium and mild steel plates which were subjected to shock loading. His results reveal the hardening of the highly deformed regions and the twinning of the steel specimens. Rohde [2.160] observed twinning in shock loaded commercially pure iron ($3 \times 10^4 - 10^5 \text{ s}^{-1}$), but did not observe it at lower stresses over the temperature range -197 to $300 \text{ }^\circ\text{C}$. Hockett and Zukas [2.53] observed twinning in annealed iron which was compressed at strain-rate of $1.2 \times 10^2 \text{ s}^{-1}$ at $140 \text{ }^\circ\text{C}$. They also mentioned that twinning occurred in the early stages of deformation and was completed at a true strain of 0.1. It has also been reported elsewhere [2.161, 2.162] that mechanical twinning can be generated in copper by shock loading. Very recently, conflicting results were obtained by Haque and Hashmi [2.163] who carried out a study on the microstructural behaviour of medium carbon steel (EN-8) deformed at low strain rate (quasi-static) and very high strain rate (up to 10^5 s^{-1}) employing different temperatures. They reported that there is no marked difference observed in the microstructure of the steel deformed either statically or dynamically at different temperatures.

1.6 EFFECT OF STRAIN-RATE ON FLOW STRESS

1.6.1 Metallic Materials

There is clear experimental evidence that most metals and alloys exhibit some increase in yield stress with increasing strain-rate. As mentioned earlier, the oldest experiments in dynamic plasticity seem to be those of Hopkinson, J [2.62] and Hopkinson, B [2.66]. They observed that the dynamic yield stress is approximately twice as high as the static yield stress. Brown and Vincent [2.164] reached a similar conclusion for mild steel. Duwez and Clark [2.165] reached a comparable conclusion by showing that under certain conditions the dynamic yield stress of annealed mild steel can be double or triple the static yield stress. The experiments conducted by Kolsky [2.61] using copper and lead showed that the dynamic elastic modulus does not differ significantly from the static one, but that the whole dynamic stress-strain curve is higher than the static one. A technique similar to that used by Kolsky was used by Davies and Hunter [2.114] who tested annealed copper, aluminium, zinc, magnesium and α -brass specimens. In all

cases, a rate effect which raised the stress level for any given strain by a factor varying from 1.0 to 3.0 was confirmed. Lindholm [2.68] used the SHPB in order to establish the dynamic properties of lead, aluminium and copper; results which are similar to those mentioned above were obtained, i.e. an increase in strain-rate increased the dynamic yield stress for all the three metals. The difference between the dynamic and static properties of various metals was also studied [2.166, 2.167], and in general the results showed that for various steels, the dynamic yield stresses are higher than the static ones, and that of all the mechanical parameters of a metal, yield stress is the most sensitive to strain-rate. Campbell [2.168] performed dynamic tests on aluminium alloy specimens. He found that the dynamic stress-strain curve is higher than the static stress-strain curve by 15-20 %. The dynamic properties of mild steel have been studied by Campbell and Duby [2.169]. They showed that the dynamic yield stress can be 2.5 times bigger than the static one.

The results of Edington [2.149] on tested copper at strain-rates up to $9 \times 10^3 \text{ s}^{-1}$ showed that although copper is insensitive to strain-rate below 10^3 s^{-1} , it is extremely sensitive to strain rate above this figure. He used long specimens, and thus concluded that previously reported high strain-rate behaviour is real and not just associated with short specimens. He deduced that at high strain-rate, the stress is a linear function of strain-rate. Dowling *et al.* [2.170] carried out tests at strain-rate up to 10^4 s^{-1} and strain up to 25%. They found that copper is very strain-rate sensitive. They also found that there was a rapid increase in flow stress above strain-rate 10^3 s^{-1} and at strain-rate below 10^3 s^{-1} there was a linear relation between yield stress and strain-rate.

From the foregoing discussions it can be concluded that, at very low strain-rates, below quasi-static, we can generally find a region of little or no strain-rate sensitivity. At higher strain-rates for most metals, the flow stress increases in a linear manner with the logarithm of the strain-rate. At very high strain-rate, the degree of sensitivity increases dramatically when the strain-rate approaches a critical value ($\dot{\epsilon}_A$). One of the explanations for this behaviour is based on the change in the rate-controlling

deformation mechanism from thermally activated to a linear viscous model. Lindholm [2.152], however, has questioned the validity of some of the experimental results upon which these conclusions have been drawn. Hereli [2.171] has raised additional questions by providing data under uniaxial strain conditions which show that there is no apparent increase in the equivalent yield stress up to equivalent strain-rate more than 10^5 s^{-1} . These results are, however, in direct conflict with the findings of Rajendran and Bless [2.172].

Follansbee and Kocks [2.173] have challenged the proposed change in rate-controlling mechanism in copper and proposed an explanation of the sudden increase in strain-rate sensitivity above 10^3 s^{-1} . They reported that in the case of copper and other metals, the accurate interpretation for this phenomena is the change of the micro-structure with strain rate. Microstructural observation supports this view by showing that the occurrence of twinning is much more common in specimens deformed at a rate above $\dot{\epsilon}_A$. However, a large variation in the value of $\dot{\epsilon}_A$ has been reported, ranging from $\sim 4 \times 10^2 \text{ s}^{-1}$ [2.151] to $\sim 2.5 \times 10^4 \text{ s}^{-1}$ [2.174]. The significance of the large variation in $\dot{\epsilon}_A$ appears to be related to specimen dimensions. In general, the larger specimens are associated with low values for $\dot{\epsilon}_A$, whilst the smaller specimens with much higher values. Gorham [2.174] showed that if $\dot{\epsilon}_A$ is an inherent materials property, no size dependency would be expected during uniform deformation. However, in practice a number of mechanisms, such as friction, inertia, and stress wave propagation lead to deviation from ideal homogeneity and offer the possibility of size dependence.

Chiddester and Malvern [2.175] investigated aluminum during compression impact tests at elevated temperatures of up to $550 \text{ }^\circ\text{C}$. They used SHPB to obtain the stress-strain-rate relationship over strain-rate ranging from 3×10^2 to $2 \times 10^3 \text{ s}^{-1}$. They reported that the strain-rate sensitivity for aluminum was found to increase with temperature. Similarly, Dean and Sturgess [2.176] investigated the behaviour of steel using compression tests at strain-rates of up to $2.5 \times 10^3 \text{ s}^{-1}$ and elevated temperatures ranging from 600 to $1200 \text{ }^\circ\text{C}$. They reported that the strain-rate sensitivity increases with

increasing test temperature and the flow stress increases either with the reduction in temperature or the increase in the strain-rate.

2.6 2 Composite Materials

Dynamic behaviour of composite materials has received very little attention. Wittman *et al.* [2.177] conducted a compression test on tungsten-nickel based matrix alloy at strain-rate up to $6 \times 10^3 \text{ s}^{-1}$ and temperature ranging from room temperature to $850 \text{ }^\circ\text{C}$. They compared the material properties of this MMC with those of pure tungsten and reported that the dominant material property for the MMC (Metal-matrix composite) and pure tungsten is the material's tendency for self heating, which results in a significant loss of the strength in the pure tungsten, but less so in the MMC. Marchand *et al.* [2.178] conducted a series of experiments at room temperature to determine the dynamic fracture initiation behaviour and dynamic stress-strain behaviour of a metal-matrix composite (2124-T6 aluminum reinforced with silicon carbide whiskers). They reported that fracture toughness in the reinforced material increases with the loading rate, but that the stress-strain behaviour does not change with the deformation rate in the range (10^{-4} - 10^3 s^{-1}). The stress-strain curves show only a small strain-rate sensitivity either for the reinforced or for the un-reinforced materials. Harding [2.179] critically assessed various techniques for determining the mechanical behaviour of fibre-reinforced composite materials at impact rates of strain.

Vaziri *et al.* [2.180] conducted experiments consisting of dynamic penetration of various reinforced and un-reinforced materials by cylindrical tungsten projectiles, fired at velocities ranging from 450 to 850 ms^{-1} . They found the MMCs superior to un-reinforced matrix materials in resisting penetration. The highly reinforced material exhibited brittle characterisation similar to ceramics. At high impact speed (750 ms^{-1}), all MMCs, behaved much like un-reinforced metals. In an attempt to simulate the impact behaviour of MMC's they implemented two strain-rate dependent deformation models; namely, Johnson-Cook model [2.88] and Zerilli-Armstrong model [2.181] into the DYNA2D code. A comprehensive review of high strain-rate experimental

techniques which have been applied to composite materials and a summary of experimental results are presented by Sierakowski [2.182].

2.6.3 Polymeric Materials

Polymers are increasingly being used in applications where they are liable to be rapidly deformed. Examples of such uses include aircraft components exposed to particle impact, crash helmets, shock absorbers, and various military applications. However, in contrast to metallic materials, little is known about their impact response. Lataillade *et al.* [2.183], listed only 17 papers during the past 25 years, whereas in contrast, a literature survey done by the author, listed over 100 papers on the topic of high speed deformation testing of metals during the same period.

The characteristics of some high polymers (Nylon, neoprene, etc.) have been studied by Hillier and Kolsky [2.184]. They determined the dynamic elastic modulus for the respective materials. Kolsky [2.61] used a modified SHPB to determine the dynamic stress-strain curves for rubber, polythene and perspex. He reported that for all the material tested, the dynamic elastic modulus is very much higher than the static elastic modulus, and that the whole dynamic stress-strain curve differs from the static one. An important *delayed recovery* phenomenon was found in the case of these materials; the strain continued to increase rapidly after the stress has passed its maximum value. Similar results for polythene were obtained by Taylor [2.185].

Bauwens-crowet *et al.* [2.186-2.188] have shown that the yield stress of polycarbonate, measured in isothermal tension tests, increases linearly with the logarithm of the strain-rate and fits to Eyring-type equation [2.189]. Later [2.190], they extended their study to strain-rates unattainable in tension tests. Using tensile creep and impact tests, it was possible for them to measure the yield stress related to strain-rates varying from 10^{-8} to 10^2 s^{-1} . Hutchings [2.191] has developed a one-dimensional elastic-plastic stress wave analysis to estimate the yield stress of materials with large yield strain. The theory has been successfully applied to experimental data for polycarbonate projectiles. He

reported that the technique is valid only for high ductility materials like polycarbonate which neither fracture under impact loading conditions nor show long-term relaxation after deformation. Recently, Walley *et al.* [2.192] have carried out an experimental investigation into the effect of strain-rate on the compressive yield stress for a wide range of polymers. They reported that all the tested polymers showed higher yield stress in the strain-rate regime 10^3 - 10^4 s⁻¹, but most exhibited a softening of behaviour within this region of strain-rates. They used a high speed camera to study failure mechanisms and associated heat evolution

CHAPTER THREE: **FORMULATION AND IMPLEMENTATION OF A NOVEL RATE-DEPENDENT CONSTITUTIVE LAW**

3.1 **INTRODUCTION**

This chapter is divided into two main sections. The first deals with the formulation of a novel constitutive law for treating strain rate dependent material, while the second deals with the use of the constitutive law in a finite-difference model of a dynamic uniaxial compression test. The finite-difference algorithms account for inertia, strain rate, strain hardening, and thermal softening. The convergence and accuracy of the developed model are examined and assessed in relation to commercially available finite-element software. Study of the energy dissipation during impact is presented.

3.2 **REVIEW OF EXISTING CONSTITUTIVE LAWS**

A *constitutive law* represents a mathematical model that describes the behaviour of a material under mechanical, thermal and shock loads. Constitutive equations can also be viewed as the vehicle by which knowledge of material behaviour enters engineering design. In this review attention is focussed on rate dependent constitutive laws only.

One of the simplest forms of describing the material behaviour under high strain rate is the semi-logarithmic equation developed by Ludwick [3.1]:

$$\sigma = \sigma_0 + \sigma_1 \ln \frac{\dot{\epsilon}}{\dot{\epsilon}_0} \quad (3.1)$$

where σ_0 , σ_1 and $\dot{\epsilon}_0$ are material constants. Constant strain rate tests were used to provide stress-strain curves for a given strain rate and temperature to determine these constants.

Earlier "overstress" models of viscoplastic laws such as those of Perzyna [3.2,3 3], and uniaxial forms like

$$\dot{\varepsilon} = g (\sigma - f(\varepsilon)) \quad (3.2)$$

used by Sokolovskii [3.4], Malvern [3.5], Malvern and Meguid [3.6] and Krempl [3.7] imply that the plastic strain rate is a function of the excess of the current stress above some equilibrium stress $f(\varepsilon)$ for the current strain ε . More modern overstress theories might adjust $f(\varepsilon)$ in equation (3.2) to account for the effects of temperature, strain hardening and strain softening.

Cowper and Symonds [3.8], employed the concept of a reference stress to develop the following dynamic equation of state:

$$\frac{\sigma}{\sigma_0} = 1 + \left[\frac{\dot{\varepsilon}^p}{D} \right]^{\frac{1}{q}} \quad (3.3)$$

where q and D are material constants, σ_0 and σ are the static and dynamic yield stresses, respectively, and $\dot{\varepsilon}^p$ is the plastic strain rate. One of the limitations of Cowper-Symonds equation is that it does not account for temperature and strain hardening effects. Tang and Kobayashi [3.9] extended the Cowper-Symonds model, whereby the constants σ_0 , q and D were taken to be both strain- and temperature-dependent.

Perzyna [3.10] suggested the following generalization of the Cowper-Symonds flow stress model to multiaxial stress situations

$$\frac{\bar{\sigma}}{\sigma_0} = 1 + \left[\frac{\sqrt{1/2 \dot{\varepsilon}_y^p \dot{\varepsilon}_y^p}}{D} \right]^{1/q} \quad (3.4)$$

where $\bar{\sigma}$ is the rate-dependent von Mises equivalent stress. The Cowper-Symonds model has been used extensively in structural dynamics applications involving blast loading [3.10-3.15]. The original Cowper-Symonds constitutive equation for rigid-perfectly plastic materials was modified by Jones [3.16] to cater for practical situations involving large plastic strains, such as structural crashworthiness problems. Lindholm [3.17] proposed that the flow stress may be related to the strain and strain rate by an equation of the form

$$\sigma = \sigma_o(\varepsilon) + \sigma_1(\varepsilon) \log\left(\frac{\varepsilon}{\varepsilon_o}\right) \quad (3.5)$$

where $\sigma_o(\varepsilon)$ is the uniaxial stress-strain at strain rate equal to unity and ε_o is a reference strain rate. The coefficient $\sigma_1(\varepsilon)$ of the logarithmic term is also an increasing function of strain. He obtained data for three different materials; namely, lead, copper, and aluminum, over the range of strain rates 10^4 to 10^3 s⁻¹. A particular form of the Lindholm model incorporated into the hydrodynamic code HEMP [3 18-3.19] is

$$\sigma = [A + B(\varepsilon^p)^n] + [C + D\varepsilon^p] \log\varepsilon^p \quad (3.6)$$

Recently, Johnson and Cook [3.20] proposed the following five-parameter empirical flow stress model:

$$\sigma = (A + B\varepsilon^n) (1 + C \ln\varepsilon^*) (1 - T^{*m}) \quad (3.7)$$

where ε is the equivalent plastic strain, and $\varepsilon^* = \varepsilon / \varepsilon_o$ is the dimensionless plastic strain rate. He took $\varepsilon_o = 1.0$ s⁻¹ as his reference strain rate, and $T^* = (T - T_{\text{room}}) / (T_{\text{melt}} - T_{\text{room}})$ is the homologous temperature for $0 \leq T^* \leq 1.0$. The five material constants are A, B, n, C, and m.

An alternative form of the Johnson-Cook model which takes into account the effect of hydrostatic pressure by an additive superposition of pressure (p) is given as

$$\sigma = (A + B\varepsilon^n) (1 + C \ln\varepsilon^*) (1 - T^{*m}) + D p \quad (3.8)$$

where D is another material constant. Equations (3.7) and (3.8) have been implemented in the EPIC codes developed by Johnson [3.21-3.22] and DYNA codes [3.23].

The Johnson-Cook model has been demonstrated to provide realistic numerical prediction of a very broad class of applications involving extreme dynamic events, such as impact, penetration, and explosive loading of ductile metals. Some lack of correlation with experimental results has been reported for cases involving low strain [3 24]. Furthermore, the thermal softening model appears to be inadequate for the simulation

of problems involving large strains. The primary disadvantage of this model, like its predecessors, is that it does not include the effect of strain rate on work hardening

3.3 FORMULATION OF A NEW CONSTITUTIVE LAW

In all the equations listed above, the temperature and strain rate influence on strain hardening were not included. Experimental observations by many researchers [3.25-3.28] show that strain hardening decreases with an increase in the strain rate, and that the initial flow stress increases with increasing strain rate. A constitutive equation which describes this behaviour and include the temperature effect is proposed by the current author; as follows:

$$\sigma_d = KG_1(T) \varepsilon^{n - \alpha(\dot{\varepsilon}, T)} [1 + (m\varepsilon)^p] \quad (3.9)$$

where

$$\alpha = \left[\frac{G}{R} \right]$$

where K is the strength coefficient (stress at strain equal to unity), G_1 is the thermal softening factor affecting the strength coefficient, G is the temperature softening parameter affecting strain hardening index, R is the strain rate parameter affecting strain hardening index, ε is the total true strain, n is the strain hardening index, α is a parameter combining strain rate and temperature effects on the strain hardening index, $\dot{\varepsilon}$ is the total true strain rate, and m and p are the material's strain rate sensitivity constants

The proposed constitutive law starts with Ludwick rate-independent flow stress law as a base ($K \varepsilon^n$). This is because all the materials tested experimentally in this study under quasi-static strain rate obey this law. This equation is then modified to cater for the effect of strain rate on flow stress using $[1 + (m\varepsilon)^p]$ which is similar to the one used by Cowper and Symond [3.8] and Malvern [3.5]. At high strain rates and large deformations, a considerable amount of temperature rise is generated. Since this rise

in temperature is known to have an effect on the material's properties, therefore, it is essential to incorporate this effect via $(K(T) \dot{\epsilon}^{n(T)})$ using factors G and G_1 (see section 3.3.1). As has been mentioned before many experimental results have revealed that the strain hardening is not constant versus strain rate, this effect has been accounted for in the proposed constitutive law using factor R (see section 3.3.2).

It should be mentioned that this equation is selected because of its simplicity and adaptability to a wide range of strains, strain rates and temperatures. For finite difference and finite element computations of plastic flow at high strain rates, a simpler constitutive equation is highly desirable for computational efficiency.

3.3.1 Effect of Thermal Softening on Strain Hardening

Most of the energy consumed during the plastic deformation is converted into heat and only a small proportion goes towards distorting the crystal structure. When a tool steel projectile is impacted against the test specimen, plastic deformation is completed within a very short period of time. In this work, the stress is considered as a function of strain, strain rate and temperature, when the strain increases from ϵ to $\epsilon + \Delta\epsilon$, the temperature rise (ΔT) during deformation is estimated by considering the plastic work done using equation (3.10) as:

$$\Delta T = \frac{f}{\rho s} \int_{\epsilon}^{\epsilon + \Delta\epsilon} \sigma(\epsilon, \dot{\epsilon}, T) d\epsilon = \frac{f \bar{\sigma} \Delta\epsilon}{\rho s} \quad (3.10)$$

where $\bar{\sigma}$ is the average value of σ over the strain interval from ϵ to $\epsilon + \Delta\epsilon$, f is a material constant and ρ is the density. The specific heat, s , is assumed to be independent of the stress level and the material is treated as incompressible. Details of the thermodynamics of inelasticity which lead to equation (3.10) have been given in reference [3.2].

Since this rise in temperature is known to have an effect on the material properties (strain hardening and flow stress decreases) and the final shape of the stress-strain

curve, it was therefore thought essential to find a general form of a temperature dependent equation over the range 20 - 400°C. The temperature dependency factors were established as a power law, based on the experimental results from the literature [3.29-3 31], as

$$G (T) = \left[\frac{T_o}{T} \right]^{\Theta} \quad (3.11)$$

$$G_1 (T) = \left[\frac{T_o}{T} \right]^{\Theta_1} \quad (3.12)$$

The magnitudes of Θ and Θ_1 were determined using the curve fitting process. The above factors are incorporated in the proposed constitutive equation to allow for the effect of thermal softening on the magnitude of the stress and the strain. Since the terms G_1 and G are based on experimental data, it could be expected that they would provide accurate results.

3 3 2 Effect of Strain Rate on Strain Hardening

Although most of the strain hardening data available in the literature relate to static conditions, it is likely that these would be applicable to high strain rate conditions with some changes. In order to develop a comprehensive constitutive equation, a general factor is established for the effect of strain rate on strain hardening using limited data from reference [3 32]. Thus

$$R (\dot{\epsilon}) = \left[\ln \left[\frac{\dot{\epsilon}}{\dot{\epsilon}_o} \right] + 1 \right]^{\beta} \quad (3.13)$$

where $\dot{\epsilon}_o$ is the reference strain rate constant [10^{-2} s^{-1}] and $\dot{\epsilon}$ is the true strain rate. The value of β is obtained as 0.28 by the curve fitting process.

3 4 THEORETICAL FORMULATIONS: FINITE-DIFFERENCE MODEL

In this study a finite-difference numerical technique, in conjunction with a lumped mass model, has been developed to analyze the impact event. The mathematical model of the entire system was represented by a lumped mass system, as shown in Figure 3.1. The main feature of this system is that the projectile and anvil deform only elastically due to their high yield stresses and the specimen deforms both elastically and plastically. Several important assumptions were made in this technique; as follows:

- (i) The geometry of the actual system may be represented by a lumped mass model, as shown in Figure 3.1. The mass of each small element of the specimen, projectile, and anvil is represented by a concentrated disc mass connected to other masses by light massless links which transmitted the axial force and strain.
- (ii) The change of density of the system during deformation is negligible.
- (iii) The deformation is homogenous and shearing does not take place between the different layers of the system.
- (iv) Uniform strain occurs in each individual link.
- (v) There is a uniform stress distribution over the cross-section of the specimen interfaces

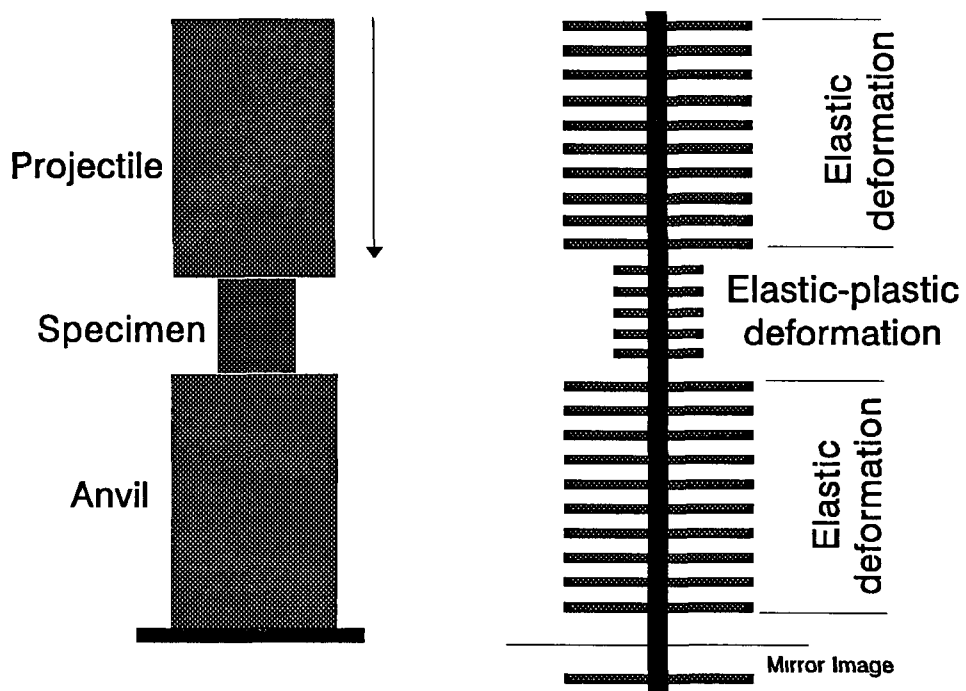


Figure 3.1 A Schematic of the System and its Equivalent Lumped Mass Model.

3.4.1 Equation of Motion

Figure 3.2a illustrates the forces acting upon a deformed element of length dX .

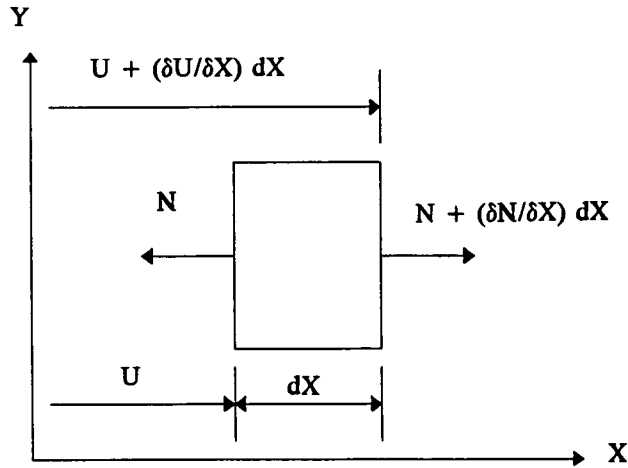


Figure 3.2a *An Element of the System and Forces Acting on it.*

The general equation of motion of an element of the system, soon after impact, can be derived by considering the internal and inertia forces acting on the element, such that

$$\frac{\partial N}{\partial X} - m\ddot{U} = 0 \quad (3.14)$$

where m is the mass per unit length, $(\)$ denotes partial double differentiation with respect to time, and all other quantities are defined in Figure 3.2a .

Equation (3.14) will be re-written in finite-difference form. To do this it is convenient to consider the system to be divided along its length into segments (elements) of initial length ΔS_0 . Let stations along the system be designated as $\dots S_{i-1}, S_i, S_{i+1}$, etc., where the element between stations S_{i-1} and S_{i+1} is termed as *ith* element and has a length ΔS_i . The mass of element i is $m_i = m\Delta S_i$ which remains constant even if the length of the segment changes during the response due to straining along the axis of the system. The finite difference equation for the element at the *ith* location of the model in Figure 3.2b is given by

$$N_{i+1,j} - N_{i,j} - m_i U_{i,j} = 0 \tag{3.15}$$

The finite-difference equation (3.15), which approximates equation (3.14), may be solved numerically for each element at successive instants of time t_j .

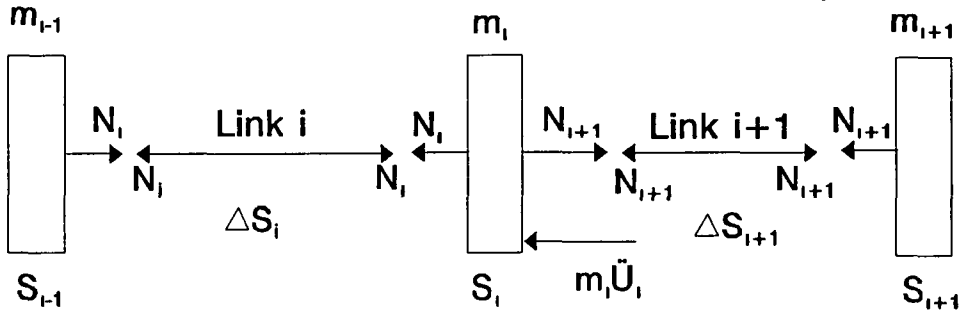


Figure 3.2b *Equivalent Finite-Difference Model.*

Since one may write in general,

$$X_j = \left[\frac{\frac{(X_{j+1} - X_j)}{\Delta t} - \frac{(X_i - X_{j-1})}{\Delta t}}{\Delta t} \right] \tag{3.16}$$

$$= \frac{X_{j+1} - 2X_j + X_{j-1}}{(\Delta t)^2}$$

Using finite-difference notation, the relation between displacement and time takes the form

$$U_j = \left[\frac{\frac{(U_{j+1} - U_j)}{\Delta t} - \frac{(U_j - U_{j-1})}{\Delta t}}{\Delta t} \right] \tag{3.17}$$

The displacement of the element at the i th location (U_i) at time $t_{j+1} = t_j + \Delta t$ may be written as.

$$U_{i,j+1} = U_{i,j} (\Delta t)^2 + 2U_{i,j} - U_{i,j-1} \tag{3.18}$$

The time increment is defined through:

$$\Delta t = t_{j+1} - t_j \quad (3.19)$$

When equation (3.15) and equation (3.18) are combined, instantaneous value of $U_{i,j+1}$ for any instant time t_{j+1} can be determined. Having $U_{i,j+1}$ for all elements, one then can determine the strain and force increments along the axis of each link.

3.4.2 The Displacement-Strain Relations

The increment of link $\delta(\Delta S)_{i,j}$ at time t_j is related to the increment of $\delta U_{i-1,j}$ and $\delta U_{i,j}$ by

$$\delta(\Delta S)_{i,j} = \delta U_{i,j} - \delta U_{i-1,j} \quad (3.20)$$

The link length at time t_j is simply:

$$\Delta S_{i,j} = \Delta S_{i,j-1} + \delta(\Delta S)_{i,j} \quad (3.21)$$

then the strain increment, strain, and strain rate occurring in the i th link during the time interval are given, respectively, by

$$\delta \varepsilon_{i,j} = \frac{\delta(\Delta S)_{i,j}}{\Delta S_{i,j}} \quad , \quad (3.22)$$

$$(3.23)$$

$$\varepsilon_{i,j+1} = \varepsilon_{i,j} + \delta \varepsilon_{i,j+1} \quad ,$$

and

$$\dot{\varepsilon}_{i,j} = \frac{\delta \varepsilon_{i,j}}{\Delta t} \quad (3.24)$$

3.4.3 Idealised Cross Section Area Model

In order to facilitate the calculation of stress which, due to friction and inertia effects may vary across the cross-section of the specimen, it is necessary to idealise the actual cross-section to an equivalent cross-section model which consists of a number of layers at which the stress is assumed to be uniform. Accordingly, the circular cross-section of the system is assumed to consist of n layers of material of circular cross-section area which can carry normal stresses (see Figure 3.3).

These layers are considered to be separated by a material which cannot carry any

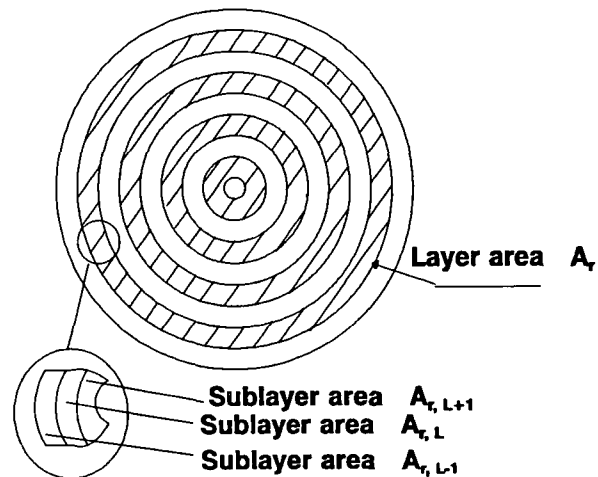


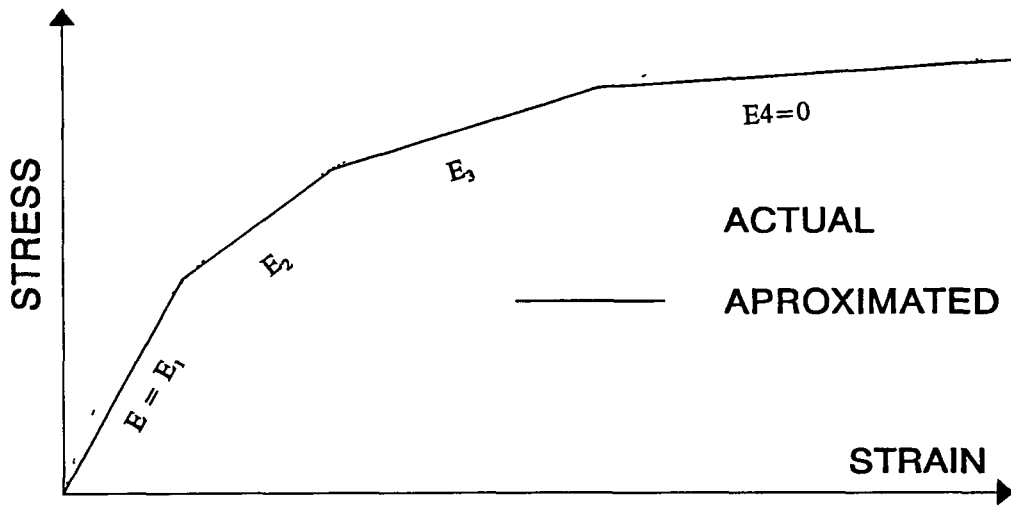
Figure 3.3 *Cross-Section Model of the System.*

normal stress, but has an infinite shear rigidity. With this simplified model the stress in the system can be defined by individual normal stresses at the n -layers without having to contravene the assumption that plane sections remain plane throughout the deformation process.

3.4 4 Stress Calculations

In order to describe the elastic-plastic stress state in the layers of the sectional model, a further idealization is made and each layer is assumed to consist of a number of sub-layers; the number of which is determined by the number of positive slopes in the approximated polygonal stress-strain curve. For example, the material whose stress-strain curves are elastic or elastic, perfectly-plastic will have one sub-layer to each layer. The polygonal stress-strain diagram for an elastic linear-strain-hardening material consists of two positive slopes and hence two sub-layers are required, whereas three sub-layers are needed to describe the stress-strain diagram shown in Figure 3.4a.

The relation between the sub-layer area and its parent layer area is established as follows:



- A -

Figure 3.4a *Approximated Polygonal Stress-Strain Curve.*

Referring to Figure 3.4b and assuming that the deformation has reached stage B, i.e. sub-layer area $A_{r,L-1}$ is loaded elastically to the condition $\sigma_1-\epsilon_1$ and the remaining sub-layer areas are loaded to the condition $\sigma_2-\epsilon_2$.

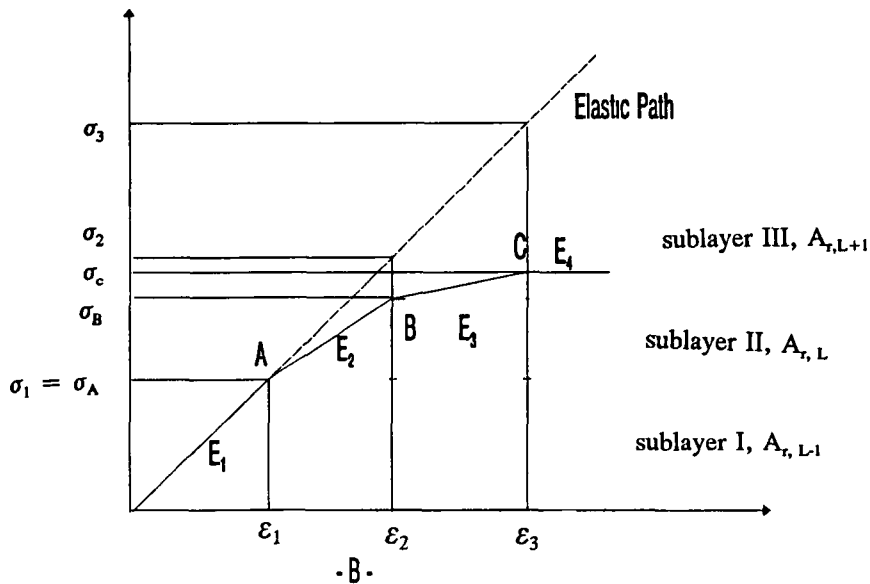


Figure 3.4b *Stress-Strain Curve Used in the Theoretical Analysis.*

It should be mentioned that the stress calculation process is strain driven. The stress σ_B is a hypothetical stress that the sub-layer area $A_{r,L}$ would have to be subjected to if it

were stressed elastically to a strain value of ε_2 . The stress σ_c is similarly related to ε_3 for the sub-layer area $A_{r,L+1}$.

So by equating forces and noting that: $A_r = A_{r,L-1} + A_{r,L} + A_{r,L+1}$

$$\sigma_2 A_r = A_{r,L-1} \sigma_1 + A_{r,L} \sigma_B + A_{r,L+1} \sigma_B \quad (3.25)$$

$$= A_{r,L-1} \sigma_1 + \sigma_B (A_{r,L} + A_{r,L+1})$$

$$= A_{r,L-1} \sigma_1 + \sigma_B (A_r - A_{r,L-1})$$

$$= A_{r,L-1} \sigma_1 + \sigma_B A_r - \sigma_B A_{r,L-1}$$

$$A_r (\sigma_2 - \sigma_B) = A_{r,L-1} (\sigma_1 - \sigma_B)$$

$$A_{r,L-1} = \frac{A_r (\sigma_2 - \sigma_B)}{(\sigma_1 - \sigma_B)}$$

$$= \frac{A_r (\sigma_B - \sigma_2)}{(\sigma_B - \sigma_1)}$$

If the slope of OA = $E_1 = \frac{\sigma_1}{\varepsilon_1} = E = \text{Young's Modulus}$

and;

$$\text{the slope of AB} = E_2 = \left(\frac{\sigma_2 - \sigma_1}{\varepsilon_2 - \varepsilon_1} \right)$$

and,

$$\text{the slope of BC} = E_3 = \left(\frac{\sigma_3 - \sigma_2}{\varepsilon_3 - \varepsilon_2} \right)$$

then;

$$A_{r,L-1} = A_r \left[\frac{(\varepsilon_2 - \varepsilon_1) (E - E_2)}{E (\varepsilon_2 - \varepsilon_1)} \right]$$

Assuming that the deformation has reached stage C.

$$= \frac{A_r}{E} [E - E_2] \quad (3.26)$$

Equating forces

$$\sigma_3 A_r = A_{r,L-1} \sigma_1 + A_{r,L} \sigma_B + A_{r,L+1} \sigma_C \quad (3.27)$$

Combining equation 3.25 and 3.27, and by using the same procedure, the sub-layer area $A_{r,L+1}$ will become:

$$A_{r,L+1} = \frac{A_r E_3}{E} \quad (3.28)$$

To find $A_{r,L}$:

$$\begin{aligned} A_{r,L} &= A_r - \frac{A_r}{E} [E_1 - E_2] - \frac{A_r E_3}{E} \\ &= \frac{A_r}{E} [E_2 - E_3] \end{aligned} \quad (3.29)$$

If the number of sub-layers is reduced to two, then the two sub-layers areas $A_{r,L}$ and $A_{r,L+1}$ are related to the parent layer area A_r by the relationships:

$$A_{r,L} = \frac{A_r}{E_1} [E_1 - E_2] \quad (3.30)$$

and

$$A_{r,L+1} = A_r \left[\frac{E_2}{E_1} \right] \quad (3.31)$$

Accordingly, the area of a sub-layer can be expressed in general terms as :

$$A_{r,l} = \frac{A_r}{E_1} [E_l - E_{l+1}] \quad (3.32)$$

Knowing the sub-layer stress $\sigma_{irL,j-1}$ at time t_{j-1} at the L^{th} sub-layer of the r^{th} layer at the i^{th} link and the strain increment $\delta\varepsilon_{ir,j}$ at time t_j at r^{th} layer of the i^{th} link, then the sub-layer stress $\sigma_{irL,j}$ at time t_j at the L^{th} sub-layer can be determined systematically as follows:

First a trial value $\sigma'_{irL,j}$ of the sub-layer stress $\sigma_{irL,j}$ is calculated by assuming an elastic path, thus

$$(3.33)$$

Once the trial value is calculated, the correct value can be ascertained by using the following conditions:

Let σ_{yL} be the sub-layer yield stress and be given by $\sigma_{yL} = E\varepsilon_L$, where ε_L is the strain defining the L^{th} corner of the approximated stress-strain diagram:

Denoting $\sigma_{irL,j}$ as σ_L for convenience, the following must apply

$$\text{IF } -\sigma_{yL} < \sigma'_L < \sigma_{yL} \text{ Then } \sigma_L = \sigma'_L$$

$$\text{IF } \sigma'_L < -\sigma_{yL} \quad \text{Then } \sigma_L = -\sigma_{yL} \quad (3.34)$$

$$\text{IF } \sigma'_L > \sigma_{yL} \quad \text{Then } \sigma_L = \sigma_{yL}$$

This procedure is applied to all sub-layers of each layer for all the links.

3.4.5 Inertia Effects

To enable an accurate determination of the stress and strain properties at high strain rates, further modifications are required to account for inertia and friction. In this study, when the test specimen is subjected to fast dynamic compression between the projectile and the anvil, radial inertia will effect plastic yielding of the specimen. It is thus necessary to make a reasonable assessment of this effect. The analysis developed by Slater [3.28] was incorporated in the numerical analysis to assess the radial inertia effect during the deformation of an element. Over a time interval, Δt , the deformation speed $U_{i,j}$ is constant and as such, the axial stress exerted on the element is given by

$$\sigma_{i,j} = \sigma_{i,j} \left[1 + \frac{3}{16} \rho \left(\frac{U_{i,j}^2}{\sigma_{i,j}} \right) \left(\frac{r_{i,j}}{h_{i,j}} \right)^2 \right] \quad (3.35)$$

The speed $U_{i,j}$ is calculated as follows:

$$U_i = \frac{\delta (\Delta S_i)}{\Delta t} \quad (3.36)$$

3.4.6 Effect of Friction

The sub-layer stress is modified to account for friction effects by using following general equation:

$$\sigma = \sigma_o \left[1 + \frac{2 \mu}{3h} (R - r) \right] \quad (3.37)$$

Rewriting equation (3.37) in a difference form, leads to

$$\sigma_{irL,j} = \sigma_{irI,j} \left[1 + \frac{2 \mu}{3h} \left(R_{ir} - R_{irL} - \frac{T^2}{12 R_{irL}} \right) \right] \quad (3.38)$$

where T is the thickness of the sublayer area. In the present study, however, a Polythene sheet was used on the two faces of the specimen, and the contact face of the projectile was also coated with petroleum jelly. It was found that the deformation is homogeneous, and hence friction effects were assumed negligible.

3.4.7 Effect of Stress Waves

Many theories have been proposed to study the effect of elastic and plastic waves during the dynamic deformation process [3.33-3.37]. Slater [3.28] reported that for velocities in excess of about 300 ms^{-1} , both elastic and plastic waves may propagate which are able to travel up and down several times during deformation. The travel of these waves can cause variation of the axial force at the specimen interfaces. Since the impact velocities for the tests conducted in this study were between 40 and 150 ms^{-1} , the effect of the stress waves is assumed insignificant and hence, has not been considered in the numerical analysis in any explicit manner. The technique itself

accounts implicitly for the stress pluses which propagate up and down the system (specimen, projectile, and anvil) since all the three components are discretised into smaller elements and calculation progresses from element to element.

Considering the effects of inertia and friction, the axial forces $N_{i,j}$ in each link are then determined from the following modified equation:

$$N_{i,j} = \sum_{r=1}^n \sum_{l=1}^k \sigma_{ir,l,j} A_{l,j} \quad (3.39)$$

where $A_{i,j}$ is the current sub-layer area.

3.4.8 Initial and Boundary Conditions

Initial condition: In order to commence the numerical computations, appropriate initial conditions must first be established. The position of the undeformed system is defined by the coordinates of the mass point $v_{i,0}$, and the velocity distribution defined by $v_{i,0}$ known at time t_0 . The positions of the mass points at time $t_j = t_0 + \Delta t$ can be evaluated

$$v_{i,j} = v_{i,0} + v_{i,0} \Delta t \quad (3.40)$$

and the general iterative procedure may then begin.

Boundary condition: The present finite difference algorithms allow one to treat the kinematic constraints, such as boundary conditions imposed in a relatively simple fashion. The forward positions of all the mass points are calculated according to the equilibrium equation (3.15). This is conducted for the sole purpose of being able to apply the same equations to every mass point, thus preserving the iterative nature of the computations. The forward positions of the restrained mass points calculated in the above manner are naturally meaningless. The forward positions of these particular restrained points are thus re-calculated on the basis of the appropriate kinematics constraints.

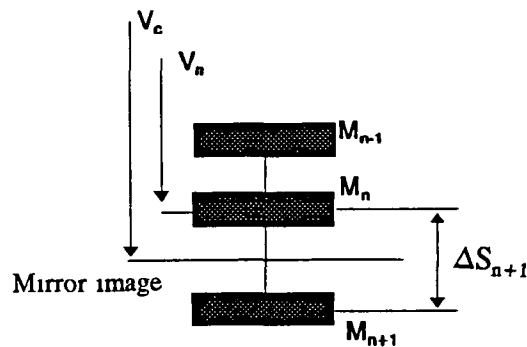


Figure 3.5 *Boundary Conditions for a Fixed End.*

For instance, if a point of a system is not free to move, the calculated position of this point is disregarded and the "new" position which the point occupies is simply its old position. For the case presented in this study, one may write (see Figure 3.5).

$$\Delta S_{n+1} = 2 (v_c - v_n) \quad (3.41)$$

This condition is needed to obtain the axial force at the fixed end, N_{n+1} , which in turn restrains the vertical motion of the mass point "n" by means of the dynamic equilibrium equations.

3 4.9 Stability of Solution and Selection of Time Increments

With reference to the numerical stability of the system the time increment Δt cannot be chosen arbitrarily. Von Neumann's method of stability analysis [3.38] is applicable to this problem. A stability criterion for such analysis is suggested as following: depending on the smallest grid size ΔS , the following stability conditions is used:

$$\Delta t < \frac{\Delta S}{\sqrt{\frac{E}{\rho}}} \quad (3.42)$$

where E is the elastic modulus and ρ is the density of the material of the system. So the numerical stability condition limits the time interval to the time taken by the bar stress wave C to travel through the length of a single link of the lumped mass model of the system. In any case, an eventual numerical instability is usually recognized at an early stage by an abnormal pattern in the behaviour of kinetic energy.

3.5 ENERGY DISTRIBUTION IN THE SYSTEM

The energy theorem for a mechanical system states that the increase of the kinetic energy within an arbitrary time interval is equal to the total work done by the external and internal forces acting on and in the system during that time interval. For the present purpose it can be written as

$$T - T_o = W_e + W_i \quad (3.43)$$

where T is the kinetic energy at an arbitrary time t of the dynamic response, T_o is the initial kinetic energy, W_e is the work done by the external forces, and W_i is the work done by the internal forces.

For an elastic-plastic material, the work done by the internal forces can be expressed as

$$W_i = - (E_e + W_p) \quad (3.44)$$

where E_e is the elastic strain energy at time t , and W_p is the mechanical work dissipated during plastic flow (plastic energy). Substituting Eq. (3.43) into Eq. (3.44), and rearranging terms gives:

$$T_o + W_e = T + E_e + W_p \quad (3.45)$$

For the case considered in the present work, W_e vanishes because there are no external applied loads; thus, one obtains:

$$T_o = T + E_e + W_p \quad (3.46)$$

which means that the initially imparted kinetic energy is subsequently partitioned among kinetic, elastic, and plastic components

The kinetic energy for each element is:

$$T = \frac{1}{2} \sum_i^n m_i U_i^2 \quad (3.47)$$

where m and U are mass and velocity of the element respectively. The total elastic strain energy appropriate to the strain-hardening model adopted in this study is obtained as the sum of the contributions of all the sub-layers in all the layers at all element stations. It can be written as

$$\begin{aligned} I &= \sum_i \sum_r \sum_L \left[\frac{\sigma_{i,r,L} A_L \Delta S_{i,o}}{2E} \right] \\ &= \frac{1}{2E} \sum_i \Delta S_{i,o} \sum_L A_L \sum_r \sigma_{i,r,L}^2 \end{aligned} \quad (3.48)$$

where E is the elastic modulus. The summations are taken over the elements i , layers r , and sub-layers L . At any time of the response, the kinetic energy (3.47) and the elastic energy (3.48) can be evaluated and the plastic energy W_p can then be obtained from equation (3.46).

3.6 IMPLEMENTATION OF FINITE-DIFFERENCE MODEL

The solution of the various finite difference equations was obtained by use of a computer. A computer program was developed to simulate the deformation behaviour during impact. The computations have been performed on PC 486DX-33MHZ with 8 MB RAM, and 100 MB Hard disk.

3.6.1 Code Description

The first step in the process is to represent the system with lumped mass and link assembly and assign the velocity to represent the motion at impact. After the initial conditions are established, the integration loop begins as shown in Figure 3.6.

The first step is to obtain the displacements of the lumped masses. The net force is used to update the element displacement.

3 6 2 Code Input and Output

Input to the code consists of a specification of the geometry of the problem, the appropriate initial velocity, mechanical & physical properties of the material. Output from the code consists of a detailed space-time history of all the important physical quantities such as force, strain, strain rate, etc.

3.6.3 Condition to Terminate the Simulation of the Deformation.

To ascertain the end of the deformation, three boundary conditions may be used:

- (i) when the projectile rebounds (contact force between the projectile and specimen becomes zero or positive), or
- (ii) when the residual kinetic energy at any time instant, j , becomes equal or greater than the kinetic energy at time $j+1$ (when the force at projectile-specimen interface reach a maximum value), or
- (iii) when the position of the element of the specimen at the interface with the projectile at time " j " does not change or the direction of the movement changes in an opposite direction to that observed at time " $j-1$ ".

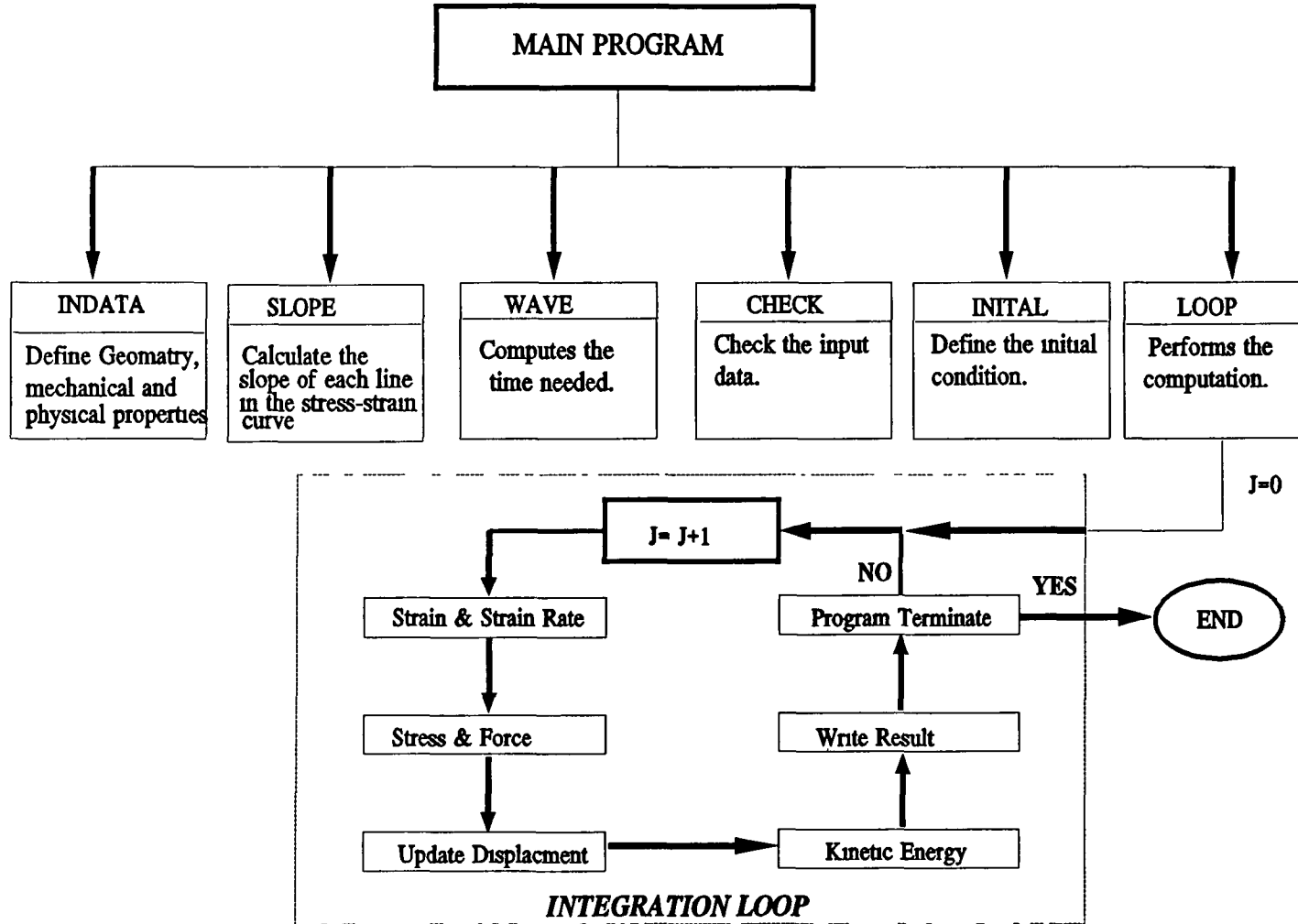


Figure 3 6 Hierarchy Chart for the Finite-Difference Code.

3.7 A COMPUTATIONAL EXAMPLE AND VALIDATION

In this section the convergence and accuracy of the developed finite-difference model are examined and assessed in relation to commercially available finite-element software (LUSAS) and finite-difference code (HEMP).

3.7.1 High Velocity Impact of a Steel Bar against a Rigid Boundary (Taylor Test)

The finite-element software used in this study is a package from Finite Element Analysis UK Ltd, named 'LUSAS'. LUSAS is a general purpose finite-element code which incorporate facilities for linear and non-linear static and dynamic analysis. Since the accuracy of LUSAS computations has been verified for Taylor impact tests (e.g Hamouda and Hashmi [3.39] and Lyons *et al.* [3.40]), LUSAS computations will be used as the 'benchmark numerical experiment' against which the results of the finite-difference code can be compared. More details about the finite-element code 'LUSAS' and other hydrocodes is given by the author in reference [3.39].

This example consists of a cylindrical steel bar striking perpendicular to a rigid boundary. Upon impact, the stress in the bar at the impact point exceeds the elastic limit of the material, and a plastic waves moves back through the bar. Within the plastic zone, the material flows radially and results in a shortening of the bar. The initial length of the bar is 23.46 mm with an initial diameter of 7.62 mm .

3.7.2 Finite-Element Model

The method of approach adopted here consists of.

- (i) model discretization;
- (ii) material property definition;
- (iii) specification of the boundary and constraint conditions,
- (iv) load definition;
- (v) mesh convergence studies; and
- (vi) computational analysis.

Model Discretization: The projectile is modelled using 4-noded one point quadrature axisymmetric elements type QAX4E as shown in Figure 3.7. This type of element is suitable for impact situations and is capable of modelling curved boundaries [3.41] An algorithm to deal with the contact between the projectile and the anvil has been developed by means of the penalty approach.

Material Properties: The projectile material is made of steel which is linearly elastic-perfectly-plastic, with an assumed modulus of elasticity, $E=211 \text{ GPa}$, a Poisson's ratio $= 0.3$, a density of 7840 kg m^{-3} and initial yield stress of 1200 MPa . No strain rate effect has been included in the deformation of the material properties.

Geometry: Because of the isotropic material definition of the model and the co-axial central impact, a rotational symmetry exists in the model, hence an axisymmetric model is used.

Support Conditions: Support conditions describing the way in which the model is grounded are specified for individual nodal freedom. All the nodes in the axis of symmetry of the model are constrained in the X-direction.

Loading: The impacting load is applied by energising the projectile with a downward velocity of 252 ms^{-1} .

Mesh Convergence Studies: Preliminary investigations were carried out on several models and a compromise between the excessive CPU demand and acceptability of the computed results had to be made. The mesh shown in Figure 3.7 proved to have an acceptable number of elements (105 elements) and reasonable mesh density distribution

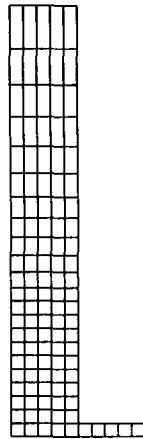


Figure 3.7 Shows the Initial Mesh in the Finite-Element Model.

3.7.3 Finite-Difference Model

In the finite difference analysis, the actual projectile was replaced with a lumped mass model which consists of a number of concentrated masses, connected to each other by a massless link system (see Figure 3.8). The deformation was simulated using the developed finite-difference code. For the sake of comparison, the material properties, boundary conditions, geometry, and loading condition are identical for both finite-element and finite-difference codes.

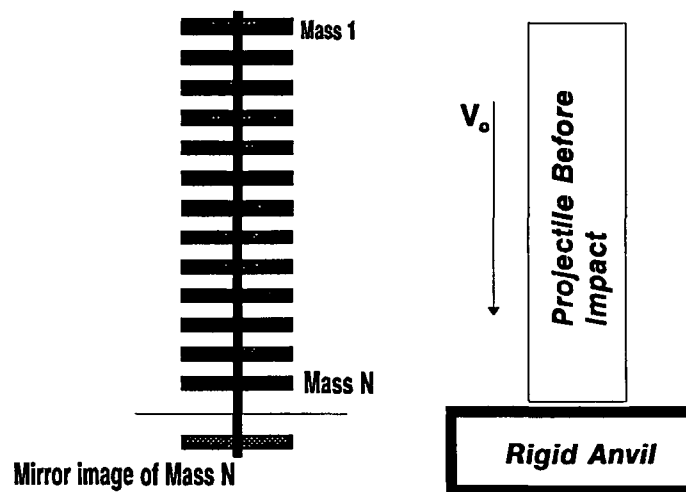


Figure 3.8 Shows the Lumped Mass Model for the Actual Projectile.

In order to verify the accuracy of the analysis, different numbers of elements were considered (10, 20, 25, 50 element). Insignificant difference in the final length of the deformed projectile was observed as long as the ratio of the length of the projectile to the link length was more than ten. The higher the number of the elements, however, the finer the predicted profile of the deformed projectile. In this example the number of element was assumed to be 25. This was found to be sufficiently large without making excessive demands on computing time.

3.7.3 Results and Comparison

The final length of the deformed projectile as approximated using the developed FD code is *19.99 mm*; this is in a very good agreement with the final length approximated using the numerical experiment, LUSAS, as *19.87 mm*.

In addition, some further validation tests were performed in an attempt to compare the results obtained using the developed FD code with the theoretical results obtained by Wilkins and Guinan [3.42] using a finite-difference computer code named "HEMP" (Hydrodynamic Elastic Magneto Plastic). The impact process of steel bars into a rigid boundary is again considered. Table 3.2 compares the ratios (L_f/L_o) obtained using the finite-difference code "HEMP" and the developed code.

Table 3.2 *Comparison of the Results for Taylor Impact Tests.*

Impact Speed (ms ⁻¹)	L _o (mm)	D _o (mm)	L _f /L _o (mm) (HEMP code)	L _f /L _o (mm) (FD code)
192	46.94	7.62	0.894	0.893
266	46.94	7.62	0.818	0.820
319	46.94	7.62	0.754	0.770
452	46.94	7.62	0.593	0.610
175	23.47	7.62	0.911	0.914
252	23.47	7.62	0.842	0.851
328	23.47	7.62	0.754	0.753
402	23.47	7.62	0.720	0.723

It can be seen from Table 3.2 that the results obtained using the developed FD code are in the most remarkable agreement with those obtained from the HEMP code.

3.8 ON THE ENERGY DISSIPATION DURING AN IMPACT TEST

3.8.1 Introduction

An air gun apparatus (or ballistic rig) similar to that used in this study is usually used to investigate the impact behaviour of materials. For exact interpretation of results, the energy losses during an impact event should be determined. The term '*energy loss*' used in this chapter is defined as "*The kinetic energy at the start of an impact event which is not converted into plastic deformation of the specimen*". In fact, depending on the boundary conditions, the projectile mass and supports may also absorb or temporarily store energy. In simple terms, any energy not used to produce a permanent deformation of the specimen is considered as a loss (including elastic strain energy). This may be expressed as a percentage loss of the original energy input.

To the author's knowledge, most of the rate-dependent flow stress laws available today were developed based on an assumption of zero loss in the initial kinetic energy¹. This section is devoted to studying the performance of the ballistic rig used and to estimate the maximum energy loss. Furthermore, the effect of this energy loss on the dynamic flow stress is also considered in chapter five.

3.8.2 Analysis

Ideal Impact Event: The ideal impact event is defined as a rigid accelerated projectile striking a target specimen which is mounted on a rigid boundary (anvil). The impact event begins with an elastic loading of the specimen and is followed by a plastic deformation for sufficiently large initial kinetic energy.

Actual Impact Event: The actual impact event is somewhat different from that described above because the boundary conditions may not be perfect. Rather than being

¹ this may cause an over estimation to the dynamic flow stress.

mounted on a perfectly rigid support, the specimen is placed on an elastic anvil, both the anvil and projectile deform elastically during the impact which modifies the deformation process as follows (see Figure 3.11):

- Stage (1) Initial impact event.
- Stage (2) Elastic-plastic deformation of the specimen until the velocity of the projectile becomes almost zero or the force at the top face of the specimen reach a maximum value. Several scenarios are possible after this stage, including the following sequence.
- Stage (3) Elastic recovery of the specimen (E_{rs}) and anvil(E_{ra}) (This may not commence simultaneously).
- Stage (4) Projectile rebound.

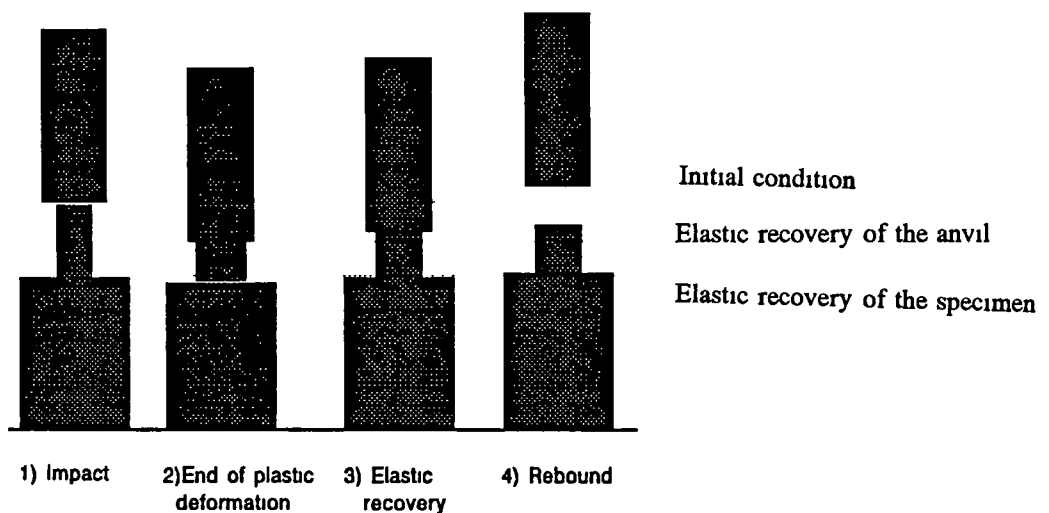


Figure 3.9 Motion of the Projectile and Anvil for a Ballistic Rig During an Impact Test.

The total energy (E_t) is equal to the kinetic energy of the projectile and is given by.

$$E_t = \frac{1}{2} m U_o^2 \quad (3.49)$$

where m and U_o are the mass and the initial velocity of the projectile, respectively.

It is likely that no further plastic deformation of the specimen occurs after stage 2. The kinetic and elastic strain energies remain in the system (projectile, specimen, and anvil) are not absorbed plastically by the specimen. Therefore, the sum of these energies (E_t) may be considered as the energy losses.

$$E_t = (E_a + E_p + E_s + E_n + E_f + E_r) \quad (3.50)$$

where

- E_a : is the elastic energy in the anvil.
- E_p : is the elastic energy in the projectile.
- E_s : is the elastic energy stored in the specimen.
- E_n : is the energy lost in a form of noise.
- E_f : is the energy losses to overcome friction.
- E_r : is the kinetic energy lost when the projectile rebounded.

The elastic strain energy in the projectile (E_p) and the anvil (E_a) can be found by subtracting the energy assuming rigid surfaces and the total energy assuming elastic projectile and anvil at fixed input energy. The energy losses as elastic strain in the projectile and anvil were found to vary with the initial impact speed, where, as the impact speed is increased the energy loss is also increased. The maximum elastic strain in the projectile and anvil is when the specimen is assumed to be rigid.

The elastic recovery of the specimen (E_s , see Figure 3.10) is calculated from:

$$E_s = E_1 - E_2 \quad (3.51)$$

where E_1 and E_2 are the total energy in the specimen with and without the elastic recovery, respectively. This has been found by terminating the simulation using the following conditions:

- (i) when the force between the projectile and specimen becomes zero, (Figure 3.11, stage 3, E_1).
- (ii) when the force at the projectile specimen interface reach a maximum value, (Figure 3.11, stage 2, E_2).

The difference between E_1 and E_2 is simply that in E_1 the specimen has recovered its elastic strain after deformation, whereas in E_2 , the simulation is stopped just before any elastic recovery taken place

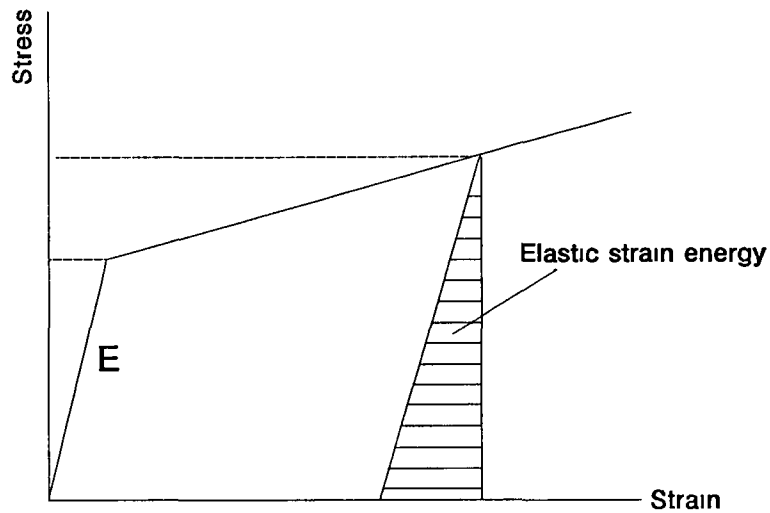


Figure 3 10 *Elastic-Linear Strain Hardening Material.*

Some of the energy will be dissipated by vibration and noise radiated (E_n). Tobias and his co-workers [3.43 and 3.44] examined the energy lost in the form of noise and vibration from a laboratory drop hammer rig. They reported that, in most of cases, the efficiency increases with a decrease of the mass ratio (λ).

$$\lambda = \left[\frac{m}{M} \right] \quad (3.52)$$

where m and M are the masses of the top plate and anvil, respectively. They reported that the efficiency increases from 81% at $\lambda = 0.25$ to 94% at $\lambda = 0.05$ at fixed input energy. In this study the mass ratio (λ) is very small (0.0014), therefore, the energy loss in the form of noise and vibration in the apparatus will be very small.

The energy losses due to friction (E_f) was estimated to be negligible due to use of an effective lubricant and uniform deformation was observed.

Part of the total kinetic energy is reconverted into kinetic energy by rebounding the projectile. The rebound velocity was measured by a laser beam and the rebound velocity was estimated to be $\sim 10\%$ of the initial impact velocity.

The total percentage of energy loss is given by:

$$\zeta = \left[\frac{E_l}{E_i} \right] \times 100 \quad (3.53)$$

CHAPTER FOUR: EXPERIMENTAL INVESTIGATIONS

4.1 INTRODUCTION

This chapter is divided into five main sections. In the first, the selection of materials and test specimen design are examined. In the second, the ballistic test apparatus used, the test procedure, and the detailed aspects of the projectile used are discussed, while in the third, some typical results are shown. Difficulties and limitations of the technique are also discussed. In the fourth, some results from the drop hammer rig are given. Finally, in the fifth, the effect of full water saturation on the mechanical properties of nylon is investigated.

4.2 SELECTION OF MATERIALS AND SPECIMEN DESIGN

Three different classes of engineering materials were used:

Metallic: High conductivity oxygen free copper; structural steel(En-9); brass; and high purity aluminium (99%). The chemical composition of these materials is shown in Table 4.1. In addition, quasi-static compression tests were conducted on these metallic alloys using an Instron 4204 universal testing machine (Plate 4.1) at cross-head speed of 5 mm min⁻¹, and the resulting quasi-static properties are summarized in Table 4.2.

Table 4.1 Shows the Chemical Composition for the Metallic Materials and Projectiles.

Materials Chemical Composition (wt %)				
Copper (C101)	Brass	Steel (EN-9)	Pure Aluminium	Tool Steel (D2)
Cu 99.9 Lead 0.005 Impurities 0.03	Cu 61.5-64% Pb < 3000 ppm impurities < 6000ppm Zn balance	C 0.55 Mn 0.7 P 0.06 S 0.06	Al 99.99 Cu 10 ppm Fe 10 ppm Si 15 ppm Mn 2 ppm Mg 2 ppm others > 3ppm	C 1.50 Cr 12.0 Mn 1.00 Fe balance



Plate 4.1 Universal Testing Machine Model [4204]

Table 4.2 *Quasi-Static Properties of Metallic Alloys*

Characteristics	Materials			
	Copper	Brass	Aluminium	Steel (En-9)
Elastic Modulus [MPa]	100	110	70.6	200
Yield Stress [MPa]	270	420	16	600
Max Reduction [%]	> 60	> 55	> 75	> 50
Flow Stress at $\epsilon=1$ [MPa]	350	500	78	800

Metal-Matrix-Composites: Extruded cylindrical rods of aluminum/copper metal matrix composite and aluminum/lithium metal matrix composite (both are reinforced with silicon carbide particles) were purchased from a commercial supplier [4.1] and used in this study. Results of the chemical analysis and the quasi-static compression tests are given in Table 4.3 and Table 4.4, respectively.

Table 4.3 *Chemical Composition of the Metal Matrix Composites.*

Chemical Compositions (Wt %)		
	Al/Cu	Al/Li
Al	77.9	81
Cu	3.3	1.2
Mg	1.2	0.8
Mn	0.4	
Li		2.0
SiC	17.8	15

Table 4.4 *Quasi-Static Properties for MMC.*

	Al/Cu Composite	Al/L1 Composite
Elastic modulus [GPa]	100	100
Yield stress [MPa]	319	308
Max Reduction(%)	60%	52%
compressive flow stress [MPa]	610 (400)	550 (359)

Polymeric: Bars of nylon 6 were purchased and used. Some of the mechanical and thermal properties as given in the literature [4.1], are given in Table 4.5.

Table 4.5 *Some Mechanical and Thermal Properties for Nylon.*

	Tensile Modulus (GPa)	Tensile Strength (MPa)	Density (g/cm ³)	Water absorption (24hrs) (%)	Thermal Conductivity (W/m K)
Nylon-6	2.6-3.0	78	1.13	2.7	0.24-0.28 (at 23°C)

4.3 HIGH STRAIN RATE TESTING

4.3.1 The Ballistic Test Apparatus

The ballistic test apparatus used for this work has been designed by Hashmi *et al.* [4.2], for firing cylindrical projectiles at speeds varying from 30-1000 ms⁻¹ onto a small cylindrical or disc shape test specimen placed upon a rigid anvil. In their work, they used a high speed camera in order to record the deformation history of small cylindrical billets.

In this study, ballistic tests were carried out using similar apparatus but without the use of a high speed camera. A schematic diagram of the ballistic rig with its accessories is shown in Figure 4.1. A photograph of the ballistic rig is given in Plate 4.2. Some modifications to the velocity measuring system, valve, as well as to the projectile shape were made.

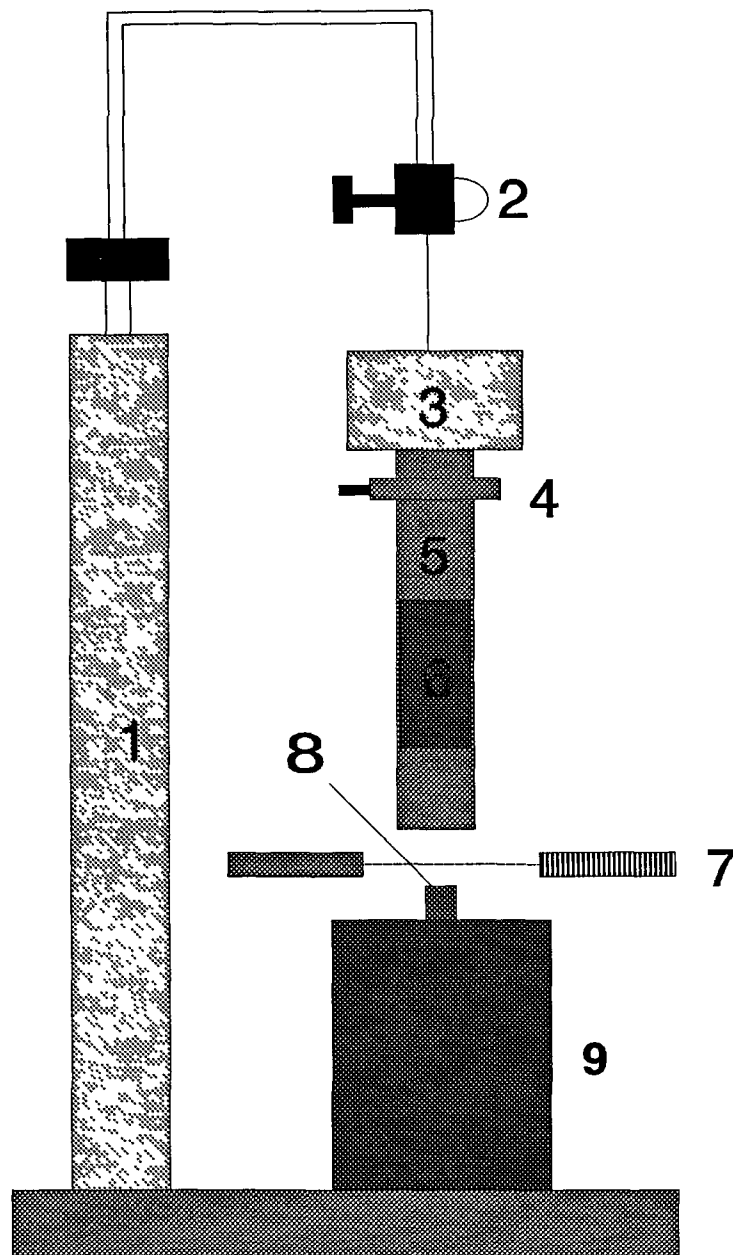


Figure 4.1 *Schematic Diagram of the Experimental Set-up.*

Gas Gun: (1) air cylinder, (2) pressure regulator, (3) air reservoir, (4) valve, (5) barrel, (6) projectile, (7) velocity measuring device, (8) specimen, and (9) anvil



Plate 4.2 Shows view of the ballistic system.



Plate 4.3 Shows the projectile position inside the loading throat.

The ballistic rig used in this study consists mainly of a movable rig, the high pressure power system, barrel parts, anvil unit and the projectile velocity measuring device. The main part of the frame of the ballistic rig is composed of a welded construction and steel angle bar. The remaining auxiliary parts are fixed by screws for the purpose of the assembly and disassembly.

In the gas propelled system, a high pressure nitrogen gas cylinder controlled by a 40 bar adjusting pressure valve supplies the compressive gas to a reservoir unit which is fixed on the rig. At the outlet of the reservoir, a two-way solenoid-controlled valve is attached.

In the barrel section, a loading throat is connected to the solenoid-controlled valve at one end, and to the primary barrel at the other end. A cut-out segment is machined on the primary barrel through which the projectile can be loaded and pushed upwards inside the projectile gripper mechanism (see Plate 4 3). A close fitting split cover is used to close the cut-out segment, and a sliding collar and a nut are used to hold the assembly firmly to prevent the high pressure gas from escaping. The projectile gripper mechanism consists of three grub screws and spring operated smooth pins incorporated at the upper end of the loading throat. An extension barrel is connected to the primary barrel at one end and is attached to a suppressor cap at the other end.

The anvil unit is composed of six individual components: (i) base plate, (ii) back-up anvil, (iii) holder plate, (iv) anvil bar, (v) top anvil, and (vi) cover plate [4.2]. The anvil bar was made from a cylindrical alloy steel En-32 bar, while the Top anvil unit was made from tool steel. The anvil bar and top anvil were heat treated and tempered to increase their strength and rigidity. The top anvil was finely ground and polished to mirror finish.

Modification of the Test Machine:

(i) The velocity measuring system (Laser Unit): The laser unit used in this study was made by Uniphase, U.S A (Helium Neon Gas Laser, model-1508) It is operated from a 230 AC power supply. The laser unit is fixed to an adjustable table which allows the unit to be move up and down vertically. The laser beam passes through the circular hole in the shield box to the photocell detector which also fixed to an adjustable table. The photocell detector is connected to a universal counter-timer (Apollo 100 Universal Counter-Timer). The counter-timer has a measuring range of $0.25\mu\text{s}$ to 10 seconds with accuracy of $\pm 1 \mu\text{s}$. The velocity of the projectile is obtained by measuring the time interval for the two ends of the projectile to pass through a reference point. The velocity is then calculated from the knowledge of the length of the projectile and the measured time interval. Before measuring, the laser beam receiver is triggered by the emissive device and the function of counter-timer is keyed at the Single Time Interval.

(ii) Solenoid Valve: In order to obtain experimental results at high impact speed, a high pressure solenoid valve was incorporated. The solenoid valve is suitable for operation at pressures ranging from 0.8 to 40 bar and temperatures between -10 and 180°C . The valve was controlled by an electric switch which operated using a 12v DC power supply. Two pressure gauges, one to measure low pressure from 0.8-10 bar and another for high pressure from 10-40 bar, were fitted to the compressed air cylinder.

(iii) Shield Box: For the purpose of safety and the convenient collection of the projectiles after each test, a close shield box was designed and manufactured (see Plate 4.4). It consisted of a welded square steel frame on which aluminium plates are fixed by screws. To allow the laser beam for the measurement of the velocity of the projectile to pass through the box, the corresponding holes on its two sides were carefully made



Plate 4.4 Shows view of the Shield Box.

4 3.2 Ballistic Test Procedure

Tests were carried out using the ballistic testing apparatus. The apparatus was first calibrated to obtain the relation between the speed of the projectile (mass=10 g) and the air pressure; the calibration curve is shown in Figure 4.2.

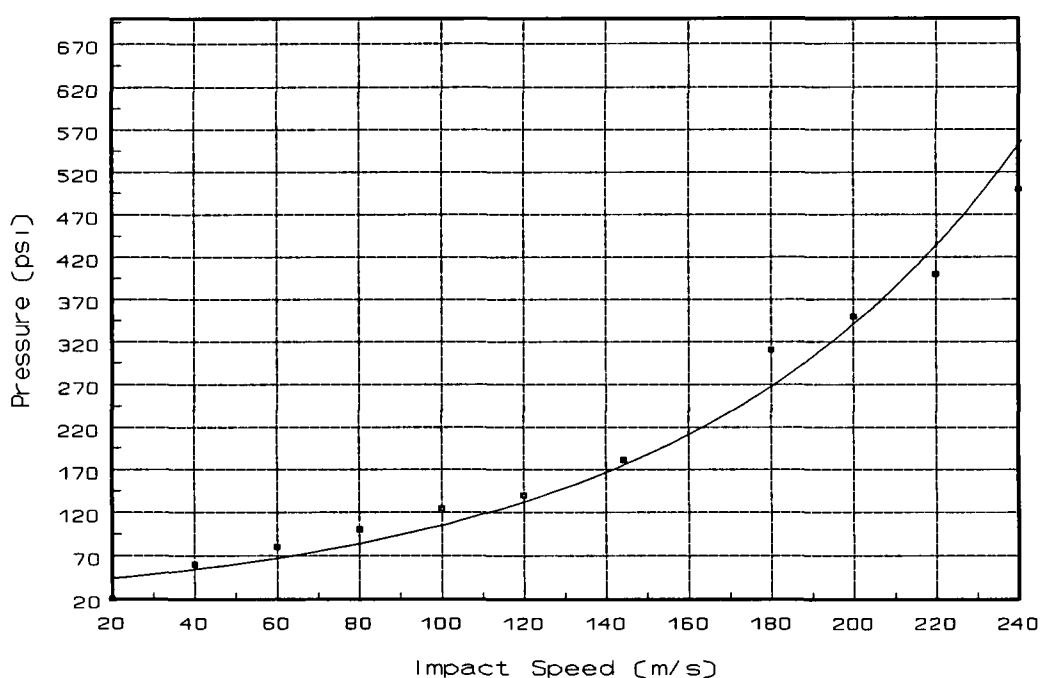


Figure 4.2 *Calibration Curve of Velocity of the Projectile Versus Pressure.*

From the calibration curve, it was possible to set the air pressure in the apparatus to fire the projectile at a specified speed. It should be noted that the curve was used as a guide-line for setting the air pressure and the exact speed of the projectile was determined in each test by means of the laser beam device. The procedural steps are as follows,

- (i) The projectile is installed inside the loading throat, then pushed up into the gripper mechanism, and kept in suspension. The slot opening is then closed with the split cover and the sliding collar is slid over and clamped using the collar-nut.
- (ii) The measuring system for the velocity of the projectile is adjusted and made ready to measure.
- (iii) The valve of the compressed air cylinder is opened slowly and kept open until the reservoir air pressure reaches the predetermined level as indicated by the pressure gage attached to it.
- (iv) The solenoid valve was opened to perform the impact test.
- (v) The reading on the display of the universal counter-timer is taken, the deformed specimen is collected and its diameter and height are accurately measured and noted.

Before carrying out each test polythene sheet of about 0.2 mm thickness was placed at both faces of the specimen to act as a lubricant. Several impact speeds were selected ranging between $35\text{-}140\text{ ms}^{-1}$. At least three specimens were tested at nominally the same impact speed. The projectile was inspected after every five firings against the test specimens and no deformation or indentation in either the projectile or the anvil was observed.

The ballistic test specimens were prepared from as-received material bars. In this investigation all the specimens were of size 5.0 mm in length and 5.0 mm in diameter. These dimensions were chosen to obtain an aspect ratio of unity. Both surfaces of the specimens were finely ground and made as flat and as parallel as possible.

4.3.3 Preparation of the Projectile

All the projectiles were made from tool steel(D2) with dimension of 19.0 mm in length and 9.5 mm in diameter. Each projectile was machined to this size to fit closely in the loading throat of the air gun apparatus. The flat surfaces of the projectile were polished to a mirror finish. The hardness of the projectile was measured to be about 800 Hv

after a series of heat treatment processes (Oil quench at 950 °C and tempered at temperature of 150 °C). Table 4 1 shows the chemical composition of the material used to make the projectile.

In order to avoid the projectile from being blocked, especially after it is used for several times, the originally designed projectiles were modified according to the configuration as shown in Figure 4 3. A 3° angle guide cone is made in the front of the projectile. Further, to guarantee the high pressure air pushing on the rear end of the projectile, a very small clearance fitting between its lateral surface and the inside face of the primary barrel of the machine is chosen.

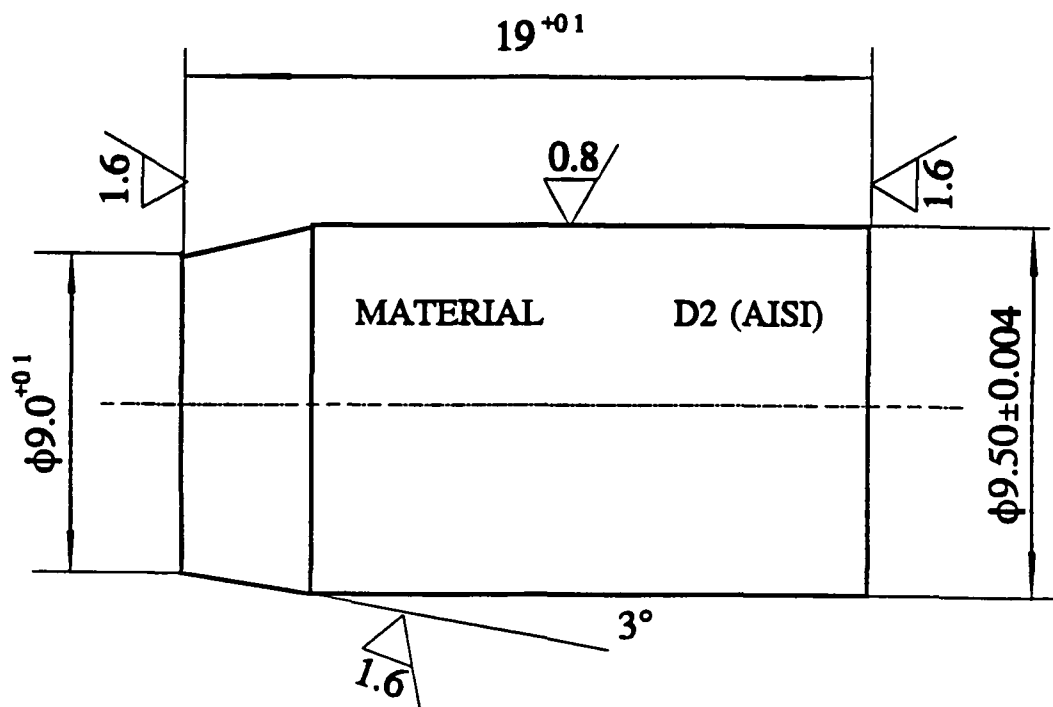


Figure 4.3 Design Details of Projectile.

4.4 TYPICAL TEST RESULTS: ADVANTAGES AND LIMITATIONS

The dynamic compression impact test were performed at room temperature. The height reductions and diameter increments have been obtained as shown in Figures 4 4a- 4.4c. Summary of all the impact tests which were carried out in this study are presented in Appendix A. These results will be used to determine the constitutive equation of these materials in the following chapters. It is worth mentioning, however, that these results were obtained quite readily. It is thus important to recognize the following advantages of the current test method:

- (i) the simplicity of the test set up and test preparation,
- (ii) the reliability of the approach adopted,
- (iii) the flexibility and adaptability of the test method to varying loading and boundary conditions.

While carrying out the initial tests, a layer of polythene sheet was used at each face of the specimen. A slight non-homogenous deformation occurred under this condition, see Plate 4 5a. This may be due to the fact that the heat rise during deformation is working to break down the lubricant on the top face. This problem was overcome by coating the contact surface of the projectile with petroleum jelly and using two layers of polythene sheet on the upper and lower faces of the test specimen. With this lubrication arrangement almost homogeneous deformation was achieved, see Plate 4.5b. High speed photographs show that no barrelling takes place during deformation under similar test conditions as reported in reference [4.3].

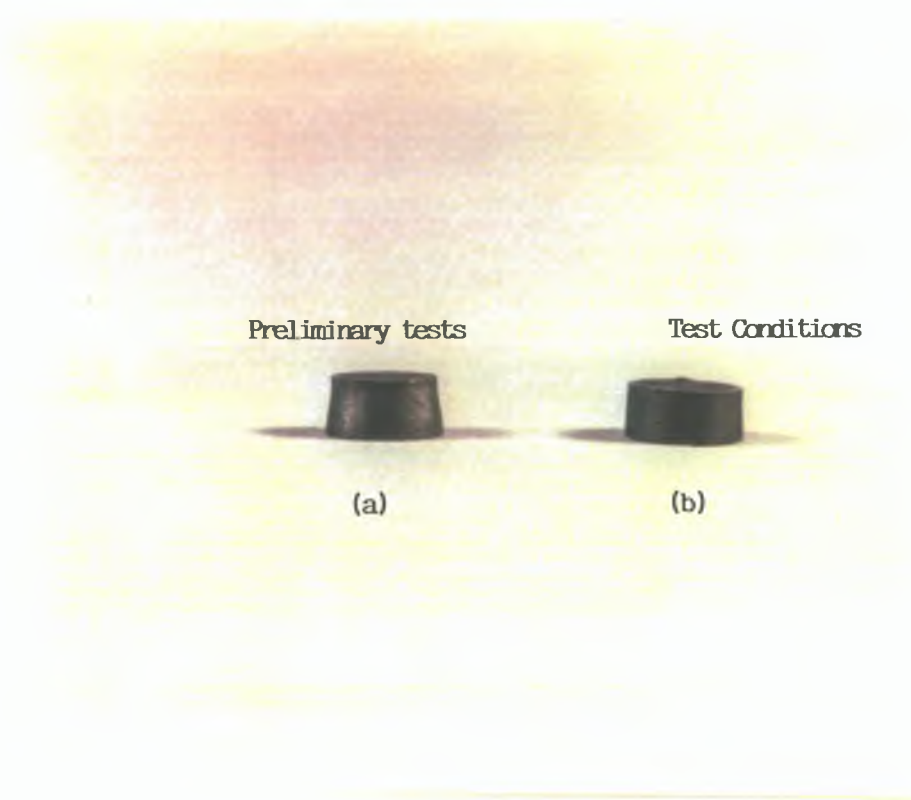
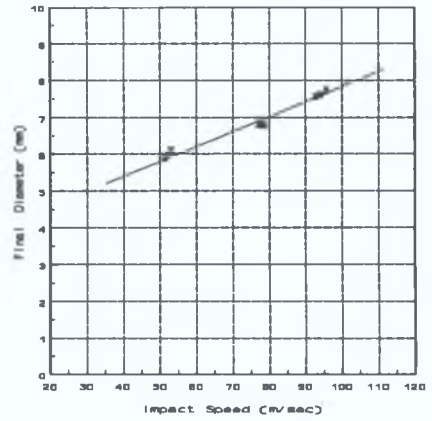
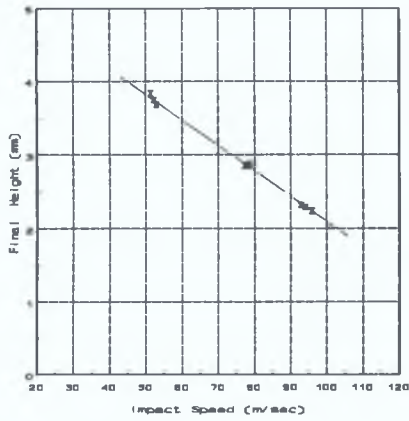
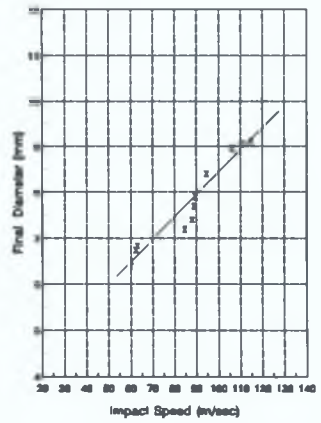
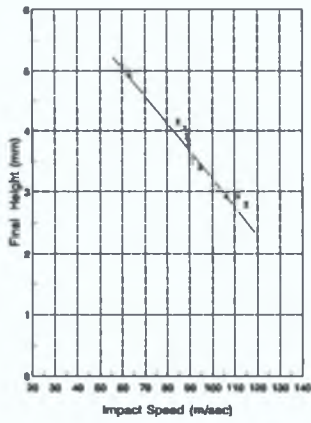


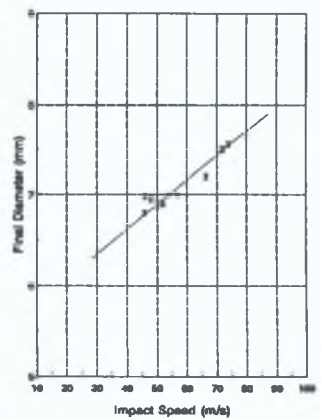
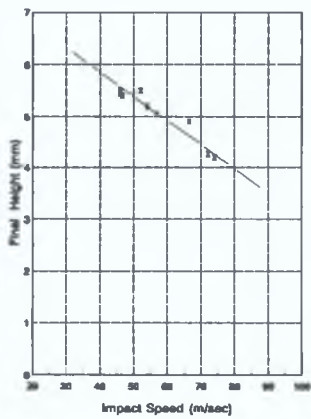
Plate 4.5 Shows the effect of the friction on the final shape of deformed test specimen.



(a) Variation of Height and Diameter for Copper.



(b) Variation of Height and Diameter for AL/CU MMC.



(c) Variation of Height and Diameter for Nylon 6.

Figure 4.4 Sample of Typical Results for Three Different Materials.

4.5 INTERMEDIATE STRAIN RATE TESTING

Three types of materials were tested at intermediate ($\sim 400 \text{ s}^{-1}$) strain rate using the drop weight apparatus at University of Manchester Institute of Science & Technology. The materials considered were (copper, Al/Cu MMC, and Al/Li MMC). In all the tests the load transmitted through the specimen to the base was measured using a piezo-electric (Kistler, type 4091) load washer. The load-time trace was stored in an oscilloscope and plotted on an X-Y plotter. More details about the drop weight apparatus are given in reference [4.4].

The experimental load-time traces for all the materials tested are shown in Figures 4.5, 4.6, and 4.7 for copper, Al/Cu MMC and Al/Li MMC respectively. Details of the specimen dimensions, impact velocity, hammer mass, etc. are given in Table 4.6.

Table 4.6 *Summary of the Drop Weight Tests.*

Drop Height (m)	Velocity (m/s)	Mass (kg)	Specimen Dimensions		Reduction in Height (%)
			Height (mm)	Diameter (mm)	
Copper					
1	4	58	10	10	50
Al/Cu MMC					
1	4	50	10	10	40
Al/Li MMC					
1	4	47	10	10	40

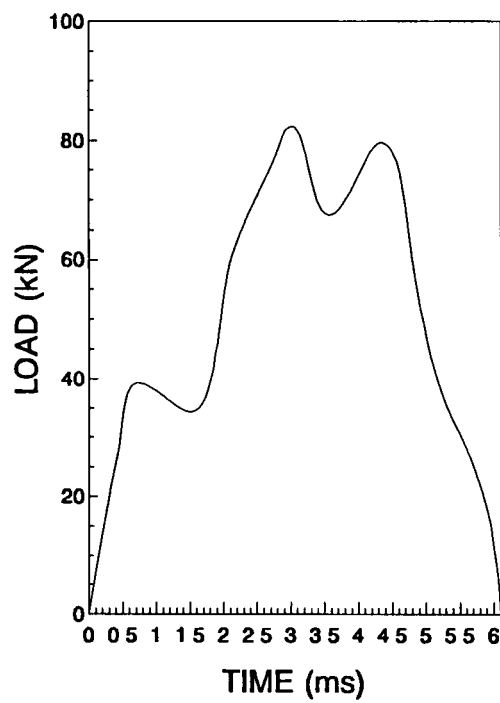
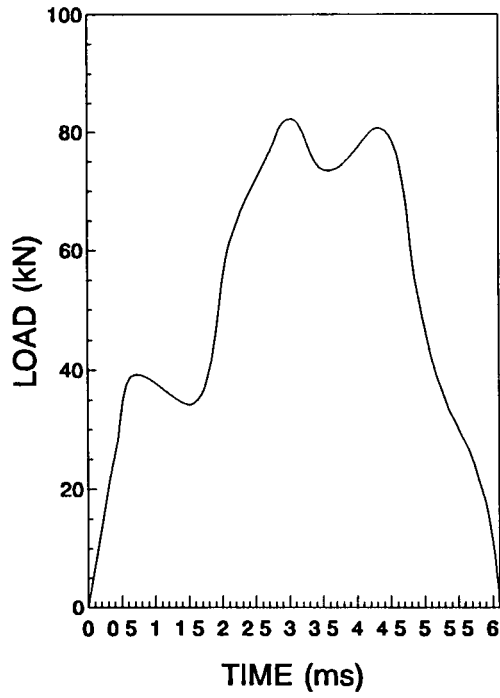


Figure 4.6 Force-time Traces for Copper from Two tests at the same Condition.

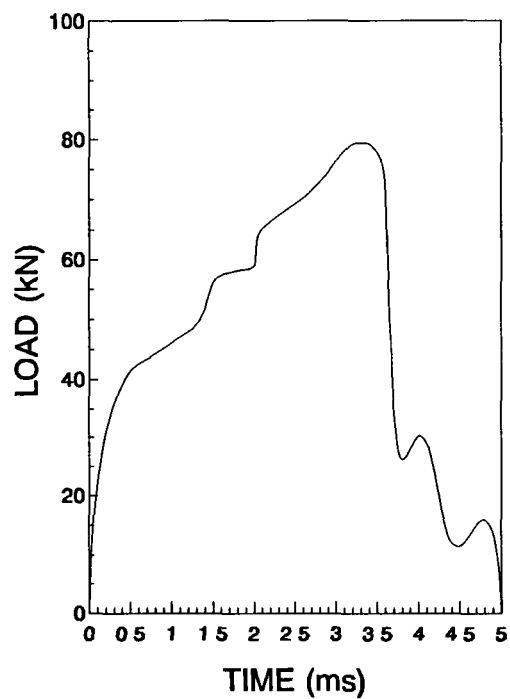
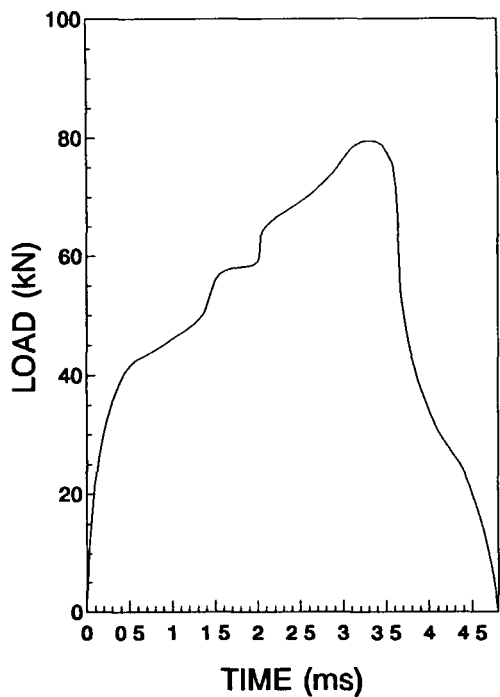


Figure 4.6 Force-time Traces for Al/Cu MMC from Two tests at the same Condition.

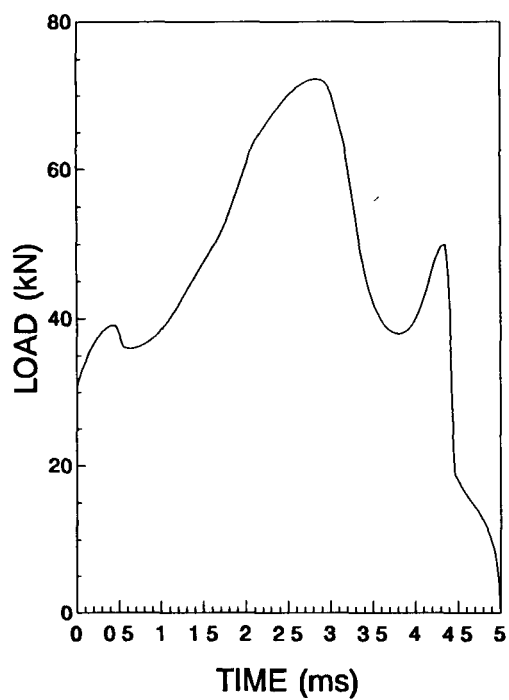
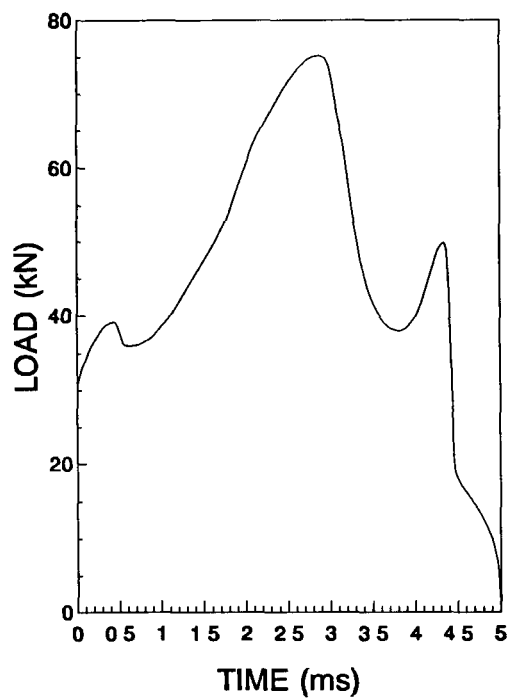


Figure 4.7 Force-time Traces for Al/Li MMC from Two tests at the same Condition

4.6 STUDY ON THE EFFECT OF WATER CONTENT ON THE MECHANICAL PROPERTIES OF NYLON

Polymers frequently contain diffused water which can have a considerable effect on their mechanical properties. In this investigation, nylon was chosen as the test material because of its sensitivity to humidity. Two sets of compression experiments were performed, the first set was carried out on dry specimens (i.e zero moisture content), and the second set was subsequently performed on specimens with different levels of moisture content. Both sets were performed under static and dynamic loading conditions and at room temperature.

All the test specimens were prepared from as-received nylon (N6) bars, which were purchased from a commercial supplier. All the specimens were machined to 6 mm diameter and had a length-to-diameter ratio of unity. Each end surface was finished as smoothly as possible, and the dimensional error was within 0.05 mm for both the diameter and the height. Prior to measurement all the specimens were dried.

The quantity of water contained in the specimens was determined by measuring the weight. An electronic scale [Mettler] with a resolution of 0.1 mg was used. The concentration of diffused moisture C_w in the polymer was evaluated according to the equation:

$$C_w = \frac{m_p - m_o}{m_o} \quad (4.1)$$

where m_p and m_o are the weight of the wet and dry specimen, respectively. The specimens were first dried in a dessicator filled with silica-gel. In this way the weight of a dry specimen was establish. Different levels of moisture content were obtained by conditioning the specimens in containers with different relative humidity levels (75.5%, 85.1%, and 94.6%), which were maintained by means of saturated salt solutions NaCl, KCl, and KNO_3 respectively, at 20°C [4.5]. Specimens were exposed to these conditions for 10-15 days depending on the kinetics of the moisture diffusion, which

changes with the percentage of air humidity. Successive weight measurements at 24-h intervals were taken to determine if the sample had reached equilibrium. It was found that 10 days were sufficient, with less than 1% variation in the amount of water gained or lost in 24-h. Results and discussion of the effect of water onto the flow stress of nylon are given in chapter 5 section 5.4

It should be noted that in this study, importance was not given to some properties of the material such as; basis weight, thickness, etc. because the aim was to study the effect of moisture on static and dynamic flow stresses. Therefore, the goal is to compare, for the same material, what effect the moisture has on the mechanical characteristics.

CHAPTER FIVE: ANALYSIS AND DISCUSSION OF RESULTS

5.1 INTRODUCTION

This chapter is divided into four main sections. In the first, the constants for the different materials investigated are provided. In the second, a detailed description of the dynamic behaviour and rate-sensitivity of the selected materials as well as comparisons between the theoretical predictions and the experimental findings are provided. In the third section, the factors affecting the compressive dynamic flow stress are investigated. Finally, in the fourth section, verification of the developed constitutive law is presented.

5.2 DETERMINATION OF MATERIALS CONSTANTS

The complete description of the newly proposed constitutive equation (3.9) necessitates the determination of the constants K and n in the static mode. The value of K is derived from the static stress-strain curve at natural strain equal to unity, and the constant n is determined from the best fit of the quasi-static data for each of the materials investigated. The temperature factors G_1 in equation (3.12) and G in equation (3.11) are obtained from the ratio of room temperature flow stress to flow stress at high temperatures obtained from the literature.

From known initial dimensions of the test specimen together with the mass and impact speed of the projectile, the deformation is simulated using the developed computer code based on the proposed constitutive equation (3.9). By iterative computation the constants m and p of the constitutive equation are established for close agreement between the experimental and simulated results in terms of the final dimensions of the deformed test specimens.

Determination of the material constants m and p in equation (3.9) involves assigning arbitrary values to these parameters. The final dimensions were then predicated theoretically in terms of the final height and final diameter at a given speed. The next step is to fix the value of m and change the value of p iteratively for a close agreement between the theoretical and experimental results at this speed. If the agreement is not close, then the value of m is changed again and the value of p is changed iteratively. This process is repeated until a very close agreement between the theoretical and experimental results is achieved. Then the same values of m and p are used to predict the final dimensions of the specimen at several impact speeds (intermediate and maximum). If similar agreements are then achieved, these values are accepted as the material strain rate sensitivity constants. If not, then a new set of m and p are determined for the intermediate and maximum speeds, and an average value of these sets of m and p are taken as the material strain rate sensitivity. However, in this study, the set of values of m and p determined in the first iteration process was found to give a good agreement over the range of impact speeds considered.

5.3 DYNAMIC BEHAVIOUR OF METALLIC ALLOYS

The experimental and computed results were compared in terms of the final dimensions of the deformed test specimens with impact speed, and the percentage discrepancy between the two was found to be 2.4 percent maximum. The best fit constants for the metallic materials investigated in this work are shown in Table 5.1.

TABLE 5.1 *Material Constants for the Constitutive Law of Metallic Alloys.*

MATERIAL	DESCRIPTION			CONSTITUTIVE EQUATION CONSTANTS			
	Density [Kg/m ³]	Specific Heat [J/Kg k]	Melting Temperature [°C]	K [MPa]	n	m [s]	p
Aluminum	2700	900	660.4	78	0.37	0.0024	0.25
Copper	8954	383	1083	350	0.07	0.0024	0.048
Brass	8522	385	937.5	500	0.0812	1x10 ⁻⁷	0.11
Steel (EN-9)	7860	465	1425	800	0.122	2x10 ⁻⁶	0.095

5.3.1 Dynamic Stress-Strain Curves

From the known material constants of the constitutive equation (3.9), the dynamic stress-strain curves for all the metallic materials investigated were obtained for strain rates varying between 10^3 - 10^5 s^{-1} , as shown in Figures 5.1 and 5.4. It can be seen from these figures that there is a significant change in the overall shape of the dynamic compressive stress-strain curve in comparison with the quasi-static curve. The conclusion that can be drawn from these figures is that the dynamic flow stress is a function of both the strain and strain rate. As the strain increases the strain rate sensitivity decreases at a constant strain rate (see also Figures 5.9-5 12). In other words, the "plastic modulus" of the dynamic curve becomes smaller than that of the static curve.

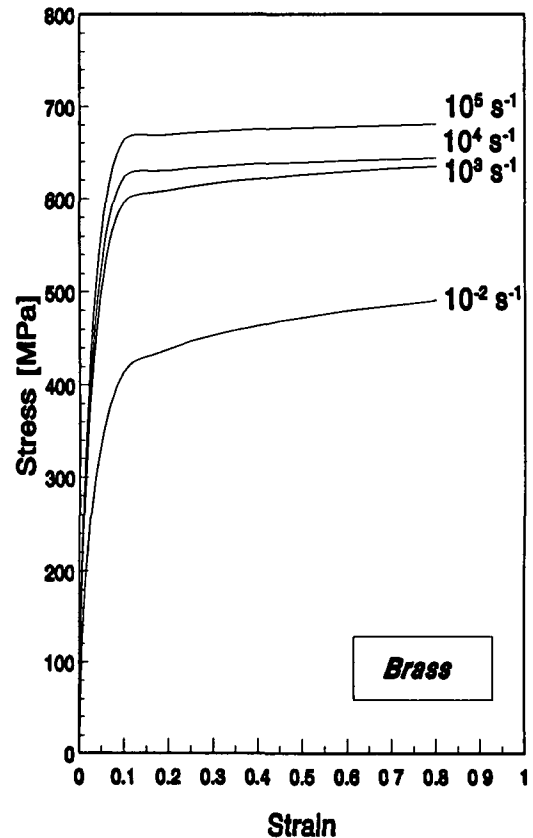
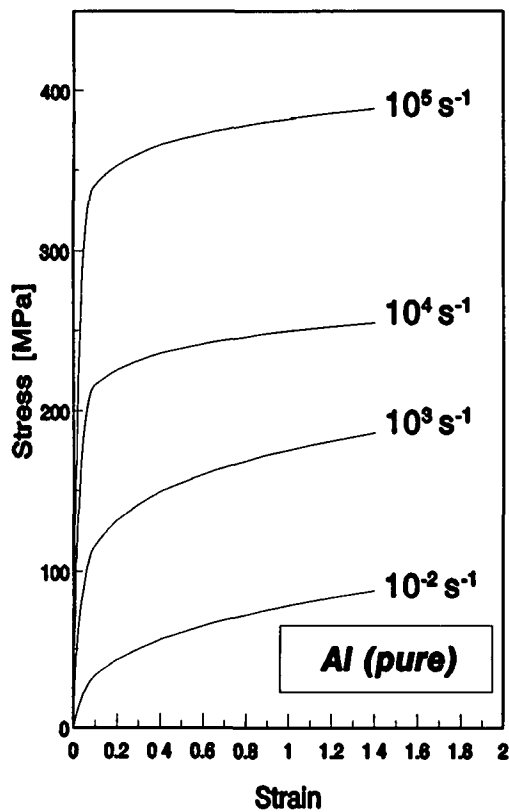


Figure 5 1 True Stress-Strain Curves for Aluminum Figure 5 2 True Stress-Strain Curves for Brass

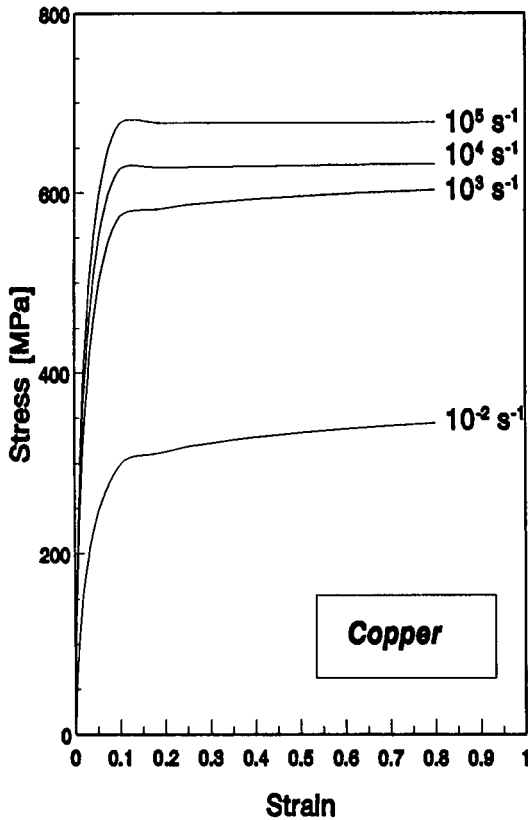


Figure 5.3 True Stress-Strain Curves for Copper

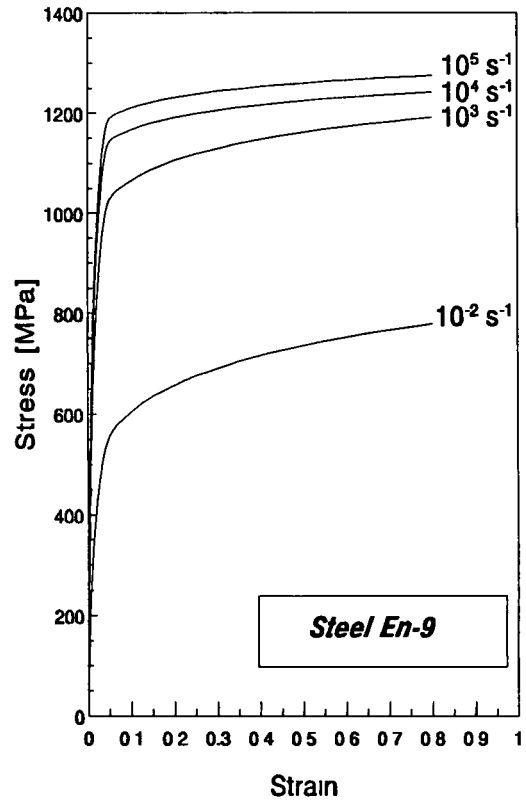


Figure 5.4 True Stress-Strain Curves for Steel

5.3.2 Adiabatic and Isothermal Stress-Strain Curves

The isothermal and adiabatic curves are established as shown in Figures 5.5 to 5.8 for aluminum, brass, copper and steel, respectively.

The adiabatic curves are obtained from equation (3.9), while the isothermal curves are obtained for G_1 , and α equal to unity in the same equation. The differences in the flow stress between the isothermal and adiabatic conditions have shown to be quite substantial. It can be seen that as the strain increases the difference between the two curves increases. In addition, it can be seen that the decrease in the flow stress is greater in the case of the steel than in brass and copper samples. At strain rate of 10^4 s^{-1} and strain 0.8 the reduction in the flow stress of aluminum, brass, copper, and steel is about 58, 70, 90, and 200 MPa, respectively.

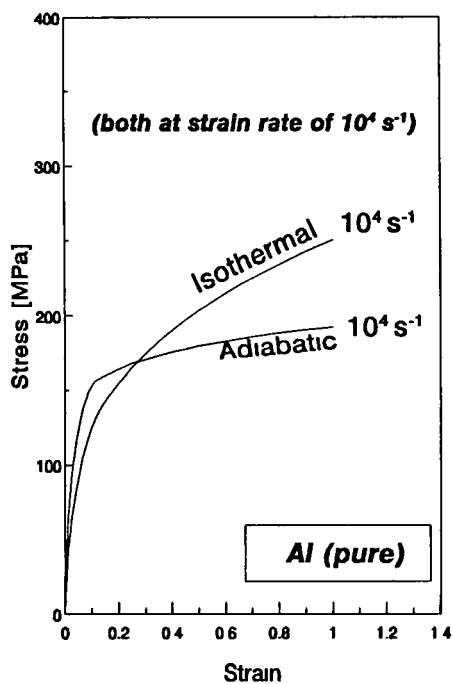


Figure 5.5 Isothermal and Adiabatic Stress-Strain Curves for Aluminum

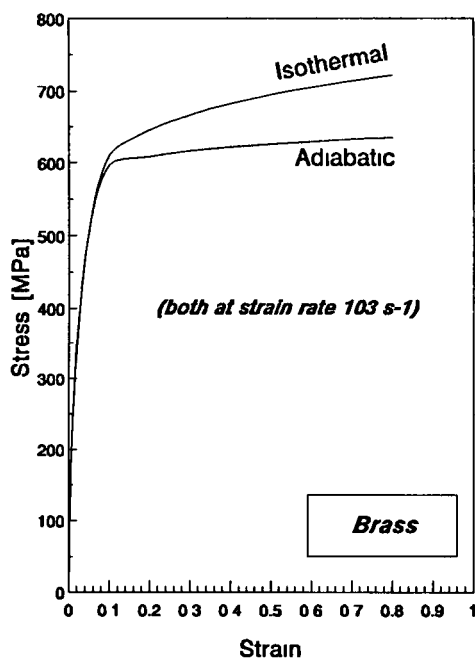


Figure 5.6 Isothermal and Adiabatic Stress-Strain Curves for Brass

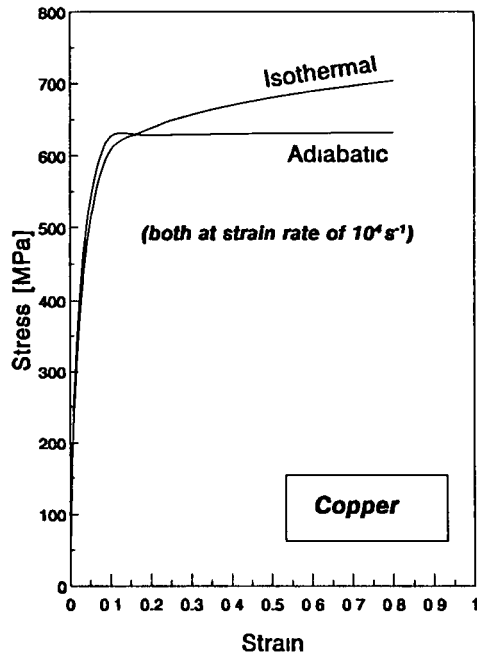


Figure 5 7 Isothermal and Adiabatic Stress-Strain Curves for Copper

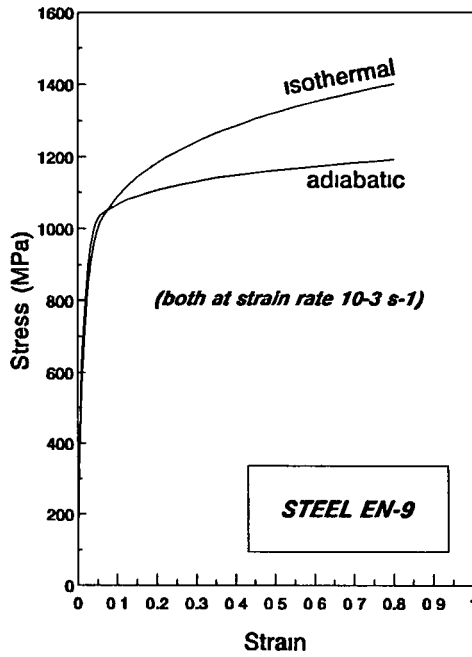


Figure 5 8 Isothermal and Adiabatic Stress-Strain Curves for Steel

5.3.3 Strain Rate Sensitivity

The strain rate sensitivity (η) may be defined as the ratio between the dynamic to static stresses at a certain strain. Thus,

$$\eta_{\epsilon} = \frac{\sigma_d}{\sigma_s} \quad (5.1)$$

In Figures 5.9 to 5.12 the strain rate sensitivity established in this study is shown against the logarithmic strain rate at various strain levels for all the metallic materials investigated. It can be seen that the rate of sensitivity of all the materials investigated varies with strain at a constant strain rate; where this sensitivity decreases as the strain increases. The rate sensitivity over the strain rate ranging from 10^3 to 10^5 s^{-1} and 10% strain were found to vary between 1.4 to 1.6 for brass 1.9 to 2.3 for copper, and 1.76 to 2.0 for steel. At a true strain of 0.7, the ratio varies between 1.29 to 1.39 for brass, 1.75 to 1.96 for copper, and 1.53 to 1.64 for steel.

The influence of strain rate on the stress level of the pure aluminum is approximately what one would expect, since in general, the strain rate sensitivity of aluminum depends on its purity, where high purity aluminum shows high strain rate sensitivity and aluminum alloys show low sensitivity [5.1]. In the present study, the stress ratio for pure aluminum investigated here has been found to vary between 3.34 to 5.9 at strain rates varying between 10^3 to 10^5 s^{-1} and strain equal to 0.1. At a strain equal to 1, the ratio was found to be varying between 2.24 to 5.3 at strain rate 10^3 to 10^5 s^{-1} . These results indicated that below the strain rate 10^3 s^{-1} the flow stress ratio corresponding to a certain strain value increases linearly with the logarithm of strain rate. This is generally acknowledged to be a consequence of the role of thermal activation in the control of the deformation mechanics. Above this critical strain rate ($\sim 10^3$ s^{-1}) the stress ratio increases more rapidly with strain rate. This behaviour is interpreted to indicate the transition to viscose-drag mechanism. Similar observations of transition to a visco-drag mechanism were reported in references [5.2-5.3]. However, Follansbee *et al.* [5.4] have observed the rapid increase of the flow stress after strain rate 10^4 s^{-1} , but reported that transition to visco-drag is not a likely explanation, and that the observed

behaviour can be more accurately interpreted as a change in the way that structure evolves with strain.

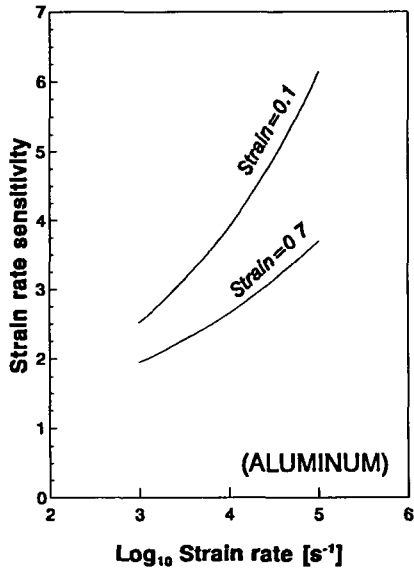


Figure 5.9 Variation of Flow Stress Ratio with Log Strain Rate for Aluminum

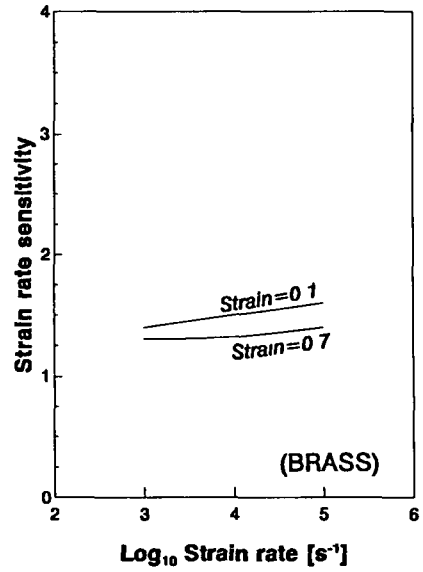


Figure 5.10 Variation of Flow Stress Ratio with Log Strain Rate for Brass.

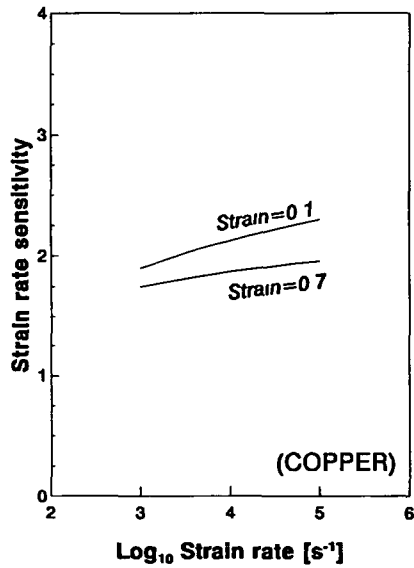


Figure 5.11 Variation of Flow Stress Ratio with Log Strain Rate for Copper

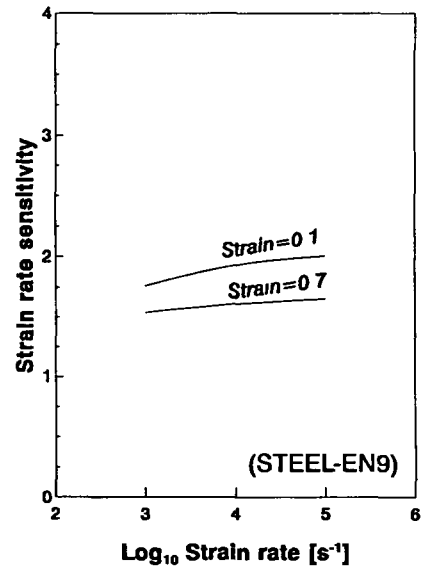


Figure 5.12 Variation of Flow Stress Ratio with Log Strain Rate for Steel

5.3 4 Comparison With Earlier Studies

Table 5 2 shows a comparison in a tabulated form between the dynamic flow stresses obtained from the present work and those reported in the literature at strain rate of 10^4 s^{-1} and 10% strain for copper.

Table 5.2 Comparison in terms of Dynamic Flow Stress for Copper

<u>REFERENCES</u>				
Strain Rate	Follansbee <i>et al</i> [5 4] Copper ($\epsilon = 0.15$)	Hashmi-Haque [5 5] C101 Copper ($\epsilon = 0.1$)	Johnson <i>et al</i> [5 6] Copper ($\epsilon = 0.1$)	Present Work C101 Copper ($\epsilon = 0.1$)
Static	200	271	233	297
10^3	275 (1 38)*	505 (1 86)	264 (1 13)	565.4 (1 9)
10^4	320 (1 6)	637.8 (2 35)	249.1 (1 19)	631.5 (2 13)
10^5	460** (2 3)	860 (3 17)	312** (1 34)	684 (2 3)

*The number between the brackets represents the strain rate sensitivity

** Extrapolated data

In order to provide direct comparison, some of these results had to be extrapolated to strain rates of up to 10^5 s^{-1} . This table shows considerable differences between the results reported by different researchers which may not be accounted for by differences in material composition, testing technique or neglect of temperature softening. Further critical testing is therefore necessary to establish the correct behaviour and to understand the difference.

Considering the data obtained for brass, it appears that there is a gradual increase in the dynamic stress (or strain rate sensitivity) with strain rate, but that this is small compared with the other materials investigated in this study. However, similar findings were obtained by Woodward and Brown [5.7] who stated that there is only a slight increase in the dynamic stress over the static value. In contrast for the mild steel there is a large increase the dynamic stress at high strain rates (10^3 to 10^4 s^{-1}).

A search of the literature of strain rate effects in pure aluminum in compression reveals some interesting data. Yoshida and Nagat [5.8] observed that the dynamic flow stress is always higher than the quasi-static one, when they conducted compression tests on pure aluminum (99% purity) at room temperature and strain rates between 10^{-2} to 10^3 s^{-1} . Bodner [5.9] also reported stress ratios of 3.11 to 3.46 for structural aluminum at strain rates ranging from 10^3 to 10^4 s^{-1} . Lindholm and Bessey [5.10] and Jiang and Chen [5.11] show that pure aluminum is strain rate dependent, however the higher strength aluminums tend to be strain rate independent over a range in strain rate approximately 10^{-4} to 10^3 s^{-1} .

There are insufficient data in the literature on structural steel EN-9 for comparison, although the effect of strain rate on flow stress of structural steel En-8 is reported by Haque and Hashmi [5.12]. The stress ratio obtained by Haque and Hashmi [5.12] is in the range of 1.8 to 2.5 at strain rate 10^3 to 10^5 s^{-1} . It can be seen that these results are slightly higher than those obtained in the present study. This could be due to the difference in the carbon percentage (0.4 for En-8 and 0.55 for En-9) [5.13]. Also, Haque and Hashmi ignored the thermal softening effect.

5.4 DYNAMIC BEHAVIOUR OF METAL MATRIX COMPOSITES

5.4.1 Primary Remarks

Metal matrix composites (MMCs) may exhibit fundamentally different behaviour from homogenous and isotropic metals. Firstly, this is due to the heterogeneity of the MMC, where not only are there two bulk phases, one of which may be brittle and the other ductile, but also an interface, which is difficult to characterize and yet plays an important role [5.14, 5.15]. Secondly, the material may be orthotropic in both elastic and plastic properties, leading to additional analytical and computational complexity. In the light of these complications, it is clear that the full characterization of the mechanical behaviour of MMC materials at very high strain rates is likely to require the use of more complicated numerical techniques and a wide range of experimental investigations. Within this context, it is felt that Particulate-Reinforced Materials (PRMs), which are more isotropic than the fibre-reinforced materials (FRMs), may be easier to model. In this study, two types of the particulate-reinforced metal matrix materials (Al/L₁ and Al/Cu MMC) were used. For simplicity, they are each treated as a material in its own right without reference to the properties of the individual constituents. Also, the material is assumed to behave as an isotropic continuum, with the properties derived from experiments [5.16].

5.4.2 Quasi-Static Properties

Quasi-static compressive tests were performed on both MMC and pure aluminum. The curves presented in Figure 5.13 indicate that the presence of reinforcement increases the compressive strength from 78 MPa for the un-reinforced material to 408 MPa for the reinforced. There is also a substantial effect on the fracture strain of the MMCs as compared with the pure materials. For the pure aluminum, the specimen was deformed up to true strain equal to 1.36 (75% reduction) and no crack developed. However, in the case of Al/L₁ MMC, a crack became evident at true strain equal to 0.78. For the Al/Cu MMC, cracking occurs at a true strain equal to 0.92.

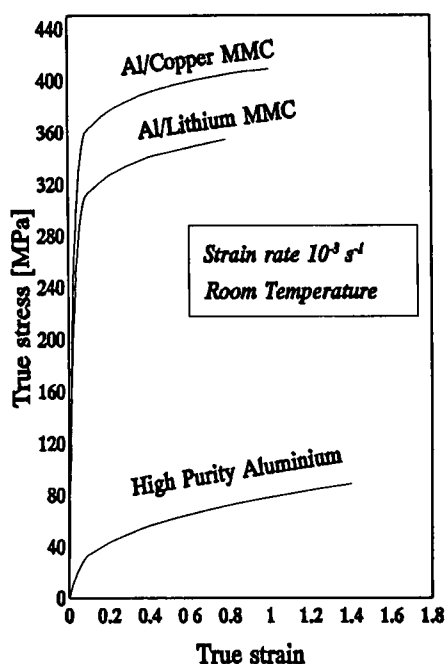


Figure 5.13 Quasi-Static Stress-Strain Behaviour in Compression of Pure and MMC Aluminum

Significant difference was found between the reported data for the standard tensile test (supplied by the company [5.17]) and the compressive data (as shown in Table 5.3) obtained during this investigation using the Instron machine. This is in agreement with what Arsenault and Wu [5.18] observed. They reported a significant difference in the tensile and compressive properties of SiC-Al composite.

Table 5.3 Comparison between compression and tensile test	Al(pure)	Al/Cu Composite	Al/Li Composite
Elastic modulus [GPa]	70.6	100	100
Yield stress [MPa]	10-35 (16) ¹	400 (319)	500 (308)
Max. Elongation/or Max. Reduction(%)	--- (> 75%)	6% (60%)	2.3% (52%)
Tensile failure stress [MPa]	50-90 (78)	610 (400)	550 (359)

¹ The numbers between the brackets are obtained from the compression tests.

5.4.3 Dynamic Stress-Strain Curves of MMC

Table 5.4 shows the material constants obtained from a best fit for Al/Cu and Al/Li MMC.

Table 5.4 *Material Constants for the Constitutive Law of MMCs.*

MATERIAL	DESCRIPTION			CONSTITUTIVE EQUATION CONSTANTS			
	Density [Kg/m ³]	Specific Heat [J/Kg k]	Melting Temperature [°C]	K [MPa]	n	m [s]	p
Al/Cu Composite	2850	875	512-660	408	0.054	8x10 ⁻⁸	0.075
Al/Li Composite	2620	875	560-590	359.5	0.06	4x10 ⁻⁹	0.06

The results are presented in two forms, viz., typical stress-strain curves at a range of strain rates for the two MMC materials (see Figures 5.14 and 5.15), and plots of flow stress ratio as a function of strain rate for one level of strain (see Figure 5.18). The typical stress-strain curves of Figures 5.14 and 5.15 should be used as a guide to the shape of the curve, keeping in mind that Figure 5.18 shows that changes in the strength with strain rate at a certain strain level.

Figures 5.14 and 5.15 show the dynamic stress-strain curves for Al/Cu and Al/Li MMCs respectively. Superimposed on these graphs are the stress-strain curves obtained from quasi-static tests at low strain rates ($\sim 10^{-3} \text{ s}^{-1}$) using the conventional screw-driven Instron testing machine. For easy of comparison the same scale is used for these two figures.

Generally, the dynamic curves show a distinct strain rate effect when compared to the quasi-static curve. In the range of the experiment, it appears that at low strain rate the flow stress increases continuously with strain, but at strain rates in the range of 10^3 to 10^5 s^{-1} a nearly constant flow stress appears. It can be seen that, the dynamic flow stress is affected differently at constant strain rate. As the strain increases the strain rate sensitivity decreases.

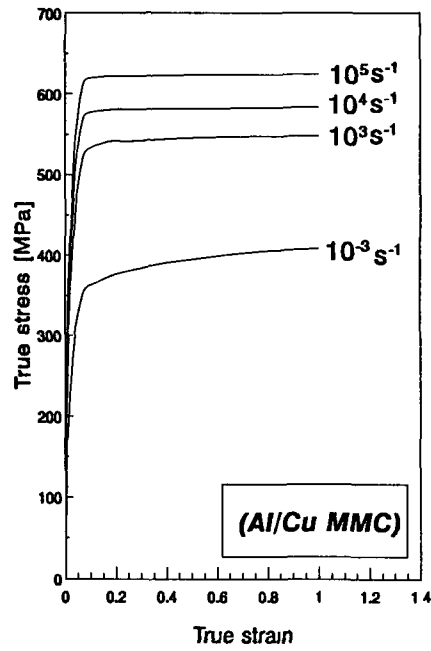


Figure 5 14 Stress-Strain Data in Compression for Al/Cu MMC

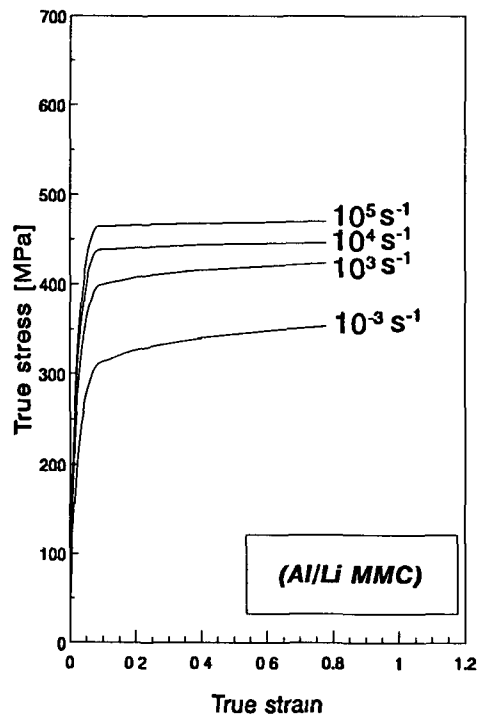


Figure 5 15 Stress-Strain Data in Compression for Al/Li MMC

5.4.4 Adiabatic and Isothermal Stress-Strain Curves

Figures 5.16 and 5.17 show the isothermal and adiabatic curves for Al/Li and Al/Cu MMC, respectively.

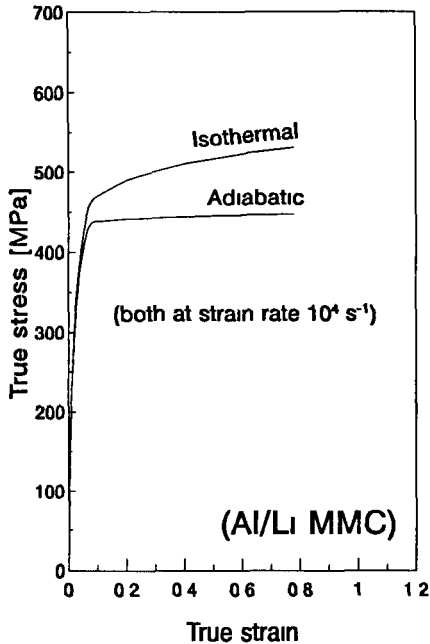


Figure 5.16 Isothermal and Adiabatic Curves for Al/Li MMC

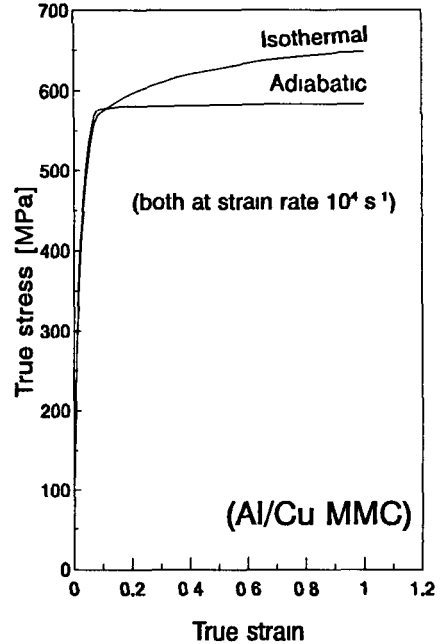


Figure 5.17 Isothermal and Adiabatic Curves for Al/Cu MMC

The initial estimation of the maximum rise in the bulk temperature, in the case of Al/Li MMC is 144 °C at impact speed 102 of ms^{-1} , and for Al/Cu MMC is 214 °C at impact speed 130 ms^{-1} . It should be noted that, in case of MMC materials, an assumption that all the work is converted into heat ($f=1$ in equation 3.10) is made, this will lead to some error as, in reality, a percentage of the work is not converted to heat. The differences in the flow stress between the isothermal and adiabatic conditions have been shown to be quite substantial. It can be seen that as the strain increases, the difference between the two curves increases. At strain rate of 10^4 s^{-1} and true strain of 0.7 the reduction in the flow stress of Al/Cu and Al/Li MMCs is about 50 and 75 MPa, respectively. It can be seen that the thermal softening effect is significant. Clearly, an isothermal model would overestimate the strength of the material and lead to erroneous prediction of the impact response.

5.4.5 Strain-Rate Sensitivity

Figure 5.18 shows the variation of the strain rate sensitivity (at a true strain of 0.5) with the logarithm of strain rate for the MMC materials, and pure aluminium. Unreinforced or pure aluminium was considered for comparison purposes. The strain rate sensitivity for the MMC at strain rate 10^3 to 10^5 s^{-1} and true strain equal to 0.12 was found to vary between 1.46 to 1.69 for Al/Cu MMC and between 1.26 to 1.46 for Al/Li MMC. At true strain equal to 0.78 the rate sensitivity varies between 1.34 to 1.54 for Al/cu MMC and between 1.19 to 1.33 for Al/li MMC.

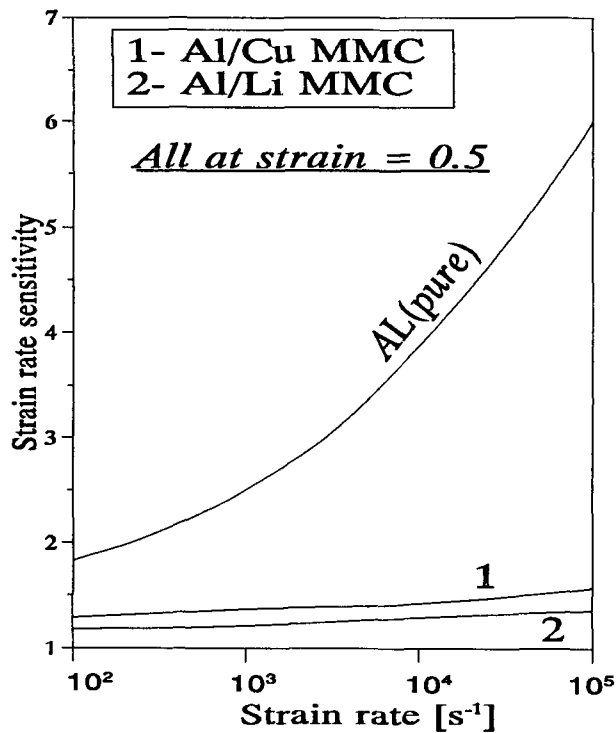


Figure 5 18 Variation of Flow Stress Ratio with Strain Rate

5 5 DYNAMIC BEHAVIOUR OF NYLON

5 5 1 Introduction

Absorbed moisture changes all the physical properties of polymers (e.g. optical, electrical). In the case of some polymers it even has a major effect on their mechanical properties. This is particularly true for thermoplastic polymers. Research has been focused on the effect of moisture on the creep behaviour of the material, quasi-static tensile properties, crack initiation, morphology of fracture, etc. On the subject of high strain rate properties of polymeric materials few studies have been carried out [5.19-5.23]. To the author's knowledge, there is no work reported on the effect of moisture content on the mechanical properties of polymers (such as nylon) at high-strain-rates. In this section, the effect of moisture content on the static and dynamic compressive flow stresses of nylon is examined

5.5.2 Primary Remarks

Nylon has been found to be particularly unstable, the environment in which the nylon is to be used needs to be considered when planning experiments relevant to an end use [5.24]. So if any trend in the behaviour is to be seen from low to high strain rates, tests must be done on specimens from the same batch, within a reasonably short period of time. In the experiments reported here, all the specimens are from the same batch and the experimental work was completed within a one month period.

5.5.3 Low Strain Rates

Figure 5 19 shows the compressive stress-strain curves for dry and fully saturated nylon. The effect of moisture on the mechanical properties of the nylon is very marked. The flow stress of fully saturated nylon is nearly half the dry nylon. It is clear from this figure that there is also a small reduction in the elastic modulus. Unloading was also measured, though not down to zero stress level. It was also observed that the fully saturated samples have a higher strain to fracture than the dry ones. This behaviour is indicative of water acting as a mild plasticizer for nylon. The strength of nylon was restored to its original characteristics after drying the fully saturated samples in an oven

for 10 hrs at a temperature of 65 °C.

The compressive yield stress is shown in Figure 5.20 for test samples having different levels of moisture content. It can be seen that with the increase of water concentration, the compressive yield stress decreases in nearly a linear manner. The dry samples have the highest compressive yield strength (57 MPa).

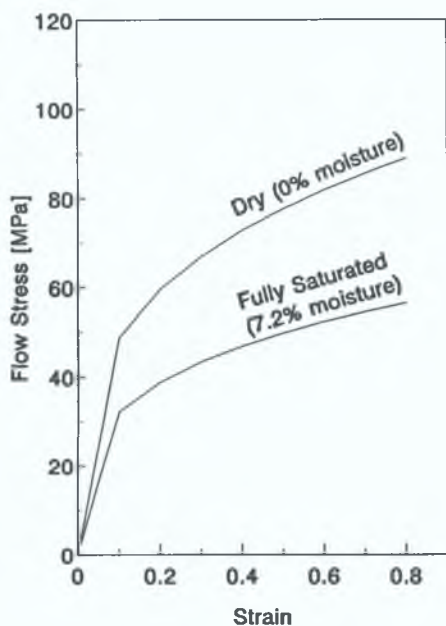


Figure 5.19 Quasi-Static Stress-Strain Curves of Nylon.

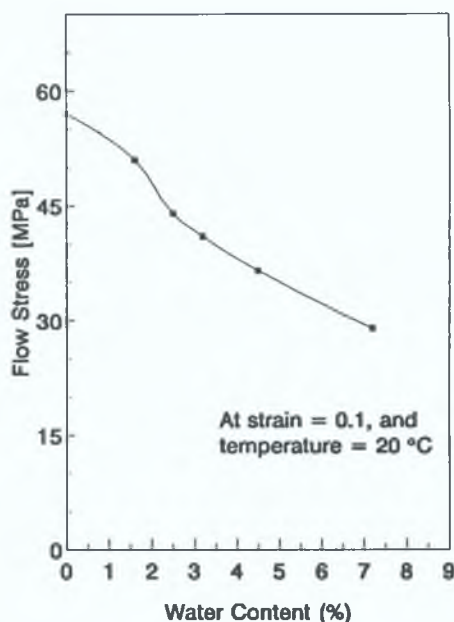


Figure 5.20 Variation of Compressive Yield Stress with Water Content.

5.5.4 Dynamic Stress-Strain Curves

Flow Stress Model: In this section, a proposal is made for a modified version of the Hashmi-Hamouda constitutive law (equation 3.9) [5.25], initially developed for metals subjected to high strain rates and large deformation.

$$\sigma_d = K(T) \varepsilon^{n(T)} \left[1 + (m(\phi) \dot{\varepsilon})^{p(\phi)} \right] \quad (5.2)$$

where K is the strength coefficient, n is the strain hardening index constant, ε is the total true strain, $\dot{\varepsilon}$ is the total true strain rate, T is the temperature, m and p are the material's strain rate sensitivity, and ϕ is the moisture content.

The constitutive equation (5.2) was implemented in an explicit finite-difference code developed by the author [see Appendix B] for the analysis of large, dynamic deformation of solids. By iterative computation the constants m and p of the constitutive equation were established for close agreement between the experimental and simulated results in terms of the final dimensions of the deformed test specimens. The experimental and computed results were compared in terms of the final dimensions of the deformed test specimens with impact speed, and the percentage discrepancy between the two was found to be 4.0 percent maximum. The best fit constants for the nylon investigated in this work are shown in Table 5.5

Table 5.5 *Material Constants in the Constitutive Law of Nylon*

Material	Description			Strain Rate Sensitivity			
	Density [kg/m ³]	Specific Heat [J/kg K]	Melting Temperature [°C]	m	p	m	P
Nylon 6	1591.5	2490	210	0.004	0.1	0.004	0.15

Using these material constants and applying them to equation (5.2), the dynamic stress-strain curves at high strain rate can be plotted. Figure 5.21 shows the dynamic stress-strain curves at different strain rates for dry and wet conditions, together with the quasi-static curve for dry condition. It can be seen that for dry specimens the stress-strain curves showed greater strain hardening than the curves obtained at higher strain rates for wet specimens. This was probably because of improved lubrication for wet specimens.

5.5.5 Strain Rate Sensitivity

Figure 5.22 shows the influence of strain rates, $\dot{\epsilon}$, on the compressive flow stress, σ . It has been found that at strain rate from 10^4 to 1 s^{-1} , the flow stress increases in a linear manner with the logarithm of strain rate. However, at very high strain rates ($\dot{\epsilon} > 10^3$), the degree of sensitivity increases dramatically. An explanation for this behaviour could be the change in the physical properties of nylon and the mode of deformation.

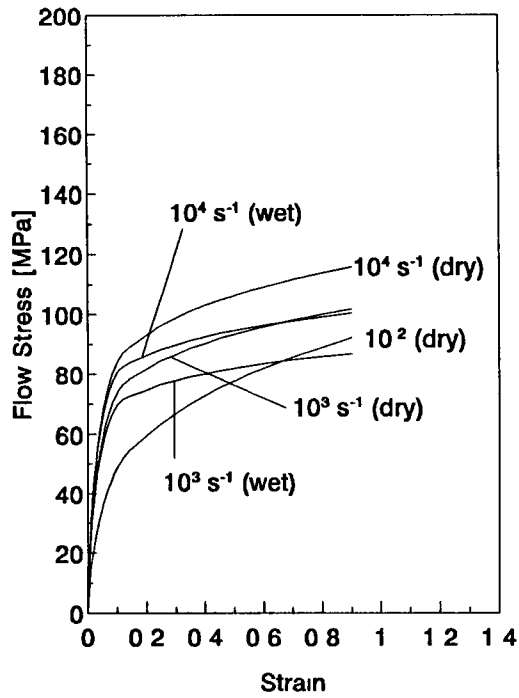


Figure 5 21 Stress-Strain Curves at Different Strain Rates for Dry and Wet Nylon

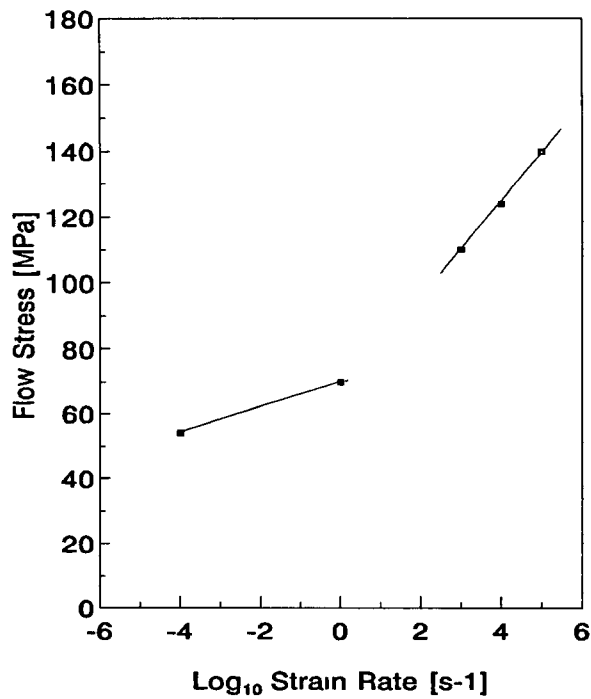


Figure 5 22 Flow Stress versus Log Strain Rate

5.5.6 Thermal Softening Effect.

The high strain rate deformation of material leads to the conversion of mechanical energy into heat. Depending on the mode of deformation this heating may produce a more uniform bulk temperature rise. The temperature rise produced during these processes can be very high and for polymers can lead to thermal decomposition or degradation [5.26] In this study, the temperature rise (ΔT) in the specimen during large plastic deformation was estimated as follows;

$$\Delta T = \frac{f}{\rho s} \int_{\varepsilon}^{\varepsilon+\Delta\varepsilon} \sigma (\varepsilon, \varepsilon, T) d\varepsilon \quad (5.3)$$

where ρ is the density, s is the specific heat, and f is the portion of the work of deformation converted into heat energy. Swallowe *et al* [5.26], reported that the value of f for nylon-6 is 0.95. The values of s and ρ are 1.4 J/kg K and 1591.5 kg/m³ respectively according to the manufacturer [5.17]. The specific heat, s , is assumed to be independent of the stress level and the material is treated as incompressible

The initial estimation of the maximum rise in the bulk temperature is about 50 °C at impact speed of 75 ms⁻¹ and strain equal to unity. During the simulation process, at each strain increment the temperature is updated based on the plastic work using equation (5.3). The computation is done in small incremental steps, which allows the stress to be calculated as a function of temperature. Since this rise in temperature is known to have an effect on the material properties it was thought essential to find a general form, temperature dependent equation, for nylon over temperatures ranging from room temperature up to 200 °C. The temperature dependency parameters were expressed in linear regressive forms as,

$$K(T) = K_0 - 0.47 T \quad (5.4)$$

$$n(T) = n_0 - 1.45 \times 10^{-3} T \quad (5.5)$$

where K_0 and n_0 are material's constants and, T is the maximum rise in the bulk temperature [°C]. The value of K_0 and n_0 are 95 MPa and 0.29 respectively, based on experimental results.

5.6 FACTORS AFFECTING STRAIN RATE SENSITIVITY

5.6.1 Interfacial Friction Effect

Interfacial friction can affect the stress level required to deform a specimen in compression mode. This effect can, however, be minimised by the use of efficient lubricant. In the present study, petroleum jelly was used to lubricate all the interfacing areas. Walley *et al.* [5.23] reported that petroleum jelly gives the lowest friction (almost zero) for similar experiments on nylon and copper. Thus it may be assumed that the friction effect is insignificant and hence was not accounted for.

5.6.2 Inertia Effects

It is now well accepted that under dynamic loading condition the specimen requires higher stress to deform larger specimens of the same material. This is due to the fact that a proportion of this stress is used up to generate radial motion. For heavier material and larger specimen this stress enhancement can be considerable. For smaller specimens and lighter material this effect is often demonstrated to be insignificant [5.27]. Maiden and Green [5.28] reported that the inertia effect can be as high as 10% at strain rates of 10^4 s^{-1} . Recently, it was shown by Gorham [5.29 and 5.30] that there is no specimen geometry for which inertia is identically zero. In this study, the inertia effect has been accounted for by means of equation (3.35). The extent of the effect of radial inertia calculated using equation (3.35) for tests giving rise to strain rates of 10^3 and 10^5 s^{-1} is found to vary between 1 to 10 percent.

5.6.3 Temperature Rise During Deformation

During plastic deformation the plastic work manifests itself in terms of increase in temperature of the specimen. This rise in temperature can have significant effect for materials having lower melting temperature, especially under high speed loading situations where virtually adiabatic conditions prevail. It was therefore thought that the inclusion of temperature effects during numerical simulation was imperative and hence temperature dependent equations were established before proceeding to determine the dynamic stress-strain properties. The works reported in references [5.26, 5.27, 5.31, 5.32] quantify the level of temperature rises estimated in this study and reinforce the need for the incorporation of temperature effect in dynamic testing

5.6.4 Energy Dissipation During Impact

Consider the experimental arrangement shown in Figure 5.23, where the kinetic energy of the impacting projectile is available for dissipation after impacting against the specimen. At the moment of maximum compression the velocity of the projectile will have been reduced to zero.

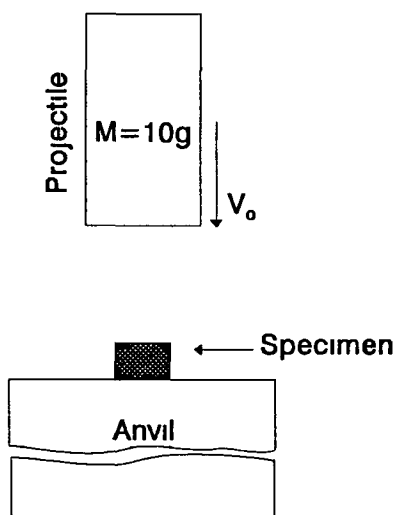


Figure 5.23 *Experimental Arrangement*

As discussed in chapter three, the kinetic energy is dissipated in the following ways, (i) as work done on the cylindrical specimen, a large fraction of this will be dissipated plastically (most of this energy results in a rise in temperature of the specimen), but a small portion will remain as elastic strain energy. The latter is recoverable and on unloading will manifest itself as vibrational energy; and (ii) transmission to the anvil foundation as elastic waves.

Some energy will be radiated as sound and some in doing work against interfacial friction, but the latter is considered to be negligible for well-lubricated specimens. Though elastic recovery of the test specimen and unloading of the projectile are not independent, the total unloading process results in the projectile rebounding to a certain height.

The energy lost as elastic strain in the projectile and anvil was found to vary with the initial impact speed, where, as the impact speed is increased the energy loss is also increased. In the case of steel the elastic strain energy loss was estimated to be between 0.7 to 0.8 % at speeds between 52.2 to 150 ms⁻¹ respectively. The energy loss due to friction was neglected, due to use of an effective lubricant, and the fact that uniform deformation was observed. The energy loss in sound and vibration in the apparatus was assumed to be very small about 0.5%.

The elastic energy stored in the specimen was estimated to be ~0.5% (using equation 3.51). Part of the total kinetic energy is reconverted into kinetic energy of the rebounding projectile. The rebound energy was estimated to be as ~4% of the initial kinetic energy the projectile. The total energy loss in the present system was found to be 5% of the initial kinetic energy maximum.

The main objective of this section is to see how the energy losses affect the dynamic flow stress. Losses up to 20% (which may be the maximum) were assumed and the dynamic flow stress was recalculated. Figure 5.24 shows the variation of strain rate sensitivity of the steel (EN-9) with the energy losses. It is evident from this figure that

as the energy losses increases, the flow stress decreases in an approximately linear manner.

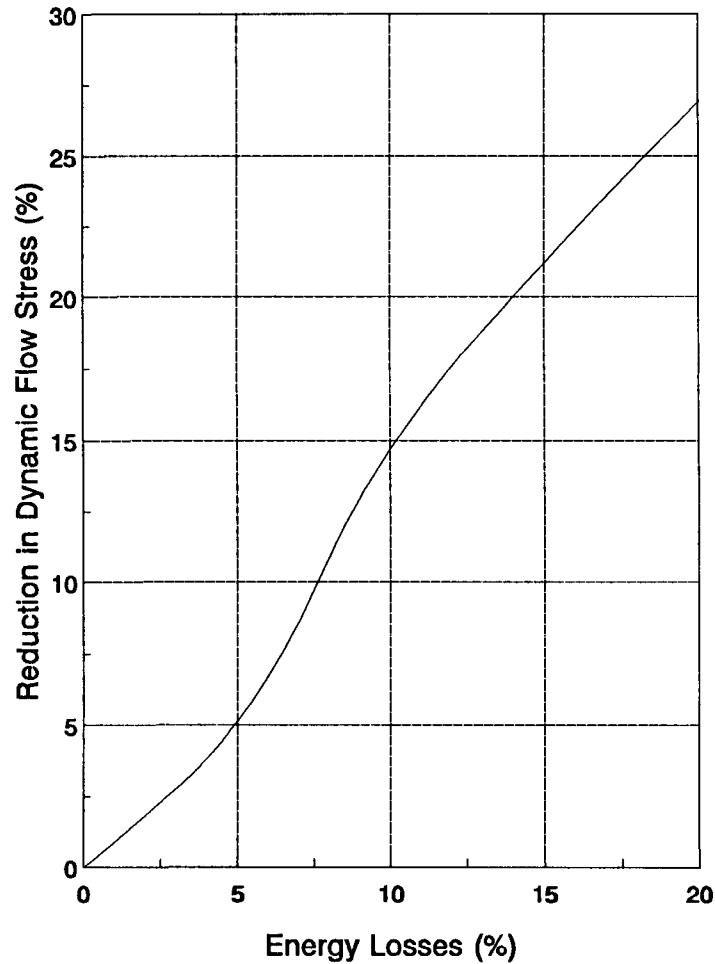


Figure 5.24 Variation of Dynamic Flow Stress of Steel with the Energy Losses

It is worth noting that the results presented here have been obtained assuming no loss in the kinetic energy due to impact, which may cause an overestimate of the dynamic flow stress. Hawkyard *et al.* [5.33] estimated the resilient energy to be less than 1 percent of the original kinetic energy, for the range of their experimental work, which would imply that no significant error will occur as a result of the neglect of this loss. However, a simple argument suggests that the calculated dynamic flow stress (σ_d) might be reduced by up to 5%.

5.7 VERIFICATION OF THE DEVELOPED CONSTITUTIVE LAW

5.7.1 Introduction

As mentioned before, the material's strain rate sensitivity constants (m & p) in the developed constitutive law were established by imposing close agreement between the experimental and computed results in terms of the final dimensions of the deformed specimen. The main difficulty with this procedure is the lack of uniqueness in the solution even if the experimental results are accurately predicted by the proposed constitutive law. At present, the capabilities of any advanced engineering or physically based law are validated through the law's ability to match various other salient features of the experimentally measured data (such force-time history). In this section, the experimentally obtained force-time history reported by Hashmi in reference [5.34] are compared with the simulated results obtained using the finite-difference code and the developed constitutive law. Furthermore, in order to extend the range of the experimental data ($\dot{\epsilon} = 400 \text{ s}^{-1}$), drop hammer tests were performed and compared

5.7.2 High Strain Rates Tests

In reference [5.34] Hashmi has used an air-gun apparatus to fire cylindrical projectiles of 25 mm length and 9.4 mm diameter into a rigid anvil at impact speeds of 100, 140 ms^{-1} . The projectiles were machined from pure commercially copper rods.

The impact load was measured using a Kistler 9081 piezo-electric load cell. The load cell had a capacity of 160 tonnes and natural frequency of 50 kHz. A Kistler charge amplifier type 5001 with a built in 33 kHz filter was used to amplify the signal from the load cell and eliminate any undesirable oscillations. A datalab DL-905 transient recorder was used to store the amplified signal from the load cell and then on a Telequipment D65 Oscilloscope and/or Hewlett Packard X-Y record type 7045-A.

In this study, a simulation of Hashmi's tests was carried out using the finite-difference computer code and the developed constitutive law. Figures 5.25 and 5.26 show the variation of the impact force with time for two impact velocities 100 and 140 ms^{-1}

respectively. It is evident from these figures that the theoretically predicted and experimentally recorded load-time histories for various impact velocities show good qualitative agreement during the contact period of up to 35 μ s. The lack of good correspondence at final stages of the contact period would not effect the validity of the technique since most of the deformation is completed, and the force rises to the maximum within the initial 10 μ s. It can also be seen that the experimentally recorded traces show considerable ripples in their shape. The cause of appreciable ripple in the experimental results may partly be attributed to the stress wave propagation through the anvil.

In order to demonstrate the effect of temperature rise during deformation, isothermal and adiabatic force-time traces were also plotted in Figure 5.25 and 5.26. Comparisons between the experimental and theoretical results in terms of the final dimensions of the projectile were also made and close agreement were obtained [5.35]

5.7.3 Intermediate Strain Rates Tests ($10^2 < \dot{\epsilon} < 10^3 \text{ s}^{-1}$)

Figures 5.27 (a), (b) and (c) show the force-time traces for copper, Al/Cu MMC and Al/L1 MMC respectively. Superimposed on those figures are the theoretically obtained force-time traces. It can be seen from this figures that the theoretically predicted maximum load is higher than the experimental one by 12%, 7%, and 6% for copper, Al/Cu MMC and Al/L1 MMC respectively. The experimentally obtained maximum load is 89, 81, and 75 kN at contact time of 2.1, 1.8, and 2.0 ms for copper Al/Cu MMC and Al/L1 MMC respectively. It can also be seen that the predicted total contact time less than the experimental one by ~ 1 ms for all the materials tested. It should be mentioned that cracks were apparent in all the metal matrix composite samples.

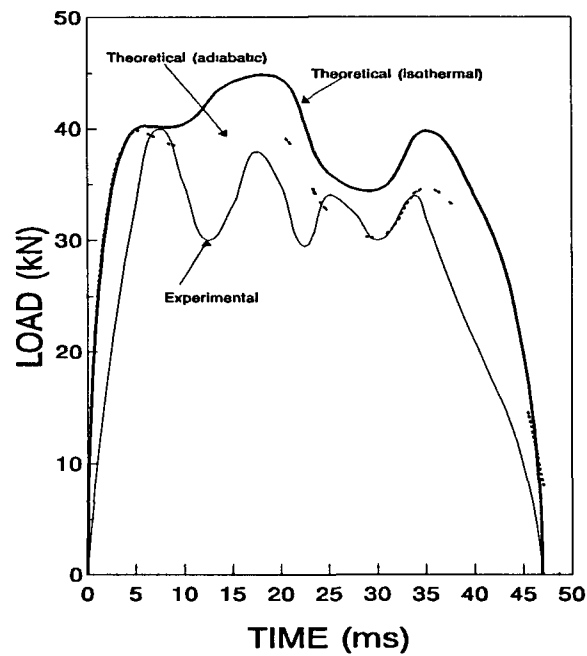


Figure 5 25 Comparison of Experimentally Obtained Force-Time History with those Predicted Theoretically for Impact Speed of 100 ms^{-1}

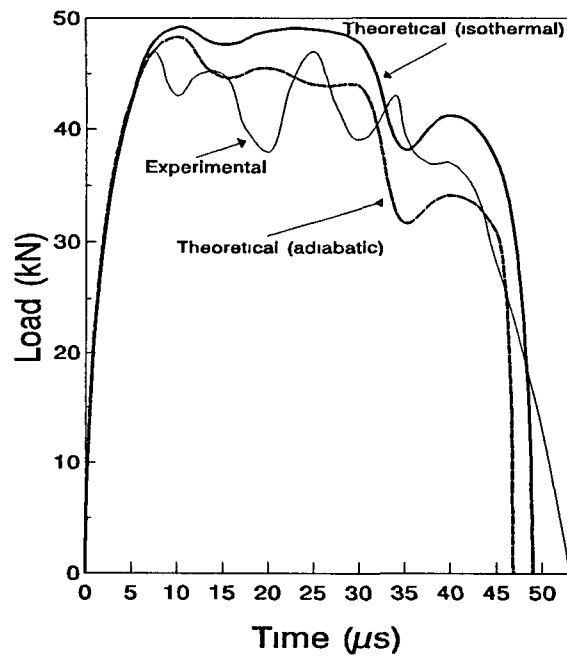


Figure 5 26 Comparison of Experimentally Obtained Force-Time History with those Predicted Theoretically for Impact Speed of 140 ms^{-1}

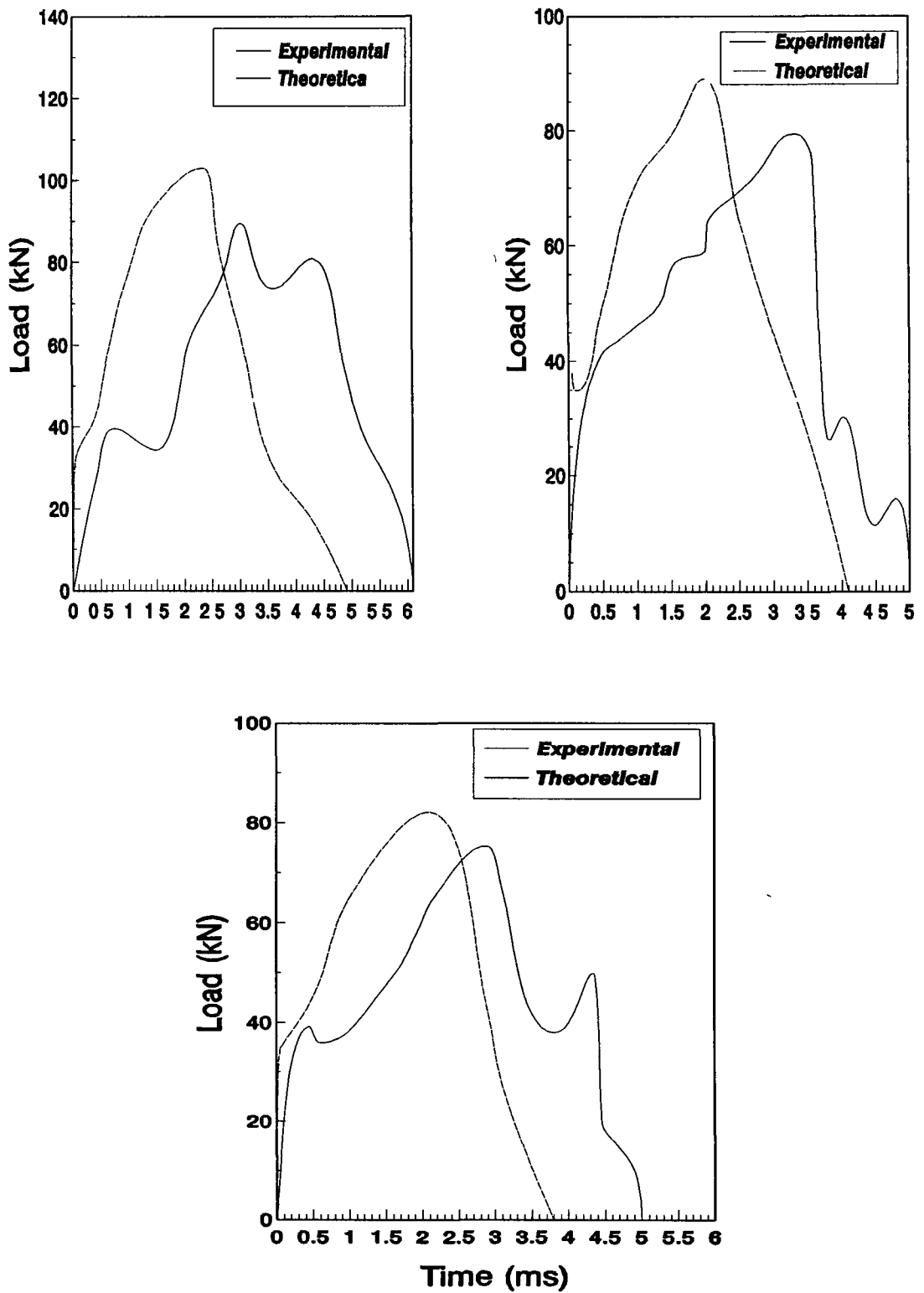


Figure 5 27 Comparison of the Experimentally Obtained Force-Time History with those Predicted Theoretical for (a) Copper (b) Al/Cu MMC and (c) Al/Li MMC of the Drop Hammer Tests

CHAPTER SIX: GENERAL CONCLUSIONS

6.1 INTRODUCTION

Chapter six provides a summary of the main headings of the current thesis. It is divided into four sections: the first defines the problem under consideration, the second identify the techniques adopted in tackling the problem; the third provides a brief summary of the conclusions and the fourth identifies the different aspects of the research which require further studies.

6.2 STATEMENT OF PROBLEM

Constitutive equations are functional relationships between sets of independent parameters describing the response of materials to mechanical, thermal and shock loading. Such equations may be modelled based on either microscopic or macroscopic approaches which are generally verified experimentally.

Recently, with the advent of numerical methods in large deformation analysis, such as the finite-element and finite-difference methods, the development of realistic rate-dependent constitutive laws has become an integral part of the design process. The development of such laws relies on the determination of the constants needed to describe the deformation state of the material under high rates of deformation. Indeed, such combined theoretical and experimental techniques generally yield a complete description of the material flow stress and its dependency upon temperature, strain and strain-rate.

Several constitutive equations exist in the literature, most of these equations describe strain-rate, cyclic dependent plastic behaviour under mostly quasi-static strain rate regimes. This may be due to the complexity of the phenomena associated with high rate loading and may be due to the difficulties associated with the experimental verification of the results. As a result, very few rate-dependent constitutive equations have been

developed; (see chapter two for details). It was therefore the objective of this work to develop a novel, rate-dependent constitutive law which is capable of describing the rate-dependent elasto-plastic behaviour of three classes of engineering materials: metallic alloys, metal-matrix composites and nylon.

6.3 SUMMARY OF THEORETICAL AND EXPERIMENTAL INVESTIGATIONS

In this study, both theoretical and experimental investigations were conducted. In the theoretical investigations, finite-difference algorithms were developed to describe the elasto-plastic behaviour of the examined materials using a novel constitutive law. The algorithms take into account the effect of inertia, friction at the interfaces, strain hardening and thermal softening. The experimental work used a ballistic test rig to obtain the materials constants and to verify the theoretical predictions

6.4 GENERAL CONCLUSIONS

The conclusions resulting from the current study are summarized under the appropriate headings.

6.4.1 A Novel Constitutive Law

- (i) A novel constitutive law which covers a wide range of strain rates and accounts for large deformation, inertia effects, thermal softening, and work hardening was developed.
- (ii) The constants for the developed constitutive law were obtained based on experimental tests at strain rates between $10^3 < \dot{\epsilon} < 10^5 \text{ s}^{-1}$, and hence justification for relying on the equation outside the range of the test data is limited.
- (iii) The basic form of the model is readily adaptable to most computer codes, since it uses variables ($\dot{\epsilon}$, ϵ , T) that are available in the codes.
- (iv) The main advantages of the model are (1) simple to implement, (2) does not required excessive computing time or memory. (3) it can be used for a variety of materials, (4) allows constants to be readily obtained from a limited number of laboratory tests, and (5) enables the effects of the important variables to be identified and separated. The primary disadvantage of this model is that it is phenomenological, and therefore, exceptional care must be exercised when using it for extrapolated values of strain, strain rate, and temperature.

6 4 2 Dynamic Behaviour of Metallic Alloys

- (i) The dynamic flow stress is a function of both strain and strain rate. As the strain increases, the rate of increase of dynamic flow stress decreases (due to thermal softening).
- (ii) It has been found that the dynamic flow stress for all the metallic materials investigated here is always higher than the static flow stress at a certain strain.
- (iii) Steel was found to have higher sensitivity than copper and brass.
- (iv) The effect of thermal softening in flow stress is greater in the case of steel than the other materials (copper, brass, aluminum).

6 4.3 Dynamic Behaviour of Composite Materials

- (i) The quasi-static results indicate that the presence of reinforcement increases the compressive strength (about 4 times more than pure aluminium), but also has a substantial effect on the fracture strain of MMCs as compared with pure materials
- (ii) The effect of thermal softening in flow stress is greater in the case of Al/L1 MMC than the Al/Cu MMC.
- (iii) The strain rate sensitivity of Al/Cu MMC is higher than that of the Al/L1 MMC, at strain rates ranging between 10^3 to 10^5 s⁻¹.
- (iv) The present study suggests that for pure aluminum the plastic deformation shows a transition from thermal activation mechanism to visco-drag mechanism at strain rate of about 10^4 s⁻¹. However, for the MMC's investigated here, no transition mechanism is evident even at strain rate of 10^5 s⁻¹. The Al/Cu MMC shows more strain rate sensitivity and ductility than the Al/L1 MMC.

6.4.4 Dynamic Behaviour of Nylon

- (i) Nylon shows large changes in mechanical properties due to the plasticisation effect of water which is, in principle, a reversible process.
- (ii) Strain rate has a great effect on the stress-strain behaviour of nylon. The effect of water content on strain rate sensitivity of nylon is significant

- (iii) In both static and dynamic tests, the strain to fracture rises to a maximum value with increased water content
- (iv) A constitutive model to predict the impact response for nylon under uniaxial loading conditions has been developed. The model incorporates the effects of temperature, strain, strain rate, and water content on the uniaxial compressive-stress response.

6.5 THESIS CONTRIBUTION

The main contribution of the current results are:

- (i) the development of a finite-difference model which is capable of describing the elasto-plastic behaviour of engineering materials using a novel constitutive law,
- (ii) the examination of the effects of inertia, strain hardening, and thermal softening of three important classes of materials: metallic alloys, metal matrix composites and polymeric materials,
- (iii) the application of a simple experimental technique using a ballistic experiment rig not only to obtain material constants but also to the theoretical predictions,
- (iv) the development of a novel theoretical investigation on the effect of energy losses during impact on the dynamic flow stress.

6.6 RECOMMENDATION FOR FUTURE WORK

- (i) To use manganin and constantan strain gauges for measuring stress-time history during impact, as the piezo-load cells usually are limited by frequency.
- (ii) To implement the developed constitutive law into commercial software such as; DYNA3D and simulate some practical cases This will require the development of FORTRAN subroutines.
- (iii) Modification of the developed rate-dependent constitutive law to cater for the effects of deformation history.
- (iv) To obtain the dynamic properties of brittle materials such as glass, ceramic, and shape memory materials.
- (v) To study the effect of specimen configurations and size on the materials strain rate sensitivity.
- (vi) Extensive experimental data is needed in order to give a clearer picture of the effects of the dynamic deformation on the microstructure.
- (vii) To modify the developed constitutive law to account in a unified sense, for many of the characteristic features of MMC. These include; (i) A significant difference in tensile and compressive strengths, (ii) increasing brittleness of the material (higher strength lower strain to fracture), (iii) increasing stiffness with increasing volume fraction of particles, (iv) effect of localized yielding, particle/matrix interface decohesion, and damage accumulation prior to fracture.

REFERENCES

CHAPTER ONE

- [1.1] BLESS, S J. and ANDERSON, Jr. C.E : Penetration of hard layers by hypervelocity rod projectiles, *Int J Impact Engng.*, 1993, **14**, 85.
- [1.2] ANDERSON, Jr. C.E, and WALKER, J.D.: Examination of long rod penetration, *Int. J. Impact Engng.*, 1991, **11**, 481.
- [1.3] SALEM, S A L and AL-HASSANI, S.T.S. · Penetration by high speed oblique jets: theory and experiment, *Int. J. Mech. Sci.*, 1983, **25**, 871.
- [1.4] GARDNER, J.W.: Calculation of the force acting upon rigid structure from an aircraft impact, *Int. J. Impact Engng* , 1984, **2**, 345.
- [1.5] JONAS, G.H and ZUKAS, J.A. · Mechanics of penetration · analysis and experiment, *Int. J. Engng Sci.*, 1978, **16**, 879.
- [1.6] PALOMBY, C and STRONGE, W J · Blunt missile preformation of thin plates and shells by discing, *Int. J. Impact Engng.*, 1988, **7**, 85.
- [1.7] WOODWARD, R L · Penetration of semi-infinite metal targets by deforming projectiles, *Int. J Mech. Sci*, 1982, **24**, 73.
- [1 8] ANDERSON, Jr.C.E, TRUCANO, T.G and MULLIN, S.A · Debris cloud dynamics, *Int. J. Impact Engng.*, 1990, **9**, 89.
- [1 9] ANDERSON, Jr.C.E and BODNER, S R · Ballistic Impact: The status of analytical and numerical modelling, *Int. J. Impact Engng.*, 1988, **7**, 9.
- [1 10] ANDERSON, Jr C E and MORRIS, B.L.: The ballistic performance of confined Al₂O₃ ceramic tiles, *Int. J. Impact Engng.*, 1992, **12**, 167.
- [1.11] EICHELBERGER, R J and GEHRING, J.W.: Effects of Meteoroid impacts on space vehicles, *ARS Journal*, 1962, **32**
- [1 12] JONES, N and WIERZBICKI, T · *Structural Crashworthiness*, 1983, (Butterworth Press).
- [1 13] WIERZBICKI, T and JONES, N.: *Structural Failure*, 1989, (John Wiley).
- [1 14] JONES, N and WIERZBICKI, T.: *Structural Crashworthiness and Failure*, 1993, (Elsevier Applied Sci).

- [1.15] REID, S.R.: *Metal Forming and Impact Mechanics*, 1985, (Pergamon Press).
- [1.16] PEDERSEN, P *et al.*: Ship Impacts: Bow collisions, *Int. J. Impact Engng.*, 1993, **13**, 163.
- [1.17] SALEM, S.A.L and AL-HASSANI, S.T.S.: Influence of salt addition and confinement on explosive welding parameters, *Int. J. Mech. Sci.*, 1983, **25**, 499.
- [1.18] Committee on Material response to ultra-high loading rates, in National Materials Advisory Board of the National Research Council, *Technical Report No. NMAB-356*, National Academy of Sciences, Washington, (1980).

CHAPTER TWO

- [2.1] JOHNSON, W and REID, S.R.: Metallic energy dissipation systems, *Appl. Mech. Rev.*, 1978, **31**, 277.
- [2.2] NURICK, C.N and MARTIN, J.B.: The measurement of the response of clamped circular plates to impulsive loading, in *Mechanical Properties at High Rates of Strain*, (Ed. J. Harding), Inst Phys Conf Ser 70, 1984, p.495.
- [2.3] JONES, N.: *Structural Impact*, 1989, (Cambridge University Press).
- [2.4] SYMONDS, P.S.: Survey of methods of analysis for plastic deformation of structures under dynamic loading, *Brown University, Division of Engineering Rep. No. BU/NSRDC/I-67*, (1967).
- [2.5] HASHMI, M.S.J.: Gross permanent deformation and fracture of model structures of strain rate material under internal blast, in *Mechanical Properties at High Rates of Strain*, (Ed. J. Harding), Inst Phys Conf Ser 70, 1984, p. 487.
- [2.6] SYMONDS, P.S.: Viscoplastic behaviour in response of structures to dynamic loading, in *Behaviour of Materials under Dynamic Loading*, (Ed. N.J Huffington), ASME Press, 1965, p. 106.
- [2.7] PERRONE, N.: On a simplified method for solving impulsively loaded structures of rate-sensitive materials, *J Appl Mech*, 1965, **32**, 489.
- [2.8] REID, S.R and REDDY, T.Y.: Effects of strain-rate on the dynamic lateral compression of tubes, in *Mechanical properties at High Rates of Strain*, (Ed. J. Harding), Inst Phys Conf Ser 47, 1979, p. 288.

- [2.9] REID, S.R and REDDY, T Y Response of one-dimensional metal ring systems to end impact, in *Mechanical Properties at High Rates of Strain*, (Ed. J. Harding), Inst Phys Conf Ser 70, 1984, p. 471.
- [2.10] JONES, N.: Some comments on the modelling of material properties for dynamic structural plasticity, *Mechanical Properties at High Rates of Strain*, (Ed. J. Harding), Inst Phys Conf Ser 102, 1989, p.435.
- [2.11] JOHNSON, W and SLATER, R.A.C.: A comparison of the energy required for slow speed and dynamic blanking using an improved linear motor, high energy forming, *Proc. Inst. Mech. Engrs* , 1964, **179**, 257.
- [2.12] JOHNSON, W and TRAVIS, T.: *Proc. Inst. Mech. Engrs*, 1966, **180**,197.
- [2.13] KASSAR, M and YU, W.W.. Effect of strain-rate on material properties of sheet steels, *J Structural Engng* , 1992, **188**, 3136.
- [2.14] BLAZYNSKI, T.Z.: *Plasticity & Modern Metal-Forming Technology*, 1989, (Elsevier Science Publishing Co).
- [2.15] HU, P *et al.*: Numerical analysis of the influence of various factors on forming the limit of hydrostatic bulging for ductile materials, *Computers & Structures*, 1994, **50**, 677.
- [2.16] HUANG, Y.M and LIU, C.H : Effects of strain rate and anisotropy upon the sheet-stretching process, *Int. J. Mech Sci.*, 1994, **36**, 105.
- [2.17] GHOSH, A.K.: The influence of strain hardening and strain-rate sensitivity on sheet metal forming, *J. Eng. Mater. Techn.*, 1977, **99**, 264.
- [2.18] MARTENSSON, N.: On the influence of the rate of deformation at cold processing, *Acta Polytech. Scandinavica, Mech. Eng. Ser.*, 1970, **52**, 6
- [2.19] JOHNSON, W.: *Impact Strength of Materials*, 1970, (Arnold, London).
- [2.20] BERMAN, I and SCHROEDER, J W (Eds.): *High Energy Forming*, 1984, (ASME press).
- [2.21] TOBIAS, S A . The state of the art of high energy rat bulk forming, *J. Mech. Working Technology*, 1984, **9**, 237
- [2.22] THOMAS, A and DENHAM, K.: Die performance in high rate forming, *Proc 12th International MATDOR Conference*, Manchester, (1971), p. 153.
- [2.23] BOOTHROYD, G and BAILEY, J.A.: Effects of strain-rate and temperature in orthogonal metal cutting, *J. Mech. Engng. Sci.*, 1966, **8**, 264.

- [2 24] SPAANS, C.: A treatise on the streamlines and stress, strain, and strain-rate distributions, and on stability in the primary shear zone in metal cutting, *J. Engng. Ind* , 1972, **84**, 690.
- [2 25] HASHMI, M.S J · Apparent strain analysis of orthogonal machining: Allowing for the effects of strain-rate and temperature , *Proc. Inst. Mech. Engrs.*, 1980, **194**, 187.
- [2.26] OXLEY, P.L.B. and HASTINGS, W.F.: Predicting the strain-rate in the zone of intense shear in which the chip is formed in machining from the dynamic flow stress properties of work material and the cutting conditions, *Proc. Roy. Soc.*, London, 1977, **356A**, 395.
- [2.27] KOMANDURI, R K.: Maching and grinding: A historical review of the classical papers, *App. Mech. Rev* , 1993, **46**, 80.
- [2.28] BOOTHROYD, G : Review of materials processing literature 1971-1972; part 1· Materials Removal Practice, *J. Engng. Ind* , 1976, **98**, 1.
- [2.29] OXLEY, P.L B.: Rate of strain effect in metal cutting, *J. Engng Ind.*, 1963, **85**, 335.
- [2.30] LE-MAITRE, F, BIZEUL, D and WEILL, R · Contribution to the study of periodic phenomena in dynamic deformation, *C.I.R P 24th General Assembly*, (1974), Kyoto, Japan
- [2.31] OXLEY, P L B and STEVENSON, M.G : Measuring stress-strain properties at very high strain-rates using a machining test. *J. Inst. Metals*, 1967, **95**, 308.
- [2.32] CURRAN, D.R.D., SHOCKEY, D.A, and SEAMAN, L Dynamic fracture criteria for a polycarbonate, *J. Appl. Phys.*, 1973, **44**, 4025.
- [2 33] JOHNSON, J.N. dynamic fracture and spallation in ductile solids, *J Appl Phys.*, 1981, **52**, 2812.
- [2 34] GRIFFITH, A.A.: *Phil Trans Roy Soc.*, 1920, **221A**, 163.
- [2.35] IRWIN, G.R.:in *Encyclopedia of Physics*, 1958, (Springer, Berlin), **6**, 551
- [2.36] KENNY, P and CAMPBELL, J D.· *Progress in Materials Science*, 1968, (Pergamon Press), p 135.
- [2 37] KLEPACZKO, J R Application of the split Hopkinson pressure bar to fracture dynamics, in *Mechanical properties at High Rates of Strain*, (Ed. J. Harding), Inst Phys Conf Ser 47, ,1979, 201.

- [2.38] BASSIM, M.N. *et al.*: Investigation of dynamic J_{1d} for alloy steel weldments using the split Hopkinson bar, *J. Test. Eval.*, 1986, 14, 229
- [2.39] KANNINEN, M.F *et al.*: in *Mechanical Behaviour of Materials Under Dynamic Loads*, (Ed. U.S. Lindholm), Springer, New York, 1968, p96.
- [2.40] NEMAT-NASSER, S.: Dynamic deformation and failure, in *Shock Wave and High-Strain-Rate Phenomena in Martials*, (Eds. M.A. Meyers, *et al.*), Marcel Dekker Publ., New York, 1992, Chapter 1.
- [2.41] LINDHOLM, U.S.: High Strain-rate Tests, in *Techniques in Metals Research*, (Ed R.F.Bunshah), Interscience, New York, 1971, 5, part 1.
- [2.42] JANGHORBAN, K and ESMAEILLI, S.: Deformation-mechanism map for Ti-6-wt% Al alloy, *J. Mat. Sci* , 1991, 26, 3362.
- [2.43] RINEHART, J.S.: Historical Perspective Metallurgical effects of high strain-rate deformation and fabrication, in *Shock Waves and High Strain Rate Phenomena in Metals*, (Eds. M.A. Meyers and L.E. Murr), Plenum Press, New York, 1981, p 3.
- [2.44] COOPER, R H and CAMPBELL, J.D.: Testing of materials at medium rates of strain, *J. Mech. Eng Sci*, 1967, 9, 278.
- [2.45] NAKKALIL, R, HORNADAY, J.R and BASSIM, M.N.: Characterization of the compression properties of rail steels at high temperature and strain rates, *Mat. Sci. & Engng.*, 1991, A141, 247.
- [2.46] FOLLANSBEE, P.S.: High strain-rate compression testing, in *ASM Handbook*, ASM Press, 8,, p 190.
- [2.47] DUVALL, G E.: *Problems in Shock Waves Research*, (Eds. R.W Rohde *et al.*), Plenum Press, New York, 1973, p 1.
- [2.48] HARDING, J.. Review of dynamic testing techniques and material behaviour, in *Mechanical Properties at High Rates of Strain*, (Ed J. Harding), Inst Phys Conf Ser 21, 1974, p 3.
- [2.49] CAMPBELL, Dynamic Plasticity: Macroscopic and microscopic aspects, *Mat. Sci. Eng* , 1973, 12, 3.
- [2.50] HARDING, J · High-rate straining and mechanical properties of materials, in *Explosive Welding, Forming and Compaction*, (Ed. T.Z Blazynski), Applied Science Pub., New York, 1983.
- [2.51] LOIZOU, N and SIMS, R.B.: The yield stress of pure lead in compression, *J. Mech. Phys. Solids*, 1953, 1, 234.

- [2.52] HOCKETT, J.E.: Compression testing at constant true strain-rates, *Proc. ASTM*, 1959, **59**, 1309.
- [2.53] HOCKETT, J.E and ZUKAS, E.G.: The response of iron to dynamic compression, in *Mechanical Properties at High Rates of Strain*, (Ed. J Harding), Inst Phys Conf Ser 21, 1974, p 53.
- [2.54] CLARK, D.S and DUWEZ, P E : Discussion of the forces acting in tension impact tests of materials, *J. App. Mech.*, 1948, **15**, A243
- [2.55] NIORDSON, F.I.: A unit for testing materials at high strain-rates, *Exp. Mech.*, 1965, **5**, 29.
- [2 56] HOGGATT, C.R and RECHT, R.F.: Stress-strain data obtained at high strain-rates using an expanding Ring, *Exp Mech.*, 1969, **9**, 441.
- [2 57] RAJENDRAN, A M and FYFE, I M : Inertia effects on the ductile failure of thin rings, *J Appl. Mech.*, 1982, **104**, 31.
- [2 58] WARNES, R H *et al.*: An improved technique for determining dynamic material properties using the expanding ring, in *Shock Waves and High-Strain-Rate Phenomena in Metals*, (Eds. M.A. Meyers and L.E Murr), Plenum Press, New York, 1981.
- [2 59] LENGYEL, B and MOHITPOUR, M.: Dynamic stress-strain data at large strains, *J Inst Metals*, 1972, **100**, 1
- [2.60] HOLZER, A.J and BROWN, R H.: Mechanical behaviour of metals in dynamic compression, *Trans ASME*, 1979, **101**, 238.
- [2.61] KOLSKY, H · An investigation of the mechanical properties of materials at very high rates of loading, *Proc Phys Soc. Lond., B*, 1949, **62**, 767.
- [2.62] HOPKINSON, J.: Further experiments on the rupture of iron wires, *Proc Manchester Lit and Phil. Soc.*, 1872, **II**, 119.
- [2 63] HOPKINSON, J On the rupture of iron by a blow, *Proc Manchester Lit and Phil Soc.*, 1872, **II**, 40.
- [2 64] HOPKINSON, B.: The effect of momentary stresses in metals, in *Scientific papers*, Cambridge University Press, 1905, p 49.
- [2 65] HOPKINSON, B.: The pressure of a blow, in *Scientific papers*, Cambridge University Press, 1912.

- [2.66] HOPKINSON, B.: A method of measuring the pressure produced in the detonation of high explosive or by the impact of bullets, *Phil. Trans. Roy. Soc. Lond. A*, 1914, **213**, 437.
- [2 67] DAVIES, R.M. A critical study of the Hopkinson pressure bar, *Proc Roy. Soc. Lond.*, 1946, **240A**, 375.
- [2 68] LINDHOLM, U.S.. Some experiments with the split Hopkinson pressure bar, *J. Mech. Phys. Solids*, 1964, **12**, 317.
- [2.69] NICHOLAS, T.: Material behaviour at high strain-rates, in *Impact Dynamics*, (Eds J Zukas *et al.*), J. Wiley & Sons Pub., New York, 1982.
- [2 70] NICHOLAS, T Measurement material properties for high rate deformation processes, *AEWAL-TR-81-4176*, (1982)
- [2.71] HARDING, J; WOOD, E D and CAMPBELL, J D Tensile testing of materials at impact rates of strain, *J Mech. Eng. Sci* , 1960, **2**, 88
- [2.72] ALBERTINI, C and MONTAGNANI, M.: Testing techniques based on the split Hopkinson Bar, in *Mechanical Properties at High Rates of Strain*, (J Harding), Inst Phys Conf Ser 21, 1974.
- [2 73] NICHOLAS, T : Tensile testing of materials at high rates of strain, *Exp. Mech* , 1980, **21**, 177
- [2.74] DUFFY, J, CAMPBELL, J.D and R.H. HAWLEY.: On the use of a torsional split Hopkinson bar to study rate effects in 1100-Aluminum, *J Appl. Mech.*, 1971, **38**, 83.
- [2.75] FRANTZ, R A and DUFFY, J : The dynamic stress-strain behaviour in torsion of 1100-Aluminum subjected to sharp increase in strain-rate, *J. Appl Mech* , 1972, **39**, 939.
- [2.76] BAKER, W.W and YEW, C.H.: Strain-rate effects in the propagation of torsional plastic waves, *J Appl Mech.*, 1966, **33**, 917.
- [2 77] NICHOLAS, T. Strain-rate and strain-rate history effects in several metals in torsion, *Exp. Mech* , 1971, **11**, 370.
- [2 78] TAYLOR, G I The use of flat ended projectile for determining dynamic yield stress: Par-I Theoretical Considerations, *Proc Roy. Soc* , Lond , 1948, **A194**, 289.
- [2.79] WIFFENS, A.: The use of flat ended projectile for determining dynamic yield stress: Par-II Experimental Considerations, *Proc. Roy. Soc.*, Lond , 1948, **A194**, 300

- [2.80] HAWKYARD, J; EATON, D and JOHNSON, W.: The mean dynamic yield strength of copper and low carbon steel at elevated temperature from measurement of the mushrooming of flat ended projectile, *Int J. Mech. Sci.*, 1968, **10**, 929.
- [2 81] HAWKYARD, J · A theory for the mushrooming of the flat-ended projectiles impinging on a rigid anvil, using energy consideration. *Int J. Mech. Sci* , 1968, **11**, 313.
- [2 82] HUTCHING, I. M and O'BRIEN, T J.: Normal impact of metal projectiles against a rigid target at low velocities, *Int. J. Mech. Sci.*, 1981, **23**, 255.
- [2.83] BALENDRA, R and TRAVIS, F.W.: An examination of the double frustum phenomena in the mushrooming of cylindrical projectiles upon high speed impact with a rigid anvil, *Int. J. Mech Sci* , 1971, **13**, 495.
- [2.84] ERLICH, D and CHARTAGNAC, J.: in *J. Phys Colloq C5*, (1985), 46, 455.
- [2 85] GILLIS, P and JONES, S A direct correlation of strength with impact velocity in Taylor test, *J. Engng. Mat. & Tech.*, 1989, **111**, 327.
- [2.86] KUSCHER, G.: Nicht-lineare ausbreitung elasto-plastischer wellwn in staben, Ernst-Mach-Inst. (EMI), (1985), (in German), Also referred by Stulp, A.J and Hohler:in *High Velocity Impact Dynamics*, Chapter 5 (1990) (Ed., Zukus, A), John Wiley & Sons, Inc.
- [2 87] WILKINS, M L and GUINAN, M W · Impact of cylinders on a rigid boundary, *J Appl. Phys* , 1973, **44**, 1200.
- [2 88] JOHNSON, G.R and COOK, W.: A constitutive model and data for metals subjected to large strains, high strain-rates and temperatures, *Procs. 7th Int. Symp. on ballistics*, Haque, The Netherlands, (1983), p. 541
- [2.89] JOHNSON, G R and HOLMQUIST, T J.: Evaluation of cylinder-impact test data for constitutive model constants, *J. Appl. Phys*, 1988, **64**, 3901
- [2 90] DYMAT'85.: *First International Conference on Mechanical and Physical Behaviour of Materials Under Dynamic Loading*, 1985, France
- [2.91] CLIFTON, R.J : Some recent development in plate impact experiments, in *Propagation of Shock Waves in Solids*, ASME Press, New York, 1976.
- [2 92] CLIFTON, R.J and KUMAR, P.: Dislocation configurations due to plate impact, *IUTAM Symposium on High Velocity Deformation of Solids*, (Eds K Kawata, and J. Shioiri), Springer-Verlag, New York, 1977, p 36.

- [2 93] KIM, K S and CLIFTON, R.J.: Pressure-shear impact of 6061-T6 aluminum, *J. Appl. Mech* , 1980, **47**, 11.
- [2.94] WATSON, H, Jr. and RIPPERGER, E.A : Dynamic stress-strain characteristics of metals at elevated temperatures, *Exp Mech.*, 1969, **9**, 289.
- [2.95] KARNES, C H and RIPPERGER, E A., Strain rate effects in cold worked high-purity aluminum, *J. Mech. Phys. Solids*, 1966, **14**, 75.
- [2 96] CHALUPNIK, J.D and RIPPERGER, E A.: *Exp. Mech.*, 1966, **6**, 547.
- [2.97] WULF, G.L.: in *Mechanical Properties of Materials at High Rates of Strain*, (Ed. J Harding), Inst Phys Conf Ser 21, 1974, p. 48
- [2 98] PARRY, D J and WALKER, A.G.: A microcomputer-based split Hopkinson pressure bar system, *Inst of Phys Meeting*, 1988, Series No. 16, 111.
- [2 99] YOKOYAMA, T and KISHIDA, K.: A microcomputer-based system for the high-speed compression test by the split Hopkinson pressure bar technique, *J. of Testing & Evaluation*, 1986, **14**, 236
- [2 100] HODGKINSON, J.M et al.: Drop-weight impact tests with the use of laser-Doppler velocimetry, *Proc Roy. Soc. Lond.*, 1982, **379A**, 133.
- [2.101] Proceedings of the *11th International Congress on High Speed Photography*, London, U.K, (1974).
- [2.102] Proceedings of the *12th International Congress on High Speed Photography*, Toronto, Canada, (1976).
- [2 103] Proceedings of the *13th International Congress on High Speed Photography and Photonics*, Tokyo, Japan, (1978)
- [2.104] Proceedings of the *19th International Congress on High Speed Photography*, Cambridge, U.K, (1990).
- [2 105] SPEYER B.: High speed still video photography for ballistic range applications, in *19th Int. Congress on High-Speed Photography and Photonics*, (1990), Cambridge, U K, p. 1215.
- [2.106] HAQUE, M M and HASHMI, M S.J.: Stress-strain properties of structural steel at strain-rates of up to 10^4 s^{-1} at sub-zero, room, and high temperatures, *Mech. Mat.*, 1984, **3**, 245.
- [2.107] PARRY, D.J *et al* The application of cylindrical blast waves to impact studies of materials, in *19th Int. Congress on High-Speed Photography and Photonics*,(1990), Cambridge, U.K, p. 1057.

- [2 108] GORHAM, D.A.: in *the proceedings of the 13th International Congress on High Speed Photography and Photonics*, Tokyo, Japan, (1978), p 313.
- [2 109] KUSCHER, G. Ph.D. Dissertation, Technische Hochschule Aachen, (in German), Also referred by Stulp, A J and Hohler (chapter 8) in *High Velocity Impact Dynamics*, (1990).
- [2.110] BIRCH, P.S and JONES, N.: Measurement of impact loads using a laser doppler velocimeter, *Proc. Instn. Mech. Engrs.*, 1990, **204**, 1.
- [2 111] SIEBEL, E.: *Stahl und Eisen*, 1925, **43**, 1295
- [2.112] BERTHOLF, L D and KARNES, C.H.: *J Mech. Phys. Solids*, 1975, **23**, 1
- [2.113] KLEPACZKO, J and MALINOWSKI, Z.: in *High Velocity Deformation of Solids*, (Eds K. Kawata and J. Shioiri), Springer-Verlag, 1978, p 403.
- [2.114] DAVIES, E.D.H. and HUNTER, S.C : The dynamic compression testing of solids by the method of split Hopkinson pressure bar, *J. Mech. Phys. Solids*, 1963, **11**,155.
- [2.115] AVITZUR, B : *Metal forming Processes and Analysis*, 1968, (McGraw-Hill, New York)
- [2.116] GORHAM, D A, POPE, P.H and COX, O.: Sources of error in very high strain rate compression tests, in *Mechanical Properties at High Rates of Strain*, (Ed. J Harding), Inst Phys Conf Ser 70, 1984, p151.
- [2.117] MALE, A.T. and COCKRAFT, M.G.: A method for the determination of the coefficient of friction of metals under conditions of bulk plastic deformation, *J Inst. Metals*, 1964, **93**, 38.
- [2.118] SHEIKH, A.D. *et al.*. The effect of impact speed and lubricant in hot forging: Part I, *Thirteen Int. MATDOR Conference*, Birmingham, (1972), 341
- [2 119] NARAYANASAMY, R *et al* : Prediction of the barrelling of solid cylinders under uniaxial compressive load, *J. Mat. Proc. Tech.*, 1988, **16**, 21
- [2.120] HASHMI, M S J : Upsetting of cylindrical billets between flat platens having unequal frictional properties, *Int. J. Mach. Tool Design & Res* , 1978, **18**, 189
- [2 121] VENUGOPAL, P , VENUGOPAL, S and SEETHARAMAN, V.: Influence of strain-rate and temperature on the friction factor of commercially pure titanium, *J Mat. Proc Techn* , 1990, **22**, 91

- [2 122] PEARSALL, W.G and BACKOFEN, W.A.: *J. Eng Ind*, 1963, **85**, 68.
- [2.123] GORHAM, D A.: in *Mechanical Properties at High Rates of Strain*, (Ed. J. Harding), Inst Phys Conf Ser 47, 1979, p.16.
- [2.124] ASM HANDBOOK, *Mechanical Testing*, Volume 8, 1992.
- [2.125] ANNUAL BOOK OF ASTM STANDARDS.: Compression testing of metallic materials at room temperature, E9, ASTM, Philadelphia, (1984).
- [2.126] HADDOW, J.B.: On the compression of a thin disk, *Int. J. Mech. Sci.*, 1965, **7**, 675.
- [2.127] STURGESS, C.E.N. and JONES, M.G.: Estimation of dynamic forces in high-speed compression using a free-flight impact forging device, *Int. J Mech. Sci.*, 1971, **13**, 309.
- [2.128] TIROSH, J and KOBAYASHI, S.: *J. Appl Mech.*, 1976, **43**, 314.
- [2.129] SAMANTA, S K.: Dynamic deformation of aluminum and copper at elevated temperatures, *J. Mech. Phys. Solids*, 1971, **19**, 117.
- [2 130] DHARAN, C and HAUSER, F.: Determination of stress-strain characteristics at very high strain-rates, *Exp Mech.*, 1970, **11**, 370
- [2.131] MALATYNSKI, M. and KLEPACZKO, J.: Experimental investigation of plastic properties of lead over a wide range of strain rates, *Int. J Mech. Sci* , 1980, **22**, 173
- [2 132] GORHAM, D A.: Specimen inertia in high strain-rate, *J. Appl. Phys.*, 1989, **22**, 1888
- [2.133] WOODWARD, R L.: Materials failure at high strain-rates, in *High Velocity Impact Dynamics*, (Ed. J. Zukas), John Wiley & Sons, Inc., 1990, p76.
- [2 134] COSTIN, L S *et al* : On the localisation of plastic flow in mild steel tubes dynamic torsional loading, in *Mechanical Properties at High Rates of Strain*, (Ed J Harding), Inst Phys Conf Ser , 70, 1984, p90
- [2 135] HARTLEY, K.A *et al*. Measurement of the temperature profile during shear band formation in steels deforming at high strain-rates, *J Mech. Phys. Soulds*, 1987, **35**, 283.
- [2.136] WOODWARD, R L *et al*.: Direct measurement of temperature in high speed torsion tests, *J Engng. Mat. Techn*, 1987, **109**, 140.

- [2 137] FROST, H.J and ASHBY, M F · *Deformation Mechanism Maps*, 1982, (Pergamon Press, Oxford).
- [2.138] DIXON, P.R and PARRY, D.J.: Thermal softening effects in type 224 carbon steel, in DYMAT'91, (1991), Strasbourg, France, p. 85.
- [2.139] FARREN, W S and TAYLOR, G.I : The heat developed during plastic extension of metals, *Proc. Roy. Soc* , 1925, **107A**, 422.
- [2.140] TAYLOR, G.I and QUINNEY, H.: The latent energy remaining in a metal after cold working, *Proc. Roy. Soc. Lond.*, 1933, **143A**, 307.
- [2 141] KIM, Y.H and WAGONER, R.H.: An analytical investigation of induced heating in tensile testing, *Int. J. Mech. Sci.*, 1987, **29**, 179.
- [2.142] BISHOP, J.F.W.: An approximation method for determining the temperatures reached in steady motion problems of plan plastic strain, *Quart. J. Mech. and Appl. Mat.*, 1956, **9**, 236.
- [2.143] SEMIATIN, S L and HOLBROOK, J.H · Failure behaviour of 304L stainless steel in torsion, *Metall Trans.*, 1983, **14A**, 2091.
- [2 144] GUNASEKERA, J. S, HAVRONEK, J and LITTLEJOHN, M H.: The effect of specimen size on stress-strain behaviour in compression, *Trans ASME*, 1982, **104**, 274.
- [2.145] HAUSER, F.E.: Techniques for measuring stress-strain relations at high strain-rates, *Exp. Mech.*, 1966, **6**, 395
- [2.146] STELLY, M and DORMEVAL, R.: *Procs. of High Velocity Deformation of Solids*, (1977), Tokyo, Japan, p. 82.
- [2.147] SAMANTA, S K.: *Int. J. Mech Sci*, 1969, **11**, 433.
- [2 148] GLENN, T and BRADLEY, W.: *Metall. Trans.*, 1973, **4**, 2343.
- [2 149] EDINGTON, J.W.: *Phil Mag.*, 1969, **19**, 1189
- [2 150] BHUSHAN, B and JAHSMAN, W.E.: *J. Solids Structures*, 1978, **14**, 739
- [2 151] KUMAR, A and KUMBLE, R G : *J. Appl. Phys.*, 1969, **40**, 3475.
- [2 152] LINDHOLM, U.S.. Deformation maps in the region of high dislocation velocity, in *High Velocity Deformation of Solids*, (Eds. K. Kawata and J. Shiori), Springer-Verlag, New York, 1978, p. 26.

- [2 153] SHIORI, J , SATOH, K and NISHIMURA, K.: in *High Velocity Deformation of Solids*, (Eds. K. Kawata and J Shiori), Springer-Verlag, New York, 1978, p.50.
- [2.154] FOLLANSBEE, P.S; REGAZZONI, G and KOCKS, U.F.: in *Mechanical Properties at High Rates of Strain*, (Ed. J Harding), Inst Phys Conf Ser 70, 1984, p. 71.
- [2.155] KISHIDA, K and SENDA,K.: *Bulletin of the JSME*, 1972, **15**, 25.
- [2.156] LESLIE, W.C.: Microstructural effects of high strain-rate deformation, in *Metallurgical Effects at High Strain-Rates*, Plenum Press, New York, 1973, p. 571
- [2.157] ARGON, A S.: *Constitutive Equations in Plasticity*, 1975, (The MIT Press, Cambridge, USA).
- [2 158] HAQUE, M.M, PICKERING, F B and HASHMI, M S.J · Investigation on microstructural change in copper deformed at strain-rates of upto 10^4 s⁻¹, DYMAT-88, (1988), *J. De Physique*, 105
- [2 159] MEGUID, S A · On the explosive hardening of one end of a metallic block, *Int. J. Mech. Sci*, 1976, **18**, 351
- [2.160] ROHDE, R.W.. Dynamic yield behaviour of shock-loaded iron from 76 to 573 K, *Acta Metall.*, 1969, **17**, 353.
- [2.161] JOHARI, O and THOMAS, G.: Substructures in explosively deformed copper and copper-aluminium alloys, *Acta Metall.*, 1964, **12**, 1153.
- [2 162] GRACE, F I.: Shock-wave strengthening of copper and nickel, *J. Appl. Phys* , 1969, **40**, 2649.
- [2 163] HAGUE, M M and M S.J Hashmi.: Investigation on microstructure of medium carbon steel deformed at strain rates of upto 10^5 per second at -30°C to 235°C, in *Advanced Materials Processing Technologies*, (Ed M.S J Hashmi), DCU Press, 1993, **1**, 583.
- [2.164] BROWN, A.F.C and VINCENT, D G.: *Proc Inst Mech. Engngs* , 1941, **141**, 126.
- [2.165] DUWEZ, P E and CLARK, D S.: *Proc. Amer Soc. Test. Mat* , 1947, **47**, 502.
- [2.166] NAKKALIL, R, HORNADAY, J.R and BASSIM, M.N.: Characterization of the compression properties of rail steels at high temperatures and strain rates., *Mat Sci. & Engng.*, 1991, **141A**, 247

- [2.167] TANAKA, K and NOJIMA, T.: Dynamic and static strength of steels, in *Mechanical Properties of Materials at High Rates of Strain*, (Ed. J. Harding), Inst Phys. Conf. Ser. 102, (1989), 166
- [2.168] CAMPBELL, J D.: An investigation of the plastic behaviour of metal rods subjected to longitudinal impact, *J. Mech. Phys. Solids*, 1953, **1**, 113.
- [2.169] CAMPBELL, J.D and DUBY, J.: *Proc. Roy. Soc., Lond.*, 1956, **A236**, 24.
- [2 170] DOWLING, A.R, HARDING, J and CAMPBELL, J D.: *J Inst. Metals*, 1970, **96**, 215.
- [2 171] HEREIL, P.L · On the strain-rate dependence of yield stresses of copper at high strain-rates. in *Impact Loading and Dynamic Behaviour of Materials*, (Chiem C.Y *et al* , Eds), (1988), DGM Informationsgesellschaft, Oberursel, Germany, p. 385.
- [2.172] RAJENDRAN, A.M and BLESS, J.S.: High strain-rate material behaviour, *AFWAL-TR-85-4009, Wright-Patterson Air Force Base, OH*, (1985).
- [2.173] FOLLANSBEE, P.S and KOCKS, U.F.: A constitutive description of the deformation of copper based on the use of the mechanical threshold stress as an internal state variable, *Acta Metall* , 1988, **36**, 81.
- [2 174] GORHAM, D.A.: The effect of specimen dimensions on high strain rate compression measurements of copper, *J. Appl Phys.*, 1991, **24**, 1489.
- [2.175] CHIDDESTER, J.L and MALVERN, L.E.: Compression impact testing of aluminum at elevated temperatures, *Proc Soc. of Experimental Stress Analysis*, (1963), 81
- [2 176] DEAN, T.A and STURGESS, C E.N. · Stress-strain characteristics of various steels over a wide range of strain-rates and temperature, *Proc. Inst. Mech. Engrs* , 1973, **187**, 523.
- [2 177] WITTMAN, C. L *et al* · High strain-rate properties and modelling of a tungsten alloy in compression and tension, in *High Strain-rate Behaviour of Refractory Metals and Alloys*, (Eds. R. Asfahani, E. Chen and A. Crowson), TMS Publisher, USA, 1992, p. 167.
- [2.178] MARCHAND, A *et al.*: An experimental study of the dynamic mechanical properties of an Al-SiCw composite, *Engng. Fracture Mech.*, 1988, **30**, 295.
- [2 179] HARDING. J.: Impact damage in composite materials, *Sci. & Engng Composite Mat.*, 1989, **1**, 41

- [2 180] VAZIRI, R *et al.*: High speed impact response of particulate metal-matrix composite materials: An experimental and theoretical investigation, *Int J. Impact Engng.*, 1993, 13, 329
- [2 181] ZERILLI, F.J and ARMSTRONG, R.W.: Dislocation-mechanics-based constitutive relations for material dynamic calculations, *J. Appl. Phys* , 1987, 61, 1816.
- [2.182] SIERAKOWSKI, R.L.: High Strain-rate testing of composites, in *Dynamic Constitutive/Failure Models*, (Eds A M. Rajendran and T. Nicholas), AFWAL-TR-88-4229, Wright-Patterson Air Force Base, OH, (1988).
- [2.183] LATAILLADE, J. L, *et al.*: in *Procs Int Congress on Rheology. Advances n Rheology*, 3, Polymers (Eds. B. Mena *et al.*), 1984, p. 137
- [2 184] HILLIER, K.W and KOLSKY, H.: An investigation of the dynamic elastic properties of some high polymers, *Proc Phys. Soc. B*, 1949, 62, 111.
- [2.185] TAYLOR, G L.: The testing of materials at high rates of loading, *J. Inst Civil Engrs.*, 1946, 2, 486.
- [2.186] BAUWENS-CROWET, C, BAUWENS, J.C and HOMES, G.: *J. Polymer. Sci.*, 1969, 7, 735.
- [2.187] BAUWENS-CROWET, C, BAUWENS, J C and HOMES, G.: *J. Polymer. Sci.*, 1969, 7, 1745.
- [2.188] BAUWENS-CROWET, C, BAUWENS, J.C and HOMES, G.: *J. Mat Sci.*, 1972, 7, 176.
- [2.189] EYRING, H.: *J. Chem. Phys.*, 1936, 4, 293.
- [2.190] BAUWENS-CROWET, C, OTS, J M, and BAUWENS, J.C.: The strain rate and temperature dependence of yield of polycarbonate in tension, tensile, and impact tests, *J. Mat Sci.*, 1974, 9, 1197
- [2.191] HUTCHINGS, M I.: Estimation of yield stress in polymers at high strain-rates using G.I Taylor's impact technique, *J. Mech. Phys Solids*, 1979, 26, 289.
- [2.192] WALLEY, S.M, *et al.*: A study of the rapid deformation behaviour of range of polymers, *Phil. Trans. Roy. Soc. Lond* , 1989, A328, 1.

CHAPTER THREE

- [3 1] LUDWICK, P.: *Elemente de Technologischen Mechanik*, 1909, (Julius Spring, Germany).
- [3.2] PERZYNA, P.: Fundamental problems in viscoplasticity, in *Advances in Applied Mechanics*, (Ed G. Kuerti), Academic Press, New York, 1966, **9**, 243
- (3.3) PERZYNA, P.: Thermodynamic theory of viscoplasticity, in *Advances in Applied Mechanics*, (Ed. C.S. Yih), Academic Press, New York, 1971, **11**, 313
- [3.4] SOKOLOVSKII, V V : Propagation of elastic-viscoplastic waves in bars, *Doklady Akademia Nank SSSR*, 1948, **68**, 775.
- [3.5] MALVERN, L.E.: The propagation of longitudinal waves of plastic deformation in a bar of material exhibiting a strain rate effect, *J Appl. Mech.*, 1951, **18**, 203.
- [3 6] MEGUID, S.A and MALVERN, L.E.: An experimental investigation into load relaxation in aluminium (HE30TB) and mild steel (EN1A), *Int. J. Mech Sci*, 1982, **24**, 299.
- [3.7] KREMPL, E.. An experimental study of room temperature rate sensitivity, creep and relaxation of AISI-type 304 stainless steel, *J. Mech. Phys Solids*, 1979, **27**, 3
- [3 8] COWPER, G.R and SYMONDS, P.S.: Strain hardening and strain rate effects in the impact loading of cantilever beams, *Tech Report No 28, ONR Contract No. 562 (10), Division of Engng, Brown University*, 1967, Providence, RI
- [3 9] TANG, M.C and KOBAYASHI, S · An investigation of shell nosing process by the finite-element method, part 2: Nosing at elevated temperatures (hot nosing), *Trans ASME, J Engng Ind.*, 1982, **104**, 312.
- [3.10] PERZYNA, P · The constitutive equations for rate sensitive plastic materials, *Quart Appl Math.*, **20**, 1963, 321.
- [3.11] KORMI, K , WEBB, D.C, and MONTAGUE, P Crash behaviour of circular tubes with large side openings, *Int. J Mech. Sci*, 1993, **35**, 193.
- [3.12] KORMI, K , WEBB, D.C, and JOHNSON, W · The crash response of circular tubes under general applied loading, *Int. J Impact Engng.*, 1993, **13**, 243

- [3.13] KORMI, K , ETHERIDGE, R.A and WEBB, D.C.: FEM simulation of the static and dynamic forming of circular plates, *J. Mat. Proc. Techn.*, 1994, **42**, 451.
- [3.14] REID, S.R.: in *Structural Crashworthiness*, 1983, (Butterworths: London), 1.
- [3.15] REID, S.R and GUI, X.G.: On the elastic-plastic deformation of cantilever beams subjected to tip impact, *Int. J. Impact Engng.*, 1987, **6**, 109.
- [3.16] JONES, N.: Some comments on the modelling of material properties for dynamic structural plasticity, in *Mechanical Properties of Materials at High Rates of Strain*. (Ed. J. Harding) Inst. Phys. Conf. Ser. 102, 1989, p. 435.
- [3.17] LINDHOLM, U.S.: Some experiments with the split Hopkinson pressure bar, *J. Mech. Phys. Solids*, 1964, **12**, 317.
- [3.18] WILKINS, M.L *et al.*: Computer simulations of ballistic experiments, *Lawrence Livermore National Laboratory, UCRL-95774*, (1974).
- [3.19] WILKINS, M.L.: Calculation of elastic-plastic flow, in *Methods in Computational Physics*, (Ed. B. Alder), 1964, **3**, 211.
- [3.20] JOHNSON, G.R and COOK, W.: A constitutive model and data for metals subjected to large strains, high strain rates and high temperatures, *Proc. 7th Int. Symp. on Ballistics*, The Hague, The Netherlands (April 1983), p.541.
- [3.21] JOHNSON, G.R.:EPIC-2, A computer program for elastic-plastic impact computations in two dimensions plus spin, *ARBRL-CR-00373*, (1978).
- [3.22] JOHNSON, G.R.:EPIC-3, A computer program for elastic-plastic impact computations in 3 dimensions, *BRL-CR-343*, (1977).
- [3.23] HOLQUIST, J.O.: LS-DYNA2D: An explicit two-dimensional hydrodynamic finite-element code with interactive rezoning and graphical display, *LSTC Report 1004, Livermore Software Technology Corporation*, (1990).
- [3.24] DUJARDIN, S.: Analysis critique des lois de comportement dynamique des materiaux metalliques, *Report Institut Franco-Allemand de Recherces Saint-Louis, France, NTIS-PB87-200416*, (1986).
- [3.25] KANAE, Y, SASAKI, T and SHIMAMURA, S.: Experimental and analytical studies on the drop-impact test with lead-shielded scale model radioactive material shipping casks, in *Structural Impact and Crashworthiness*, (Ed. J. Morton), Elsevier, NY, 1984, **2**, 343.
- [3.26] RAJENDRAN, A.M *et al.*: Effect of strain rate of plastic flow and fracture in pure tantalum, *J. Mat. Shaping Technol.*, 1991, **9**, 7.

- [3.27] WITTMAN, C.L *et al.*: High strain rate properties and modelling of a tungsten alloy in compression and tension, in *High Strain Rate Behaviour of Refractory Metals and Alloys*, (Eds. R. Asfahani, E. Chen, and A. Crowson), TMS Publ., 1992, p. 167.
- [3.28] SLATER, R.A.C.: *Engineering Plasticity*, 1977, (MacMillan), p. 272.
- [3.29] HAWKYARD, J; EATON, D and JOHNSON, W.: The mean dynamic yield strength of copper and low carbon steel at elevated temperature from measurement of the mushrooming of flat ended projectile, *Int. J. Mech. Sci.*, 1968, **10**, 929.
- [3.30] AL-HADDID, T.N.: High strain rate properties of structural aluminium, PhD Thesis, *Sheffield City Polytechnic*, (1987).
- [3.31] WOODWARD, R.L and BROWN, R.H.: Dynamic stress-strain properties of a steel and a brass at strain rates up to 10^4 per second, *Proc. Inst. Mech. Engrs*, 1975, **189**, 107.
- [3.32] SAXENA, A and CHATFIELD, D.A. The effect of strain rate on strain hardening exponent, *ASE paper 760209*, (1976).
- [3.33] TANIMOTO, N, FUKUOKA, H and FUJITA, K.: One-dimensional numerical analysis of a bar subjected to longitudinal impulsive loading, *Int. J. Japan Soc. Mech. Engrs.*, 1993, **36A**, 137.
- [3.34] LUBLINER, J.: A generalized theory of strain rate dependent plastic wave propagation in bars, *J. Mech. Phys. Solids*, 1964, **12**, 59.
- [3.35] HILL, R.: Constitutive laws and waves in rigid/plastic solids, *J. Mech. Phys. Solids*, 1962, **10**, 89.
- [3.36] HASHMI, M.S.J.: Stress wave theory applied to simple upsetting, *Symposium on Manufacturing Engineering*, June 14-15, 1977, Leciester Polytechnic, p B3.
- [3.37] JOHNSON, W and MELLOR, P.B.: *Engineering Plasticity*, 1975, Van Nostrand Reinhold Company LTD.
- [3.38] O'BRIEN, G.G., HYMAN, M.A, and KAPLAN, S.: A study of the numerical solution of a partial differential equations, *J. Mat. Phys.*, 1951, **29**, 223.
- [3.39] HAMOUDA, A.M.S and HASHMI, M.S.J.: Modelling the impact and penetration events: Computer characteristics and material models, *J. Mat. Proc. Technology*, 1994, (in press)
- [3.40] LYONS, P. *et al.*: Plasticity and element formulations for impact analysis in LUSAS, in *Proc of NAFEMS*, June 1991, South Africa.

- [3 41] LUSAS THEORY MANUAL, *FEA Ltd* , Ver. 11, 1994.
- [3.42] WILKINS, M.L and GUINAN, M.W.: Impact of cylinders on a rigid boundary, *J. Appl. Phys.*, 1973, **44**, 1200.
- [3.43] GREGORIAN. V, SADEK, M.M and TOBIAS, S.A.: Noise generated by a laboratory drop hammer and its interrelation with structural dynamics and problem parameters, *In. J Mach Tool Des. Res.*, 1976, **16**, 301.
- [3.44] DAS, M.K and TOBIAS, S.A.. The efficiency of energy transfer and the determination of load in impact forming machines, *4th Int. Conf of the Center for High Energy Forming*, USA, (1973)

CHAPTER FOUR

- [4.1] GOODFELLOW CAMBRIDGE LIMITED, U.K , *Goodfellow Catalogue-1994*
- [4 2] HASHMI, M.S.J *et al.*: High strain rate properties of material: Design and development of a test equipment and methodology, *Int. J. Mach. Tool. Des. and Res* , 1985, **25**, 39.
- [4.3] HAQUE, M.M. and HASHMI, M.S.J : Stress-strain properties of structure steel at strain rates of up to 10^5 per second at subzero, room, and high temperatures, *Mech. of Mat.*, 1984, **3**, 245.
- [4.4] REID, S.R, REDDY, T Y and GRAY, M D.: Static and dynamic axial crushing of foam-filled sheet metal tubes, *Int J. Mech. Sci*, 1986, **28**, 295.
- [4.5] GREENSPAN, L.: Humidity fixed points of binary saturated aqueous solutions, *J. Research of the National Bureau of Standards*, 1977, **81A**, 89.

CHAPTER FIVE

- [5.1] HOLT, D L *et al.*: The strain rate dependence of the flow stress in some alloys, *Trans ASM*, 1967, **60**, 152
- [5.2] HAQUE, M.M, PICKERING, F.B and HASHMI, M.S.J.: Investigation on microstructural change in copper deformed at strain-rates of upto 10^4 s⁻¹, *DYMAT-88*, (1988), *J. De Physique*, 105.

- [5.3] CHIEM, C Y. in *Impact Loading and Dynamic Behaviour of Materials*, (Eds. C.Y. Chiem *et al*), Interscience Publisher, China, 1988, p. 57.
- [5.4] FOLLANSBEE, P.S. REGAZZONI, G and KOCKS, U F · in *Mechanical Properties at High Rates of Strain*, (Ed J Harding). Inst. Phys Conf Ser 70, 1984, p 71.
- [5.5] HASHMI, M.S.J and HAQUE, M.M.: High strain rate properties of an aluminum and high purity copper at room temperature, *Procs. Int. Conf. of Metal under Dynamic Loading*, (Ed. Z. Zheng), China Science Press, 1986.
- [5.6] JOHNSON, G R *et al.*: Response of various metals to large torsional strain over a large range of strain rates-Part I Ductile materials, *J. Eng Mats and Techn. Trans ASME*, 1983, **105**, 42
- [5.7] WOODWARD, R.L and BROWN, R.H.: Dynamic stress-strain properties of a steel and a brass at strain rates up to 10^4 per second, *Proc. Inst Mech Engrs.*, 1975, **189**, 107.
- [5 8] YOSHIDA, S and NAGATA, N · Deformation of polycrystalline aluminum at high strain rates, *Trans of National Res. Inst. for Metals*, 1967, **9**, 20.
- [5 9] BODNER, S R · Strain rate effects in dynamic loading of structures, *Winter Annual Meeting of the ASME*, Chicago, (1965), 93.
- [5.10] LINDHOLM, U S and BESSEY, R L.: A survey of rate dependent strength properties of metals, *AFWAL-TR-69-119*, Wright-Patterson Air Force Base, OH, (1969).
- [5.11] JIANG, C.W and CHEN, M.M.: Dynamic properties of materials, Part II-Aluminum alloys, *Report No AMMRC CTR 74-23*, Watertwon, MA, (1974).
- [5 12] HAQUE, M.M and HASHMI, M.S.J.: Stress-strain properties of structural steel at strain-rates of up to 10^4 s⁻¹ at sub-zero, room, and high temperatures, *Mech Mat.*, 1984, **3**, 245.
- [5 13] DAVIES, E.D.H. and HUNTER, S C.: The dynamic compression testing of solids by the method of split Hopkinson pressure bar, *J. Mech Phys. Solids*, 1963, **11**,155.
- [5.14] HAMOUDA, A M.S and HASHMI, M S J : High strain rate testing of composite materials: Advances and Challenges, *To be presented at 2nd Int. Conf. in Advanced Materials Processing and Technology*, 1995, Dublin, Ireland.

- [5.15] HAMOUDA, A.M.S and HASHMI, M.S.J.: Mechanical properties of aluminium metal matrix composites under impact loading, *J. Mat. Proc. Technology*, 1994, (in press).
- [5.16] VAZIRI, R, OLSON, M.D, and ANDERSON, D.L.: Finite-element analysis of fibrous composite structures: A plasticity approach, *Computers & Structures*, 1992, **44**, 103.
- [5.17] GOODFELLOW CAMBRIDGE LIT , U K , *Goodfellow Catalogue-1994*
- [5.18] ARSENAULT, R J and WU, S.B.: The strength differential and Bauschinger effects in SiC-Al composites, *Mater. Sci. Eng.*, 1987, **96**, 77
- [5.19] BILLINGTON, E.B and BRISSENDEN, C.: Mechanical properties of various polymeric solids tested in compression, *Int. J. Mech. Sci.*, 1971, **13**, 531.
- [5.20] BRISCOE, B.J and HUTCHINGS, M.I : Impact yielding of high density polyethylene, *Polymer*, 1976, **17**, 1099.
- [5.21] HAMOUDA, A.M.S. and HASHMI, M.S J.: Mechanical behaviour of nylon at high strain rates, *Key Engineering Material*, 1993, **86-87**, 109.
- [5.22] LABIBES, K, LILI, W, and PLUVINAGE, G.: On determining the viscoplastic constitutive equation of polymers at high strain-rates, *DYMAT Journal*, 1994, **1**, 135.
- [5.23] WALLEY, S.M *et al.*: The rapid deformation behaviour of various polymers, *J. Phys III France*, 1991, **1**, 1889.
- [5.24] ASHBY, M.F and JONES, D.R.H · *Engineering Material 2*, 1986, (Pergamon Press, Oxford), p 201.
- [5.25] HASHMI, M.S.J and HAMOUDA, A.M.S.: Development of 1D constitutive equation for metals subjected to high strain rate and large strains, *J. of Strain Analysis, Proc IMechE*, 1994, **29**, 117.
- [5.26] SWALLOWE, G.M, FIELD, J.E and HORN, L.A.: Measurements of transient high temperatures during deformation of polymers, *J. Mat Sci.*, **21**, 1986, 4089
- [5.27] DIXON, P R and PARRY, D J · Thermal softening effects in type 225 carbon steel, *DYMAT-91, J De Physique*, 1991, **1**, 85.
- [5.28] MAIDEN, C.J and GREEN, S J : Compression strain rate tests on six selected materials at strain rates from 10^{-3} to 10^4 s⁻¹, *Trans ASME*, 1966, 496

- [5 29] GORHAM, D.A . Specimen inertia in high strain-rate, *J. Appl Phys.*, 1989, **22**, 1888.
- [5.30] GORHAM, D.A.. An effect of specimen size in the high strain rate compression test, in *3rd Int Conf on Mechanical & Physical Behaviour of Materials under Dynamic Loading*, Strasbourg, France, (October 1991), p 411.
- [5 31] VINH, T and KHALIL, T · Adiabatic and viscoplastic properties of some polymers at high strain and high strain rate, in *Mechanical Properties at High Rates of Strain*, (Ed. J. Harding). Inst. Phys Conf Ser 70, 1984, p 39
- [5 32] GILAT and WU, X.: Elevated temperature testing with torsional split Hopkinson bar, *Exp. Mech.*, **34**, 1994, 166
- [5 33] HAWKYARD, J · A theory for the mushrooming of the flat-ended projectiles impinging on a rigid anvil, using energy consideration. *Int J. Mech Sci.*, 1968, **11**, 313.
- [5.34] HASHMI, M S J.: Strain rate sensitivity of commercially pure copper at room temperature and strain rates up to 10^6 per second, *Technical Report No. SCP/MPE/R-106*, Department of Mechanical & Production Engng , Sheffield City Polytechnic, (Oct. 1978)
- [5.35] HAMOUDA, A.M.S and HASHMI, M S J : High speed impact of elastic-plastic work hardening material into a rigid boundary, 4th Int Sci. Conf on Achievements in the Mechanical and Material Engineering (AMME'95), Poland, 1995, (in press).

Appendix (A)

SUMMARY OF ALL THE BALLISTIC COMPRESSION TESTS

Table A1 Results of the Ballistic Compression Tests for Aluminum

Initial Height = 6 mm Initial Diameter = 6 mm

Test No.	Impact Speed (ms ⁻¹)	Final Height (mm)	Final Diameter (mm)
1	25.1	4.34	7.28
2	38.1	3.40	8.00
3	45.2	2.80	8.60
4	52.4	2.52	9.15
5	59.1	2.16	9.98
6	65.9	1.89	10.7
7	70.4	1.72	11.31

Table A2 Results of the ballistic compression tests for Brass

Initial Height = 5 mm Initial Diameter = 5 mm

Test No.	Impact Speed (ms ⁻¹)	Final Height (mm)	Final Diameter (mm)
1	38.9	4.34	5.14
2	41.1	4.06	5.34
3	45.2	4.15	5.30
4	48.9	4.15	5.26
5	58.7	3.84	5.49
6	61.5	3.64	5.66
7	64.2	3.61	5.66
8	67.9	3.70	5.75
9	74.7	3.19	6.11
10	75.9	3.20	6.00
11	76.5	3.14	6.14
12	76.9	3.10	6.24
13	78.3	3.11	6.14
14	78.3	3.05	6.07
15	78.5	3.10	6.11
16	91.7	2.62	6.85
17	99.2	2.45	6.95
18	102.4	2.55	6.90

Table A3 Results of the Ballistic Compression Tests for Copper

Initial Height = 5 mm

Initial Diameter = 5 mm

Test No	Impact Speed (ms ⁻¹)	Final Height (mm)	Final Diameter (mm)
1	51.4	3.84	5.90
2	52.2	3.75	6.01
3	52.9	3.69	6.12
4	77.2	2.86	6.81
5	77.9	2.86	6.82
6	78.6	2.88	6.79
7	92.8	2.32	7.56
8	94.1	2.29	7.62
9	95.8	2.24	7.74

Table A4 Results of the Ballistic Compression Tests for Stainless-steel (304)

Initial Height = 5 mm

Initial Diameter = 5 mm

Test No	Impact Speed (ms ⁻¹)	Final Height (mm)	Final Diameter (mm)
1	73.16	4.07	5.67
2	73.18	4.09	5.67
3	76.4	4.08	5.69
4	83.44	3.70	5.92
5	85.3	3.65	6.10
6	85.8	3.62	6.10
7	94.6	3.32	6.54
8	97.0	3.39	6.31
9	99.3	3.36	6.35
10	100.0	3.20	6.53
11	109.0	3.14	6.72
12	119.0	3.01	6.80

Table A5 Results of the Ballistic Compression Tests for Steel En-9

Initial Height = 5 mm Initial Diameter = 5 mm

Test No	Impact Speed (ms ⁻¹)	Final Height (mm)	Final Diameter (mm)
1	51.2	4.45	5.25
2	52.1	4.54	5.29
3	53.3	4.46	5.25
4	73.0	3.90	5.61
5	81.1	3.91	5.66
6	82.0	3.90	5.70
7	95.8	3.29	6.26
8	104.5	3.19	6.25
9	105.5	3.40	6.21
10	109.3	2.65	6.89
11	115.7	2.66	7.20
12	120.0	2.20	7.95
13	122.3	2.34	7.55
14	123.1	2.70	6.96
15	125.0	2.34	7.50
16	125.7	2.45	7.39
17	126.1	2.60	6.98
18	133.1	2.10	7.70
19	136.7	1.96	7.90
20	143.7	2.15	8.00
21	152.9	2.10	7.79
22	170.6	2.04	8.08

Table A6 Results of the Ballistic Compression Tests for Al/Cu MMC

Initial Height = 6 mm

Initial Diameter = 6 mm

Test No.	Impact Speed (ms ⁻¹)	Final Height (mm)	Final Diameter (mm)
1	23.4	5.90	6.05
2	60.0	5.05	6.5
3	62.35	5.0	6.75
4	63.16	4.95	6.85
5	77.58	4.26	7.15
6	84.81	4.15	7.2
7	87.8	4.05	7.4
8	88.9	3.9	7.7
9	89.5	3.8	7.9
10	90.57	3.5	8.0
11	94.57	3.4	8.4
12	106.2	2.95	8.95
13	111.2	2.95	9.05
14	115.1	2.8	9.10
15	133.0	2.5	9.5

Table A7 Results of the Ballistic Compression Tests for Nylon 6

Initial Height = 6 mm

Initial Diameter = 6 mm

Test No	Impact Speed (ms ⁻¹)	Final Height (mm)	Final Diameter (mm)
1	45.8	5.5	6.9
2	46.7	5.4	6.9
3	52.0	5.5	6.9
4	56.8	5.0	7.0
5	66.48	4.9	7.1
6	72.11	4.2	7.5
7	75.0	3.92	7.7

Table A8 Results of the Ballistic Compression Tests for Al/Li MMC

Initial Height = 6 mm

Initial Diameter = 6 mm

Test No	Impact Speed (ms ⁻¹)	Final Height (mm)	Final Diameter (mm)
1	25.4	5.85	6.15
2	40.5	5.40	6.39
3	65.0	4.67	6.98
4	72.1	4.27	7.15
5	76.4	4.15	7.24
6	102.0	3.14	9.10
7	115.7	2.64	9.47

Appendix (B)

COMPUTER CODE DESCRIPTION

The FDIC (Finite-Difference Impact Calculations) computer program contains the formulation presented in chapter three. A description of some the characteristics of the computer code is given in the following subsections.

Program Organization and Subroutines

The organization of the FDIC code is shown in Figure 3.6 page 52. It consists of the main program FDIC and over 14 subroutines for total of 40 Byte. The following is a brief description of the main program and subroutines (listed alphabetically):

FDIC	This the main program which calls the subroutines.
AREA	This subroutine computes the cross-sectional area of each layer and sublayer in the element.
CONST	This subroutine calculates some auxiliary constants.
ENERGY	This subroutine computes system data such as energy for the projectile, target and anvil, it also writes this data into file.
EQUILI	This subroutine computes the displacement of each element in system
INDATA	This subroutines reads the input data file
INITAL	This subroutine generates the initial condition of the system.
LOOP	This subroutine computes the mechanical properties at each time increment.
OUTDAT	This subroutine prints all the input data for checking.
PRINT	This subroutines reads and prints the output results of space-time history of all the important physical quantities such as stress, strain rate, etc.
SLOPE	This subroutine computes the slopes for each part of the stress-strain curve.
STRAIN	This subroutine computes the strain and strain rate in each element.
STRESS	This subroutine computes the stress in each element
TEMPER	This subroutine computes the temperature rise during deformation in each element.
WAVE	This subroutine computes the time interval.

Glossary of Abbreviated Terms Used in the Computer Code

AFC	The Area of the Friction Cone	M	The Total Number of Calculations
AFL	The Area of each Layer in the Element	M1	The First Number of Calculations after which the Results are Printed
ARR	The Mean Radius of each Layer in the Element	M2	Number of Calculations after which the Results are Printed
ASFL	The Area of each Sublayer in the Layer	N	Number of Divisions of the System
BIGL	The Initial Height of the Specimen	NFL	Number of Divisions of each Element
BIGLA	The Initial Height of the Anvil	NSFL	Number of Divisions of each Layer
BIGLP	The Initial Height of the Projectile	PI	Constant
BIGLT	The Initial Height of the System	PLAST	The Energy Consumed on the Plastic Deformation.
BIGN	The Force in each Element.	RFC	The Radius of the Friction Cone
BIGR	The Current Radius of each Element	RHO	The Density of the Specimen
BIGRO	The Initial Radius of the Specimen	SIGMA	The Static Stress of the Specimen
BIGROA	The Initial Radius of the Projectile	SIGMAL	The Static Stress of the Projectile
C1	Auxiliary Variable	SN	The Stress in each Sublayer
CINET	The Current Kinetic Energy	SNO	The Fictitious Stress of the Specimen
CIENTO	The Initial Kinetic Energy	SNOA	The Fictitious Stress of the Projectile
DDS	The Difference in Displacement between Two Elements	STR	The Strain for each Element
DELTAT	The Time Interval	STRT	The Strain-rate for each Element
DELTS	The Current Height of each Element	T	The Distance between the Centre and the Radius of the Layer
DV	The Displacement of each Element	TIME	The Cumulative Time
E	Young's Modulus of the Specimen	V	The Position of each Element
EA	Young's Modulus of the Projectile	VDOTO	The Velocity of the Projectile
ELAST	The Energy Consumed on Elastic Deformation in the Specimen	WE	The Mass of each Element
ELASTA	The Energy Consumed on Elastic Deformation in the Anvil	WP	The Mass of the Projectile
ELASTP	The Energy Consumed on Elastic Deformation in the Projectile		
EPSIL	The Strain of the Specimen		
EPSILA	The Strain of the Projectile		
FMU	Friction Coefficient		
FN	Auxiliary Variable for the Force Counter		
J			

CALL INTAL

C-----
C Calculation of the energy spent (in the projectile, specimen and anvil) during deformation
C-----

CALL ENERGP
CALL ENERGS
CALL ENERGA
CALL PRINT
BIGN(1)=0 0

C-----
C To Calculate the mechanical properties at each time increment
C during deformation
C-----

120 J=J+1
QQ=CIENT
QH=V(2)
DO 92 I=1, N1
C1(I)=E(1)/DELTS(I)
92 CONTINUE

C-----
C Conditions to terminate the simulation after the elastic recovery
C-----

128 IF(BGN(2) GT 0)THEN
WRITE (6,*) 'Force becomes tension'
TIME=DELTAT*FLOAT(J)
CALL ENERGP
CALL ENERGS
CALL ENERGA
CALL PRINT
GOTO 210
END IF

C-----
C Boundary conditions of mass (N1)
C-----

DDS(N1)=-2 0*DV(N)
V(N1)=V(N1)-DV(N)
DDS(1)=0 0

C-----
C Calculation of strain in each link
C-----

CALL STRAIN

C-----
C Condition to terminate the simulation before any elastic recovery
C-----

IF(V(2) GT QH)THEN
WRITE (6,*) 'Element no 2 goes up'
TIME=DELTAT*FLOAT(J)
CALL ENERGP
CALL ENERGS

```

CALL ENERGA
CALL PRINT
GOTO 210
END IF
C-----
C    Calculations of temperature rise in each element during deformation
C-----
CALL TEMPER
C-----
C    Calculations of the elastic-plastic stresses on the specimen
C-----
CALL STRESS
C-----
C    Calculation of the elastic stresses in the projectile and anvil
C-----
CALL PROESS
C-----
C    Calculations of the displacement of each element
C-----
CALL EQUILI
CALL ENERGP
CALL ENERGS
CALL ENERGA
C-----
C    Condition to terminate the simulation when the kinetic energy
C    is almost zero
C-----

IF(CINET GT QQ)THEN
    WRITE(6,*) 'Energy is almost zero'
    TIME=DELTAT*FLOAT(J)
    CALL ENERGP
    CALL ENERGS
    CALL ENERGA
    CALL PRINT
    GOTO 210
END IF
C-----
C    Print out of the results
C-----
IF(J-M1)120,140,210
140  CALL LOOP
    CALL ENERGP
    CALL ENERGS
    CALL ENERGA
    WRITE(6,*)SUM
210  END

```

```

C=====
SUBROUTINE INDATA
C=====
IMPLICIT REAL * 8(A-H,O-Z)
COMMON V,DV,DELTS,DELT,DDS,BIGN,EPSIL,SIGMA,SIGMALE,BIGR,SNO,ARR,AFL,
ASFL,SN,TIME,DELTSO,CINETO,H,C1,C2,C5,C6,C7,T,STN,RHO,BIGRO,PI,P,
DELTAT,FMU1,FMU2,STNRT,N,N1,NFL,NSFL,J,WP,WE,M,M1,M2,BIGL,VDOTO,D,
A,S,SUM,SUM1,CINET,Hf,C,SUM4,SUM3,SUM5,SB,ELAST,ELASTS,ELASTA, ELASTP,
PLAST,SNOA,BIGLT,BIGLA,BIGLP,EA,BIGROA,K1,K2,R1,R2,EPSILA,
SUM6,SUM7,SUM8,SF,SUM9,STSS,SUMS,SNY,TO,F,W1,Z

DIMENSION V(94),DV(94),DELTS(94),DDS(94),BIGN(94),EPSIL(4),
SIGMA(4),E(4),BIGR(94),SNO(4),ARR(5,94),AFL(5,94),ASFL(4,5,94),
SN(4,5,94),STN(94),STNRT(94),C1(94),T(5,94),STSS(94),TO(94)
SNOA(4),EA(4),EPSILA(4),SIGMAL(4)

READ(1,1) N,NFL,NSFL,M,M1,M2,BIGRO,RHO,DELTAT,FMU1,FMU2,WP,F,
. W,Z,SB,Hf,VDOTO,A,S,BIGL,PI,SIGMA(1),(EPSIL(L),L=1,NSFL)
1 FORMAT(6(10X,I10/),20(10X,D14 8/))
CLOSE (UNIT=1,STATUS='KEEP')
RETURN
END

```

```

C=====
SUBROUTINE SLOPE
C=====
IMPLICIT REAL * 8 (A-H,O-Z)
COMMON V,DV,DELTS,DELT,DDS,BIGN,EPSIL,SIGMA,SIGMALE,BIGR,SNO,ARR,AFL,
ASFL,SN,TIME,DELTSO,CINETO,H,C1,C2,C5,C6,C7,T,STN,RHO,BIGRO,PI,P,
DELTAT,FMU1,FMU2,STNRT,N,N1,NFL,NSFL,J,WP,WE,M,M1,M2,BIGL,VDOTO,D,
A,S,SUM,SUM1,CINET,Hf,C,SUM4,SUM3,SUM5,SB,ELAST,ELASTS,ELASTA, ELASTP,
PLAST,SNOA,BIGLT,BIGLA,BIGLP,EA,BIGROA,K1,K2,R1,R2,EPSILA,
SUM6,SUM7,SUM8,SF,SUM9,STSS,SUMS,SNY,TO,F,W1,Z

DIMENSION V(94),DV(94),DELTS(94),DDS(94),BIGN(94),EPSIL(4),
SIGMA(4),E(4),BIGR(94),SNO(4),ARR(5,94),AFL(5,94),ASFL(4,5,94),
SN(4,5,94),STN(94),STNRT(94),C1(94),T(5,94),STSS(94),TO(94)
SNOA(4),EA(4),EPSILA(4),SIGMAL(4)

E(1)=SIGMA(1)/EPSIL(1)
EA(1)=E(1)
DO 4 L=2,NSFL
SIGMA(L)=A*(EPSIL(L)**S)
4 CONTINUE
IF(NSFL-1)16,16,14
14 DO 15 L=2,NSFL
E(L)=(SIGMA(L)-SIGMA(L-1))/(EPSIL(L)-EPSIL(L-1))
15 CONTINUE
16 E(NSFL+1)=0
EA(2)=0
RETURN
END

```

```
C=====
SUBROUTINE AREA
C=====
```

```
IMPLICIT REAL * 8 (A-H,O-Z)
```

```
COMMONV,DV,DELTS,DELT,DDS,BIGN,EPSIL,SIGMA,SIGMALE,BIGR,SNO,ARR,AFL,
.ASFL,SN,TIME,DELTSO,CINETO,H,C1,C2,C5,C6,C7,T,STN,RHO,BIGRO,PI,P,
.DELTAT,FMU1,FMU2,STNRT,N,N1,NFL,NSFL,J,WP,WE,M,M1,M2,BIGL,VDOTO,D,
.A,S,SUM,SUM1,CINET,Hf,C,SUM4,SUM3,SUM5,SB,ELAST,ELASTS,ELASTA,ELASTP,
.PLAST,SNOA,BIGLT,BIGLA,BIGLP,EA,BIGROA,K1,K2,R1,R2,EPSILA,
.SUM6,SUM7,SUM8,SF,SUM9,STSS,SUMS,SNY,TO,F,W1,Z
```

```
DIMENSION V(94),DV(94),DELTS(94),DDS(94),BIGN(94),EPSIL(4),
.SIGMA(4),E(4),BIGR(94),SNO(4),ARR(5,94),AFL(5,94),ASFL(4,5,94),
.SN(4,5,94),STN(94),STNRT(94),C1(94),T(5,94),STSS(94),TO(94)
.SNOA(4),EA(4),EPSILA(4),SIGMAL(4)
```

```
EPSILA(1)=0.0125
SIGMAL(1)=EA(1)*EPSILA(1)
N1=N+1
K1=20
K2=21
R1=26
R2=25
BIGROA=4.75E-3
BIGLA=5.0*BIGL
BIGLP=4.0*BIGL
BIGLT=BIGL+BIGLA+BIGLP
DELTSO=BIGLT/FLOAT(N)
DELT=DELTSO/2.0
DO 24 I=K2,R2
BIGR(I)=BIGRO
24 CONTINUE
DO 22 I=1,K1
BIGR(I)=BIGROA
22 CONTINUE
DO 2 I=R1,N1
BIGR(I)=BIGROA
2 CONTINUE
WE=RHO*(BIGRO**2)*PI*DELTSO
C WEA=RHO*(BIGROA**2)*PI*DELTSO
WEA=WP/K1
FLONFL=NFL
DO 3 I=1,N1
DO 4 K=1,NFL
T(K,I)=BIGR(I)/FLONFL
ARR(K,I)=FLOAT(K+K-1)*T(K,I)/2.
AFL(K,I)=2.0*PI*ARR(K,I)*T(K,I)
4 CONTINUE
3 CONTINUE
DO 474 I=1,K1
DO 484 K=1,NFL
DO 494 L=1,1
ASFL(L,K,I)=AFL(K,I)*(EA(L)-EA(L+1))/EA(1)
```

```

      SNOA(L)=EA(1)*EPSILA(L)
494  CONTINUE
484  CONTINUE
474  CONTINUE
      DO 17 I=K2,R2
      DO 18 K=1,NFL
      DO 19 L=1,NSFL
      ASFL(L,K,I)=AFL(K,I)*(E(L)-E(L+1))/E(1)
      SNO(L)=E(1)*EPSIL(L)
19   CONTINUE
18   CONTINUE
17   CONTINUE
      DO 47 I=R1,N1
      DO 48 K=1,NFL
      DO 49 L=1,1
      ASFL(L,K,I)=AFL(K,I)*(EA(L)-EA(L+1))/EA(1)
      SNOA(L)=EA(1)*EPSILA(L)
49   CONTINUE
48   CONTINUE
47   CONTINUE
      RETURN
      END

```

```

C=====
      SUBROUTINE OUTDAT

```

```

C=====

```

```

      IMPLICIT REAL * 8 (A-H,O-Z)
      COMMONV,DV,DELTS,DELT,DDS,BIGN,EPSIL,SIGMA,SIGMALE,BIGR,SNO,ARR,AFL,
      ASFL,SN,TIME,DELTSO,CINETO,H,C1,C2,C5,C6,C7,T,STN,RHO,BIGRO,PI,P,
      DELTAT,FMU1,FMU2,STNRT,N,N1,NFL,NSFL,J,WP,WE,M,M1,M2,BIGL,VDOTO,D,
      A,S,SUM,SUM1,CINET,Hf,C,SUM4,SUM3,SUM5,SB,ELAST,ELASTS,ELASTA,ELASTP,
      PLAST,SNOA,BIGLT,BIGLA,BIGLP,EA,BIGROA,K1,K2,R1,R2,EPSILA,
      SUM6,SUM7,SUM8,SF,SUM9,STSS,SUMS,SNY,TO,F,W1,Z

```

```

      DIMENSION V(94),DV(94),DELTS(94),DDS(94),BIGN(94),EPSIL(4),
      SIGMA(4),E(4),BIGR(94),SNO(4),ARR(5,94),AFL(5,94),ASFL(4,5,94),
      SN(4,5,94),STN(94),STNRT(94),C1(94),T(5,94),STSS(94),TO(94)
      SNOA(4),EA(4),EPSILA(4),SIGMAL(4)

```

```

      WRITE(6,31)N,NFL,NSFL,M,BIGRO,RHO,DELTAT,D,P,VDOTO,BIGL,
      (L,EPSIL(L),SIGMA(L),L=1,NSFL)
31   FORMAT(5H N= ,I5,6H NFL= ,I5,7H NSFL= ,I5,5H M= ,I5/
      . 9H BIGRO= ,D12 5,7H RHO= ,D12 5,10H DELTAT= ,D12 5,/
      5H D= ,D12 5/5H P= ,D12 5,/
      8H VDOTO= ,D12 5,17H      BIGL= ,D12 5,/
      39H L  EPSIL  SIGMA      /(I5,2D12 5))
      RETURN
      END

```

```

C=====
SUBROUTINE INITAL
C=====
IMPLICIT REAL * 8 (A-H,O-Z)
COMMONV,DV,DELTS,DELT,DDS,BIGN,EPSIL,SIGMA,SIGMALE,BIGR,SNO,ARR,AFL,
ASFL,SN,TIME,DELTSO,CINETO,H,C1,C2,C5,C6,C7,T,STN,RHO,BIGRO,PI,P,
DELTAT,FMU1,FMU2,STNRT,N,N1,NFL,NSFL,J,WP,WE,M,M1,M2,BIGL,VDOTO,D,
A,S,SUM,SUM1,CINET,Hf,C,SUM4,SUM3,SUM5,SB,ELAST,ELASTS,ELASTA,ELASTP,
PLAST,SNOA,BIGLT,BIGLA,BIGLP,EA,BIGROA,K1,K2,R1,R2,EPSILA,
SUM6,SUM7,SUM8,SF,SUM9,STSS,SUMS,SNY,TO,F,W1,Z

DIMENSION V(94),DV(94),DELTS(94),DDS(94),BIGN(94),EPSIL(4),
SIGMA(4),E(4),BIGR(94),SNO(4),ARR(5,94),AFL(5,94),ASFL(4,5,94),
SN(4,5,94),STN(94),STNRT(94),C1(94),T(5,94),STSS(94),TO(94)
SNOA(4),EA(4),EPSILA(4),SIGMAL(4)

J=0
TIME=0 0
DO 50 I=1,N1
V(I)=DELT*(2*I-1)
TO(I)=20 0D0
DV(I)=0 0
DELTS(I)=DELTSO
BIGN(I)=0
DDS(I)=0 0D0
50 CONTINUE
DO 444 I=1,K1
DO 804 K=1,NFL
DO 494 L=1,1
SN(L,K,I)=0 0
494 CONTINUE
804 CONTINUE
444 CONTINUE
DO 54 I=K2,R2
DO 40 K=1,NFL
DO 39 L=1,NSFL
SN(L,K,I)=0 0
39 CONTINUE
40 CONTINUE
54 CONTINUE
DO 44 I=R1,N1
DO 80 K=1,NFL
DO 49 L=1,1
SN(L,K,I)=0 0
49 CONTINUE
80 CONTINUE
44 CONTINUE
DO 448 I=1,K1
DV(I)=DELTAT*VDOTO
448 CONTINUE
RETURN
END

```


C=====
SUBROUTINE CONST

C=====
IMPLICIT REAL * 8 (A-H,O-Z)

COMMON V,DV,DELTS,DELT,DDS,BIGN,EPSIL,SIGMA,SIGMAL,E,BIGR,SNO,ARR,AFL,
ASFL,SN,TIME,DELTSO,CINETO,H,C1,C2,C5,C6,C7,T,STN,RHO,BIGRO,PI,P,
DELTAT,FMU1,FMU2,STNRT,N,N1,NFL,NSFL,J,WP,WE,M,M1,M2,BIGL,VDOTO,D,
A,S,SUM,SUM1,CINET,Hf,C,SUM4,SUM3,SUM5,SB,ELAST,ELASTS,ELASTA, ELASTP,
PLAST,SNOA,BIGLT,BIGLA,BIGLP,EA,BIGROA,K1,K2,R1,R2,EPSILA,
SUM6,SUM7,SUM8,SF,SUM9,STSS,SUMS,SNY,TO,F,W1,Z

DIMENSION V(94),DV(94),DELTS(94),DDS(94),BIGN(94),EPSIL(4),
SIGMA(4),E(4),BIGR(94),SNO(4),ARR(5,94),AFL(5,94),ASFL(4,5,94),
SN(4,5,94),STN(94),STNRT(94),C1(94),T(5,94),STSS(94),TO(94)
SNOA(4),EA(4),EPSILA(4),SIGMAL(4)

C2=DELTAT**2/RHO/BIGRO**2/PI/DELTSO
C4=DELTAT**2/RHO/BIGROA**2/PI/DELTSO
RETURN
END

C=====
SUBROUTINE WAVE

C=====
IMPLICIT REAL * 8 (A-H,O-Z)

COMMON V,DV,DELTS,DELT,DDS,BIGN,EPSIL,SIGMA,SIGMALE,BIGR,SNO,ARR,AFL,
ASFL,SN,TIME,DELTSO,CINETO,H,C1,C2,C5,C6,C7,T,STN,RHO,BIGRO,PI,P,
DELTAT,FMU1,FMU2,STNRT,N,N1,NFL,NSFL,J,WP,WE,M,M1,M2,BIGL,VDOTO,D,
A,S,SUM,SUM1,CINET,Hf,C,SUM4,SUM3,SUM5,SB,ELAST,ELASTS,ELASTA, ELASTP,
PLAST,SNOA,BIGLT,BIGLA,BIGLP,EA,BIGROA,K1,K2,R1,R2,EPSILA,
SUM6,SUM7,SUM8,SF,SUM9,STSS,SUMS,SNY,TO,F,W1,Z

DIMENSION V(94),DV(94),DELTS(94),DDS(94),BIGN(94),EPSIL(4),
SIGMA(4),E(4),BIGR(94),SNO(4),ARR(5,94),AFL(5,94),ASFL(4,5,94),
SN(4,5,94),STN(94),STNRT(94),C1(94),T(5,94),STSS(94),TO(94)
SNOA(4),EA(4),EPSILA(4),SIGMAL(4)

Ce=(E(1)/RHO)**0.5
DELTAT1= DELTSO/Ce
DELTAT = DELTAT1/M2
RETURN
END

```

C=====
      SUBROUTINE LOOP
C=====
      IMPLICIT REAL * 8 (A-H,O-Z)
      COMMONV,DV,DELTS,DELT,DDS,BIGN,EPSIL,SIGMA,SIGMALE,BIGR,SNO,ARR,AFL,
      ASFL,SN,TIME,DELTSO,CINETO,H,C1,C2,C5,C6,C7,T,STN,RHO,BIGRO,PI,P,
      DELTAT,FMU1,FMU2,STNRT,N,N1,NFL,NSFL,J,WP,WE,M,M1,M2,BIGL,VDOTO,D,
      A,S,SUM,SUM1,CINET,Hf,C,SUM4,SUM3,SUM5,SB,ELAST,ELASTS,ELASTA, ELASTP,
      PLAST,SNOA,BIGLT,BIGLA,BIGLP,EA,BIGROA,K1,K2,R1,R2,EPSILA,
      SUM6,SUM7,SUM8,SF,SUM9,STSS,SUMS,SNY,TO,F,W1,Z

      DIMENSION V(94),DV(94),DELTS(94),DDS(94),BIGN(94),EPSIL(4),
      SIGMA(4),E(4),BIGR(94),SNO(4),ARR(5,94),AFL(5,94),ASFL(4,5,94),
      SN(4,5,94),STN(94),STNRT(94),C1(94),T(5,94),STSS(94),TO(94)
      SNOA(4),EA(4),EPSILA(4),SIGMAL(4)

140  M1=M1+M2
      IF(M-M1)141,142,142
141  M1=M
142  TIME=DELTAT*FLOAT(J)
      RETURN
      END

C=====
      SUBROUTINE STRAIN
C=====
      IMPLICIT REAL * 8 (A-H,O-Z)
      COMMONV,DV,DELTS,DELT,DDS,BIGN,EPSIL,SIGMA,SIGMALE,BIGR,SNO,ARR,AFL,
      ASFL,SN,TIME,DELTSO,CINETO,H,C1,C2,C5,C6,C7,T,STN,RHO,BIGRO,PI,P,
      DELTAT,FMU1,FMU2,STNRT,N,N1,NFL,NSFL,J,WP,WE,M,M1,M2,BIGL,VDOTO,D,
      A,S,SUM,SUM1,CINET,Hf,C,SUM4,SUM3,SUM5,SB,ELAST,ELASTS,ELASTA, ELASTP,
      PLAST,SNOA,BIGLT,BIGLA,BIGLP,EA,BIGROA,K1,K2,R1,R2,EPSILA,
      SUM6,SUM7,SUM8,SF,SUM9,STSS,SUMS,SNY,TO,F,W1,Z

      DIMENSION V(94),DV(94),DELTS(94),DDS(94),BIGN(94),EPSIL(4),
      SIGMA(4),E(4),BIGR(94),SNO(4),ARR(5,94),AFL(5,94),ASFL(4,5,94),
      SN(4,5,94),STN(94),STNRT(94),C1(94),T(5,94),STSS(94),TO(94)
      SNOA(4),EA(4),EPSILA(4),SIGMAL(4)

      SUM=0.0D0
      SUM1=0.0D0
      SUM3=0.0D0
      SUM4=0.0D0
      SUM5=0.0D0
      DO 10 I=2,N
          DDS(I)=DV(I)-DV(I-1)
10  CONTINUE
      DO 2004 I=2,N1
          SUM1=SUM1+DDS(I)
2004 CONTINUE
      DO 30 I=1,N
          V(I)=V(I)+DV(I)
30  CONTINUE
      DO 40 I=1,K1
          DELTS(I)=DELTS(I)+DDS(I)

```

```

IF(DELTS(I)-0 01*DELTSO)31,32,32
31 DELTS(I)=0 01*DELTSO
32 DELTS(I)=DELTS(I)+DDS(I)
BIGR(I)=(DELTSO*BIGROA**2/DELTS(I))**0 5
40 CONTINUE
DO 124 I=K2,R2
DELTS(I)=DELTS(I)+DDS(I)
SUM=SUM+DELTS(I)
BIGR(I)=(DELTSO*BIGRO**2/DELTS(I))**0 5
SUM3=SUM3+(2 *BIGR(I))
124 CONTINUE
DO 244 I=R1,N1
DELTS(I)=DELTS(I)+DDS(I)
BIGR(I)=(DELTSO*BIGROA**2/DELTS(I))**0 5
244 CONTINUE
DO 444 I=1,K1
FLONFL=NFL
DO 440 K=1,NFL
T(K,I)=BIGR(I)/FLONFL
ARR(K,I)=FLOAT(K+K-1)*T(K,I)/2
AFL(K,I)=2 *PI*ARR(K,I)*T(K,I)
DO 446 L=1,1
ASFL(L,K,I)=AFL(K,I)*(EA(L)-EA(L+1))/EA(1)
446 CONTINUE
440 CONTINUE
444 CONTINUE
DO 64 I=K2,R2
FLONFL=NFL
DO 50 K=1,NFL
T(K,I)=BIGR(I)/FLONFL
ARR(K,I)=FLOAT(K+K-1)*T(K,I)/2
AFL(K,I)=2 *PI*ARR(K,I)*T(K,I)
DO 60 L=1,NSFL
ASFL(L,K,I)=AFL(K,I)*(E(L)-E(L+1))/E(1)
60 CONTINUE
50 CONTINUE
64 CONTINUE
DO 644 I=R1,N1
FLONFL=NFL
DO 540 K=1,NFL
T(K,I)=BIGR(I)/FLONFL
ARR(K,I)=FLOAT(K+K-1)*T(K,I)/2
AFL(K,I)=2 *PI*ARR(K,I)*T(K,I)
DO 640 L=1,1
ASFL(L,K,I)=AFL(K,I)*(EA(L)-EA(L+1))/EA(1)
640 CONTINUE
5401 CONTINUE
644 CONTINUE
NSFL=3
SUM3=SUM3/N
RETURN
END

```

```

C=====
  SUBROUTINE STRESS
C=====
  IMPLICIT REAL * 8 (A-H,O-Z)
  COMMONV,DV,DELTS,DELT,DDS,BIGN,EPSIL,SIGMA,SIGMALE,BIGR,SNO,ARR,AFL,
ASFL,SN,TIME,DELTSO,CINETO,H,C1,C2,C5,C6,C7,T,STN,RHO,BIGRO,PI,P,
DELTAT,FMU1,FMU2,STNRT,N,N1,NFL,NSFL,J,WP,WE,M,M1,M2,BIGL,VDOTO,D,
A,S,SUM,SUM1,CINET,Hf,C,SUM4,SUM3,SUM5,SB,ELAST,ELASTS,ELASTA, ELASTP,
PLAST,SNOA,BIGLT,BIGLA,BIGLP,EA,BIGROA,K1,K2,R1,R2,EPSILA,
SUM6,SUM7,SUM8,SF,SUM9,STSS,SUMS,SNY,TO,F,W1,Z

  DIMENSION V(94),DV(94),DELTS(94),DDS(94),BIGN(94),EPSIL(4),
SIGMA(4),E(4),BIGR(94),SNO(4),ARR(5,94),AFL(5,94),ASFL(4,5,94),
SN(4,5,94),STN(94),STNRT(94),C1(94),T(5,94),STSS(94),TO(94)
SNOA(4),EA(4),EPSILA(4),SIGMAL(4)

  SUMS=0.0D0
  DO 100 I=2,N1
  SNDS=C1(I)*DDS(I)
  BIGN(I)=0
  DO 90 K=1,NFL
  FN=0.0D0
54  DO 80 L=1,NSFL
  SN(L,K,I)=SN(L,K,I)+SNDS
  IF(SN(L,K,I)-SNO(L))30,70,11
  11  SNY=(SNO(L)*(1+(ABS(STNRT(I))*D)**(P)))
  IF(SN(L,K,I)-SNY)70,70,20
  20  SN(L,K,I)=SNY
  GO TO 70
  30  IF(SN(L,K,I)+SNO(L))31,70,70
  31  SNY=(SNO(L)*(1+(ABS(STNRT(I))*D)**(P)))
  IF(SN(L,K,I)+SNY)40,70,70
  40  SN(L,K,I)=-SNY
  70  FN=FN+SN(L,K,I)*(ASFL(L,K,I))
  80  CONTINUE

C  THE SIGN OF THE SECOND TERM IN THE NEXT EQUATION SHOULD
C  CORRESPOND WITH THE SIGN OF -FN- AND NOT ADDED TO -FN- ,
C  BECAUSE -FN- MIGHT EITHER HAS A NEGATIVE VALUE OR A POSITIVE ONE
C
C  FN=FN+(PI*ARR(K,I)*T(K,I)**3 *RHO*(DDS(I)/DELTAT)**2*(BIGR(I)**2
C  -ARR(K,I)**2-(T(K,I)**2/4 ))/4 /DELTS(I)**2)
C
C  TO CHANGE THIS THE EQUATION WILL BE DIVIDED TO CALCULATE THE
C  RESULTANT FORCE FROM RADIAL INERTIA AND COMPARE ITS SIGN WITH
C  THE SIGN OF -FN- AND CHANGE ITS SIGN IF NECESSARY THEN ADD IT
C  TO -FN-

  FRI=(3 *PI*AFL(K,I)*RHO*(DDS(I)/DELTAT)**2*(BIGR(I)**2
  -ARR(K,I)**2-(T(K,I)**2/4 ))/8 /DELTS(I)**2)
  FRI=DSIGN(FRI,FN)
  FN=FN+FRI
  BIGN(I)=BIGN(I)+FN
  90  CONTINUE
  100 CONTINUE

```

```

    BIGN(1)=0
    NSFL=3
    RETURN
5   END

```

```

C=====
  SUBROUTINE EQUILI

```

```

C=====
  IMPLICIT REAL * 8 (A-H,O-Z)
  COMMONV,DV,DELTS,DELT,DDS,BIGN,EPSIL,SIGMA,SIGMALE,BIGR,SNO,ARR,AFL,
  ASFL,SN,TIME,DELTSO,CINETO,H,C1,C2,C5,C6,C7,T,STN,RHO,BIGRO,PI,P,
  DELTAT,FMU1,FMU2,STNRT,N,N1,NFL,NSFL,J,WP,WE,M,M1,M2,BIGL,VDOTO,D,
  A,S,SUM,SUM1,CINET,Hf,C,SUM4,SUM3,SUM5,SB,ELAST,ELASTS,ELASTA, ELASTP,
  PLAST,SNOA,BIGLT,BIGLA,BIGLP,EA,BIGROA,K1,K2,R1,R2,EPSILA,
  SUM6,SUM7,SUM8,SF,SUM9,STSS,SUMS,SNY,TO,F,W1,Z

```

```

  DIMENSION V(94),DV(94),DELTS(94),DDS(94),BIGN(94),EPSIL(4),
  SIGMA(4),E(4),BIGR(94),SNO(4),ARR(5,94),AFL(5,94),ASFL(4,5,94),
  SN(4,5,94),STN(94),STNRT(94),C1(94),T(5,94),STSS(94),TO(94)
  SNOA(4),EA(4),EPSILA(4),SIGMAL(4)

```

```

    DO 20 I=1,N
    IF(I GE K2 AND I LE R2)THEN
    DV(I)=DV(I)+C2*(BIGN(I+1)-BIGN(I))
    ELSE
    DV(I)=DV(I)+C4*(BIGN(I+1)-BIGN(I))
    END IF
20  CONTINUE
    RETURN
    END

```

```

C=====
  SUBROUTINE PRINT

```

```

C=====
  IMPLICIT REAL * 8 (A-H,O-Z)
  COMMONV,DV,DELTS,DELT,DDS,BIGN,EPSIL,SIGMA,SIGMALE,BIGR,SNO,ARR,AFL,
  ASFL,SN,TIME,DELTSO,CINETO,H,C1,C2,C5,C6,C7,T,STN,RHO,BIGRO,PI,P,
  .DELTAT,FMU1,FMU2,STNRT,N,N1,NFL,NSFL,J,WP,WE,M,M1,M2,BIGL,VDOTO,D,
  A,S,SUM,SUM1,CINET,Hf,C,SUM4,SUM3,SUM5,SB,ELAST,ELASTS,ELASTA, ELASTP,
  PLAST,SNOA,BIGLT,BIGLA,BIGLP,EA,BIGROA,K1,K2,R1,R2,EPSILA,
  .SUM6,SUM7,SUM8,SF,SUM9,STSS,SUMS,SNY,TO,F,W1,Z

```

```

  DIMENSION V(94),DV(94),DELTS(94),DDS(94),BIGN(94),EPSIL(4),
  SIGMA(4),E(4),BIGR(94),SNO(4),ARR(5,94),AFL(5,94),ASFL(4,5,94),
  SN(4,5,94),STN(94),STNRT(94),C1(94),T(5,94),STSS(94),TO(94)
  SNOA(4),EA(4),EPSILA(4),SIGMAL(4)

```

```

    WRITE(6,90)J,TIME,CINET,ELAST,PLAST,(I,V(I),DELTS(I),
    BIGN(I),STN(I),BIGR(I),STNRT(I),I=1,N1)
90  FORMAT(5H J= ,I5,6HTIME= ,D12 5,8HKINTIC= ,D12 5,
  9HELASTIC= ,D12 5,9HPLASTIC= ,D12.5/
  40H I    V    HIGHT    FORCE
  39H strain    RADIUS    STNRT    /(I5,6D12 5))

```

```

    WRITE(6,*)SUM

```

```

WRITE(6,*)SUM3
WRITE(6,*)SUM4
WRITE(6,*)SUM5
WRITE(6,*)SUM8
RETURN
END

```

```

C=====
SUBROUTINE TEMPER

```

```

C=====

```

```

IMPLICIT REAL * 8(A-H,O-Z)
COMMON V,DV,DELTS,DELT,DDS,BIGN,EPSIL,SIGMA,SIGMAL, E,BIGR,SNO,ARR,AFL,
ASFL,SN,TIME,DELTSO,CINETO,H,C1,C2,C5,C6,C7,T,STN,RHO,BIGRO,PI,P,
DELTAT,FMU1,FMU2,STNRT,N,N1,NFL,NSFL,J,WP,WE,M,M1,M2,BIGL,VDOTO,D,
A,S,SUM,SUM1,CINET,Hf,C,SUM4,SUM3,SUM5,SB,ELAST,ELASTS,ELASTA, ELASTP,
PLAST,SNOA,BIGLT,BIGLA,BIGLP,EA,BIGROA,K1,K2,R1,R2,EPSILA,
SUM6,SUM7,SUM8,SF,SUM9,STSS,SUMS,SNY,TO,F,W1,Z

```

```

DIMENSION V(94),DV(94),DELTS(94),DDS(94),BIGN(94),EPSIL(4),
SIGMA(4),E(4),BIGR(94),SNO(4),ARR(5,94),AFL(5,94),ASFL(4,5,94),
SN(4,5,94),STN(94),STNRT(94),C1(94),T(5,94),STSS(94),TO(94)
SNOA(4),EA(4),EPSILA(4),SIGMAL(4)

```

```

SUM8=0.0D0
DO 24 I=K2,R2
W=(ABS(DDS(I)*BIGN(I))/(PI*(BIGR(I)**2)*DELTS(I)))
TO(I)=(F*W/(RHO*SB))+TO(I)
SUM8=SUM8+TO(I)
24 CONTINUE
SUM8=SUM8/5
RETURN
END

```

```

C=====
SUBROUTINE PROESS

```

```

C=====

```

```

IMPLICIT REAL * 8 (A-H,O-Z)
COMMON V,DV,DELTS,DELT,DDS,BIGN,EPSIL,SIGMA,SIGMALE,BIGR,SNO,ARR,AFL,
ASFL,SN,TIME,DELTSO,CINETO,H,C1,C2,C5,C6,C7,T,STN,RHO,BIGRO,PI,P,
DELTAT,FMU1,FMU2,STNRT,N,N1,NFL,NSFL,J,WP,WE,M,M1,M2,BIGL,VDOTO,D,
A,S,SUM,SUM1,CINET,Hf,C,SUM4,SUM3,SUM5,SB,ELAST,ELASTS,ELASTA, ELASTP,
PLAST,SNOA,BIGLT,BIGLA,BIGLP,EA,BIGROA,K1,K2,R1,R2,EPSILA,
.SUM6,SUM7,SUM8,SF,SUM9,STSS,SUMS,SNY,TO,F,W1,Z

```

```

DIMENSION V(94),DV(94),DELTS(94),DDS(94),BIGN(94),EPSIL(4),
SIGMA(4),E(4),BIGR(94),SNO(4),ARR(5,94),AFL(5,94),ASFL(4,5,94),
SN(4,5,94),STN(94),STNRT(94),C1(94),T(5,94),STSS(94),TO(94)
SNOA(4),EA(4),EPSILA(4),SIGMAL(4)

```

```

DO 100 I=1,K1
SNDS=C1(I)*DDS(I)
BIGN(I)=0.0D0
DO 90 K=1,NFL
FN=0.0D0

```

```

54 DO 80 L=1,1
   SN(L,K,I)=SN(L,K,I)+SNDS
   IF(SN(L,K,I)-SNOA(L))30,70,11
11  SNY=(SNOA(L)*(1+(ABS(STNRT(I))*D)**(P)))
   IF(SN(L,K,I)-SNY)70,70,20
20  SN(L,K,I)=SNY
   GO TO 70
30  IF(SN(L,K,I)+SNOA(L))31,70,70
31  SNY=(SNOA(L)*(1+(ABS(STNRT(I))*D)**(P)))
   IF(SN(L,K,I)+SNY)40,70,70
40  SN(L,K,I)=-SNY
70  FN=FN+SN(L,K,I)*(ASFL(L,K,I))
80  CONTINUE

```

$$FRI = (3 * \pi * AFL(K,I) * RHO * (DDS(I) / DELTAT) ** 2 * (BIGR(I) ** 2 - ARR(K,I) ** 2 - (T(K,I) ** 2 / 4)) / 8 / DELTS(I) ** 2)$$

$$FRI = DSIGN(FRI, FN)$$

$$FN = FN + FRI$$

$$BIGN(I) = BIGN(I) + FN$$

```
90 CONTINUE
```

```
100 CONTINUE
```

```

DO 104 I=R1,N1
  SNDS=C1(I)*DDS(I)
  BIGN(I)=0 OD0
  DO 94 K=1,NFL
    FN=0 OD0
    DO 84 L=1,1
      SN(L,K,I)=SN(L,K,I)+SNDS
      IF(SN(L,K,I)-SNOA(L))34,74,14
14   SNY=(SNOA(L)*(1+(ABS(STNRT(I))*D)**(P)))
      IF(SN(L,K,I)-SNY)74,74,24
24   SN(L,K,I)=SNY
      GO TO 74
      IF(SN(L,K,I)+SNOA(L))34,74,74
34   SNY=(SNOA(L)*(1+(ABS(STNRT(I))*D)**(P)))
      IF(SN(L,K,I)+SNY)44,74,74
44   SN(L,K,I)=-SNY
74   FN=FN+SN(L,K,I)*(ASFL(L,K,I))
84   CONTINUE

```

$$FRI = (3 * \pi * AFL(K,I) * RHO * (DDS(I) / DELTAT) ** 2 * (BIGR(I) ** 2 - ARR(K,I) ** 2 - (T(K,I) ** 2 / 4)) / 8 / DELTS(I) ** 2)$$

$$FRI = DSIGN(FRI, FN)$$

$$FN = FN + FRI$$

$$BIGN(I) = BIGN(I) + FN$$

```
94 CONTINUE
```

```
104 CONTINUE
```

$$BIGN(1) = 0$$

```

NSFL=3
RETURN
END

```

```

C=====
SUBROUTINE ENERGP
C=====
IMPLICIT REAL * 8 (A-H,O-Z)
COMMONV,DV,DELTS,DELT,DDS,BIGN,EPSIL,SIGMA,SIGMALE,BIGR,SNO,ARR,AFL,
ASFL,SN,TIME,DELTSO,CINETO,H,C1,C2,C5,C6,C7,T,STN,RHO,BIGRO,PI,P,
DELTAT,FMU1,FMU2,STNRT,N,N1,NFL,NSFL,J,WP,WE,M,M1,M2,BIGL,VDOTO,D,
A,S,SUM,SUM1,CINET,Hf,C,SUM4,SUM3,SUM5,SB,ELAST,ELASTS,ELASTA,ELASTP,
PLAST,SNOA,BIGLT,BIGLA,BIGLP,EA,BIGROA,K1,K2,R1,R2,EPSILA,
SUM6,SUM7,SUM8,SF,SUM9,STSS,SUMS,SNY,TO,F,W1,Z

DIMENSION V(94),DV(94),DELTS(94),DDS(94),BIGN(94),EPSIL(4),
SIGMA(4),E(4),BIGR(94),SNO(4),ARR(5,94),AFL(5,94),ASFL(4,5,94),
SN(4,5,94),STN(94),STNRT(94),C1(94),T(5,94),STSS(94),TO(94)
SNOA(4),EA(4),EPSILA(4),SIGMAL(4)

CINET=0.0D0
DO 10 I=1,K1
CINET=CINET+(DV(I)**2/C4/2)
10 CONTINUE
ELASTP=0.0D0
IF (J)30,20,30
20 PLAST=0
CINETO=CINET
GO TO 4
30 DO 60 L=1,1
SUM2=0
DO 50 I=1,K1
DO 40 K=1,NFL
SUM2=SUM2+SN(L,K,I)**2*ASFL(L,K,I)
40 CONTINUE
50 CONTINUE
ELASTP=ELASTP+SUM2
60 CONTINUE
ELASTP=ELASTP/(EA(1)/DELTSO)
C PLAST=CINETO-CINET-ELAST
4 DO 80 I=2,K1
STN(I)=LOG(ABS(DELTS(I)/DELTSO))
STNRT(I)=DDS(I)/DELTSO/DELTAT
80 CONTINUE
NSFL=3
RETURN
END

```



```

C=====
  SUBROUTINE ENERG8
C=====
  IMPLICIT REAL * 8 (A-H,O-Z)
  COMMONV,DV,DELTS,DELT,DDS,BIGN,EPSIL,SIGMA,SIGMALE,BIGR,SNO,ARR,AFL,
  ASFL,SN,TIME,DELTSO,CINETO,H,C1,C2,C5,C6,C7,T,STN,RHO,BIGRO,PI,P,
  DELTAT,FMU1,FMU2,STNRT,N,N1,NFL,NSFL,J,WP,WE,M,M1,M2,BIGL,VDOTO,D,
  A,S,SUM,SUM1,CINET,Hf,C,SUM4,SUM3,SUM5,SB,ELAST,ELASTS,ELASTA, ELASTP,
  PLAST,SNOA,BIGLT,BIGLA,BIGLP,EA,BIGROA,K1,K2,R1,R2,EPSILA,
  SUM6,SUM7,SUM8,SF,SUM9,STSS,SUMS,SNY,TO,F,W1,Z

  DIMENSION V(94),DV(94),DELTS(94),DDS(94),BIGN(94),EPSIL(4),
  SIGMA(4),E(4),BIGR(94),SNO(4),ARR(5,94),AFL(5,94),ASFL(4,5,94),
  SN(4,5,94),STN(94),STNRT(94),C1(94),T(5,94),STSS(94),TO(94)
  SNOA(4),EA(4),EPSILA(4),SIGMAL(4)

  DO 12 I=K2,R2
  CINET=CINET+(DV(I)**2/C2/2 )
12  CONTINUE
  ELASTS=0.0D0
  IF (J)32,22,32
22  PLAST=0
  CINETO=CINET
  GO TO 4
32  DO 62 L=1,NSFL
  SUM2=0
  DO 52 I=K2,R2
  DO 42 K=1,NFL
  SUM2=SUM2+SN(L,K,I)**2*ASFL(L,K,I)
42  CONTINUE
52  CONTINUE
  ELASTS=ELASTS+SUM2
62  CONTINUE
  ELASTS=ELASTS/(E(1)/DELTSO)
C  PLAST=CINETO-CINET-ELAST
4  DO 80 I=K2,R2
  STN(I)=LOG(ABS(DELTS(I)/DELTSO))
  STNRT(I)=DDS(I)/DELTSO/DELTAT
80  CONTINUE
  RETURN
  END

```

```

C=====
  SUBROUTINE ENERGA
C=====
  IMPLICIT REAL * 8 (A-H,O-Z)
  COMMONV,DV,DELTS,DELT,DDS,BIGN,EPSIL,SIGMA,SIGMALE,BIGR,SNO,ARR,AFL,
  ASFL,SN,TIME,DELTSO,CINETO,H,C1,C2,C5,C6,C7,T,STN,RHO,BIGRO,PI,P,
  DELTAT,FMU1,FMU2,STNRT,N,N1,NFL,NSFL,J,WP,WE,M,M1,M2,BIGL,VDOTO,D,
  A,S,SUM,SUM1,CINET,Hf,C,SUM4,SUM3,SUM5,SB,ELAST,ELASTS,ELASTA, ELASTP,
  PLAST,SNOA,BIGLT,BIGLA,BIGLP,EA,BIGROA,K1,K2,R1,R2,EPSILA,
  SUM6,SUM7,SUM8,SF,SUM9,STSS,SUMS,SNY,TO,F,W1,Z

  DIMENSION V(94),DV(94),DELTS(94),DDS(94),BIGN(94),EPSIL(4),
  SIGMA(4),E(4),BIGR(94),SNO(4),ARR(5,94),AFL(5,94),ASFL(4,5,94),
  SN(4,5,94),STN(94),STNRT(94),C1(94),T(5,94),STSS(94),TO(94)
  SNOA(4),EA(4),EPSILA(4),SIGMAL(4)

  DO 14 I=R1,N1
    CINET=CINET+(DV(I)**2/C4/2.)
14  CONTINUE
    ELASTA=0.0D0
    ELAST=0.0D0
    IF (J)34,24,34
24  PLAST=0
    CINETO=CINET
    GO TO 4
34  DO 64 L=1,1
    SUM2=0
    DO 54 I=R1,N1
    DO 44 K=1,NFL
    SUM2=SUM2+SN(L,K,I)**2*ASFL(L,K,I)
44  CONTINUE
54  CONTINUE
    ELASTA=ELASTA+SUM2
64  CONTINUE
    ELASTA=ELASTA/(EA(1)/DELTSO)
C  PLAST=CINETO-CINET-ELAST
4  DO 80 I=R1,N1
    STN(I)=LOG(ABS(DELTS(I)/DELTSO))
    STNRT(I)=DDS(I)/DELTSO/DELTAT
80  CONTINUE
    ELAST=ELAST+ELASTP+ELASTS+ELASTA
    PLAST=CINETO-CINET-ELAST
    RETURN
  END

```

Appendix (C)

LIST OF PUBLICATIONS

1. A.M.S. HAMOUDA AND M.S.J. HASHMI · High Strain Rate Constitutive Equations for Steel and Copper at Room Temperature, *Key Engineering Material*, 1992, Vol 74, pp 575-582.
2. A M.S. HAMOUDA AND M.S.J. HASHMI.:Simulation of the Impact of a Tool Steel Projectile into Copper, Mild-steel, Stainless-steel (304) Test Specimens, in *Structures Under Shock and Impact*, (Edited by P.S Bulson), Computational Mechanics Publications, 1992, p51-61.
3. A M.S. HAMOUDA AND M.S.J. HASHMI.:High Strain Rate Constitutive Equations for Brass and En-9 Steel at Room Temperature, in *Procs. of Advances in Engineering Plasticity and its Applications*, (Edited by W. Lee), Published by Elsevier, 1993, p251-558.
4. A.M.S. HAMOUDA AND M.S.J. HASHMI.:Mechanical Behaviour of Nylon at High Strain Rate and Room Temperature, *J. Key Engineering Material*, 1993, Vol 86-87, pp 109-114.
5. A M.S. HAMOUDA AND M.S.J. HASHMI.:High Strain Rate Constitutive Equation for Al Metal Matrix Composites, in: *Procs of Advanced Composites*, (Edited T.Chandra and A.K. Dhingra), Published by The Minerals, Metals, Materials Society, 1993, pp 1119-1124.
6. M S J HASHMI AND A.M.S. HAMOUDA.: Development of 1D Constitutive Equations for Metals Subjected to High Strain Rate and Large Strains, *Journal of Strain Analysis*, 29, (2), pp 117-127.
7. A M S. HAMOUDA AND M.S.J. HASHMI.: Modelling the Impact and Penetration Events of Modern Engineering Materials: Computer Codes Characteristics and Materials Models, *Journal of Materials Processing Technology*, 1994 , (in press).
8. A.M S HAMOUDA AND M.S.J. HASHMI.: Mechanical Properties of Al MMC Under Impact Loading, *Journal of Materials Processing Technology*, 1994, (in press).
9. A.M.S. HAMOUDA AND M S J. HASHMI.: The Influence of Water Absorbed on the Mechanical Behaviour of Nylon Under Static and Dynamic Loading:in *Proc. of Mechanics of Solids and Materials Engineering*, Vol (C) Mechanics of Materials, 1995, pp. 753-758.
10. A M S. HAMOUDA AND M.S.J. HASHMI : Dynamic Flow Stress Constitutive Equation For Type 304 Stainless-Steel, in *Procs. of Computational Plasticity, Fundamentals and Applications*,(Edited by D.R.J. Owen and E. Onate), 1995, pp 1779-1791.
11. A.M.S. HAMOUDA AND M S.J. HASHMI.: Testing of Composite Materials at High Strain Rate: Advances & Challanges, in: *Procs. Advanced Materials Processing Technologies*, (Ed M S.J. Hashmi), 1995, pp. 1488-1501.
12. A.M S. HAMOUDA AND M.S.J. HASHMI · A Simple Technique for Evaluating Material Constants for Solid Materials for Various Flow Stress Models, *First Australasian Congress on Applied Mechanics, 19-21 February 1996, Melbourne, Australia.*